Dipartimento di Informatica, Bioingegneria,
Robotica ed Ingegneria dei Sistemi

Hydrological cycle during droughts: large-scale analyses for process understanding and modelling

by

Giulia Bruno

DIBRIS, Università di Genova
Via Opera Pia, 13 16145 Genova, Italy
http://www.dibris.unige.it/

Università degli Studi di Genova

Dipartimento di Informatica, Bioingegneria,

Robotica ed Ingegneria dei Sistemi

Ph.D. Thesis in Computer Science and Systems Engineering
Systems Engineering Curriculum

Hydrological cycle during droughts: large-scale analyses for process understanding and modelling

by

Giulia Bruno

March, 2023

Dottorato di Ricerca in Informatica ed Ingegneria dei Sistemi
Indirizzo Informatica
Dipartimento di Informatica, Bioingegneria, Robotica ed Ingegneria dei Sistemi
Università degli Studi di Genova

DIBRIS, Univ. di Genova
Via Opera Pia, 13
I-16145 Genova, Italy
http://www.dibris.unige.it/

Ph.D. Thesis in Computer Science and Systems Engineering
Systems Engineering Curriculum

Submitted by Giulia Bruno
DIBRIS, Univ. di Genova

Date of submission: December 2022

Title: Hydrological cycle during droughts: large-scale analyses for process understanding and modelling

Advisors:

Prof. Dr. Luca Ferraris
Università di Genova and CIMA Research Foundation

Dr. Simone Gabellani
CIMA Research Foundation

Dr. Francesco Avanzi
CIMA Research Foundation

Ext. Reviewers:

Prof. Dr. Manuela Brunner
ETH Zurich and WSL Institute for Snow and Avalanche Research SLF

Dr. Andrea Toreti
European Commission Joint Research Centre

Abstract

Droughts strongly affect the environment and human activities with long-term and far-reaching impacts that will increase in the next decades under global changes. Thus, we need an in-depth understanding of drought processes and their robust modelling to cope with drought risk. For hydrologists, recurring challenges include predicting the impacts of precipitation (P) deficits in the form of soil moisture, streamflow (Q), or groundwater deficits. Water stored in catchments and evapotranspiration (ET) regulate drought evolution, that is the propagation of P deficits through the hydrological cycle and the subsequent recovery. Yet, analyses explicitly considering the joint contribution of storage and ET to drought evolution across different hydroclimatic regimes are rare. Furthermore, many hydrological models poorly simulate Q during droughts, but previous studies have rarely assessed model performances during droughts in multi-variable and spatially-distributed evaluations. This PhD thesis aimed to answer two main research questions: (i) do storage changes and ET affect drought evolution across climates and landscapes?; (ii) does a distributed hydrological model properly represent Q, ET, and storage during droughts? I performed a large-sample data-based analysis of Q, ET, and changes in the subsurface storage (in soil and groundwater) over the period 2010-2019 for 102 Italian catchments to answer the first question. To address the second question, I evaluated Q, ET, and storage simulations from the process-based distributed hydrological model Continuum over the Po river basin (northern Italy) during recent droughts, including the severe 2022 event. From the large-sample data-based analysis, I found that annual subsurface storage changes represented on average 11% of annual P across the study catchments, and mostly buffered Q deficits during drought years and their recovery. ET, instead, both buffered and aggravated Q deficits, and it had a decoupled response to P. These results revealed the prominent role of subsurface storage in driving the evolution of annual droughts. From model evaluation, I showed worse model performances in simulating Q for severe than for moderate droughts (mean KGE across the 38 study sub-catchments = 0.55±0.25 during moderate droughts and 0.18±0.69 in 2022) and I linked them to a degraded simulation of ET, rather than storage, especially in the human-affected croplands (mean r = -0.03 and nRMSE

= 1.8 across the croplands in 2022). By calibrating the model during a moderate drought, I showed similar model performances during the severe event (mean KGE = 0.18±0.63), which further point to specific human-water processes during this event. Therefore, I delineated possible ways forward for model improvement during severe droughts, such as an enhanced consideration of human interference, especially in ET. The findings of the thesis provided a consistent picture of the different role ET and storage have in drought evolution and in our modelling capabilities, coherently with recent literature, also on multi-year droughts. Moreover, these results emphasized the need for a holistic approach across the hydrological cycle for process understanding and model evaluation during droughts, with the ultimate goal of improving drought modelling for water resources management, disaster risk reduction, and climate change impact assessments.

Acknowledgements

My gratitude goes to many people who supported this work in different ways:

- my advisors Prof. Dr. Luca Ferraris and Dr. Simone Gabellani for their trust in my work and interest in my progress, and Dr. Francesco Avanzi for his guidance into the scientific world, our weekly meetings, and his positive notes on my desk;
- Dr. Doris Duethmann who hosted me for six months during my PhD at the Leibniz Institute for Freshwater Ecology and Inland Fisheries (IGB), for warmly welcoming me in her group and fruitful discussions on my thesis;
- Prof. Dr. Manuela Brunner and Dr. Andrea Toreti for their availability in being external reviewers of my thesis, suggestions that helped me to improve the presentation of my results, and insights for future work;
- my coauthors, I have learned something on research from each of, for insightful collaborations;
- people at CIMA Research Foundation where I spent my PhD time, for the nice working environment they contribute to;
- all the colleagues I have met in the Hydrology and Hydraulics Group over the past four years for their always kind answers to my many questions, who helped me collecting data for my thesis, and Giulia for her constant advice on hydrological, modelling, and programming issues;
- Anna and Endalk, with who I spent most of my PhD in Savona, for sharing experiences on doing a PhD, and friends from CIMA for our swimming after work and farinata in the evening to enjoy the most Savona;
- PhD students and postdocs at IGB for enriching discussions and for making my staying in Berlin more enjoyable;
- people I have met (virtually or in person) during courses and conferences for discussions that shaped my hydrological understanding and my vision of current research on hydrology and drought;
- my friends and family for their understanding and encouragement during this journey.

Table of Contents

[1]Part of this chapter is published as G. Bruno, F. Pignone, F. Silvestro, S. Gabellani, F. Schiavi, N. Rebora, P. Giordano, M. Falzacappa, Performing Hydrological Monitoring at a National Scale by Exploiting Rain-Gauge and Radar Networks: The Italian Case, Atmosphere (2021) 12, 771. https://doi.org/10.3390/atmos12060771

[2]This chapter is adapted from G. Bruno, F. Avanzi, S. Gabellani, L. Ferraris, E. Cremonese, M. Galvagno, and C. Massari, Disentangling the role of subsurface storage in the propagation of drought through the hydrological cycle, Advances in Water Resources (2022) 104305, https://doi.org/10.1016/j.advwatres.2022.104305

[3]This chapter is adapted from G. Bruno, D. Duethmann, F. Avanzi, L. Alfieri, A. Libertino, and S. Gabellani, Parameter transferability of a distributed hydrological model to droughts, Hydrol. Earth Syst. Sci. Discuss. [preprint], 2022, https://doi.org/10.5194/hess-2022-416, in review

Chapter 1

Introduction

1.1 Drought risk

Drought is 'a sustained period of below-normal water availability' [1] and is a recurring phenomenon all over the world. Much of Europe is currently facing a severe drought caused by a persistent lack of precipitation since winter 2021 and a summer heatwave, with the 7% of Europe in warning conditions for low soil water content and 17% in alert conditions due to vegetation stress in August 2022 [2]. Key droughts with severe hydrological implications over recent years were the European summer droughts in 2003 [3], 2015 [4], and 2018 [5, 6, 7] - which turned into a multi-year drought in some areas [8, 9, 10] -, the Millennium drought in south-eastern Australia (ca. 1997-2010, [11]), the Chilean megadrought (2010-2020, [12]), and the 2012-2016 California drought [13]. Severe droughts also occurred in previous centuries, such as the 1930s Dust Bowl in North America [14] and past events that might even have contributed to the collapse of civilizations [15].

Droughts originate from a lack of precipitation and/or anomalously high temperatures (meteorological droughts or snow droughts in snow-dominated regions [16]), and then propagates through the hydrological cycle to generate soil moisture and hydrological - streamflow and groundwater - droughts [17] (Figure 1.1). Similarly, the recovery of droughts to normal conditions propagates through the hydrological cycle [18], according to local conditions [19] and human activities [20]. Local conditions that govern drought evolution (propagation and recovery) across the landscape include for instance dominant vegetation types, with their different water use strategies during dry periods [21], morphological and climatic features, that make some catchments more prone to store water than others, and antecedent catchment conditions [22]. Today, human activities intensify or induce hydrological drought events too [23] (anthropogenic droughts [24]). Since

water is essential for ecosystems and human life, drought events can further translate into ecological droughts, that negatively affect ecosystems [25], and socio-economic droughts [17], which impact human society and economy (Figure 1.1).

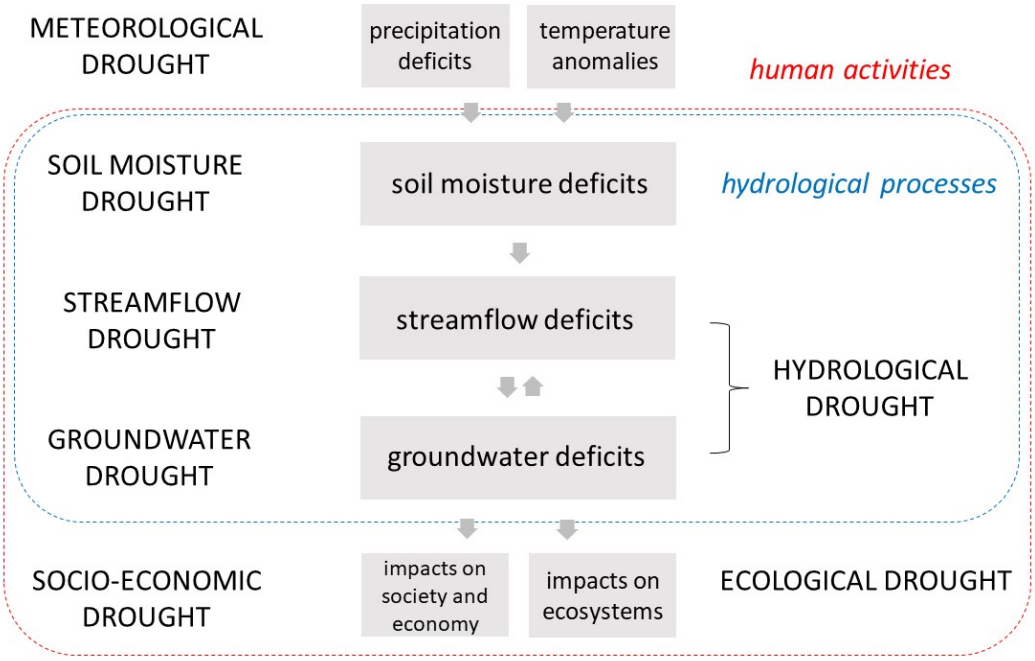

Figure 1.1: Schematic representation of drought propagation, inspired by [17] and [26]. In capital letters drought definitions and in gray background main features of each drought type.

Droughts generally have a long duration and a wide spatial extent [27], with long-term and far-reaching impacts that require regional management and ultimately undermine a sustainable development [28]. Droughts have direct and indirect impacts on various sectors of economy, society, and ecosystems [26] (Figure 1.2). Direct impacts of droughts are reduction in agricultural production [29] and in water supply [30], as well as forest disturbance [31]. Indirect drought impacts can be, for instance, decreased water quality [32, 33], famine [34], epidemic outbreaks [35], migrations [36], conflicts [37], gender disparities [38], and mental health deterioration [39]. Moreover, droughts occur with and trigger other natural hazards, like heatwaves and wildfires, resulting in compound and cascading events [40] and impacts [41]. For these reasons, properly estimating drought impacts is challenging [42]; yet, [43] reported US$128 billion lost and 1.43 billion people affected by droughts worldwide between 2000 and 2019. This ranked droughts as the fourth most impactful natural risk in terms of economic losses and the second one in terms of affected population [43].

Data have shown clear changes in drought characteristics for some regions of the world over the recent decades, such as an increase in streamflow drought spatial extent across the USA between 1981 and 2018 [44], and an intensification in frequency and duration of meteorological droughts

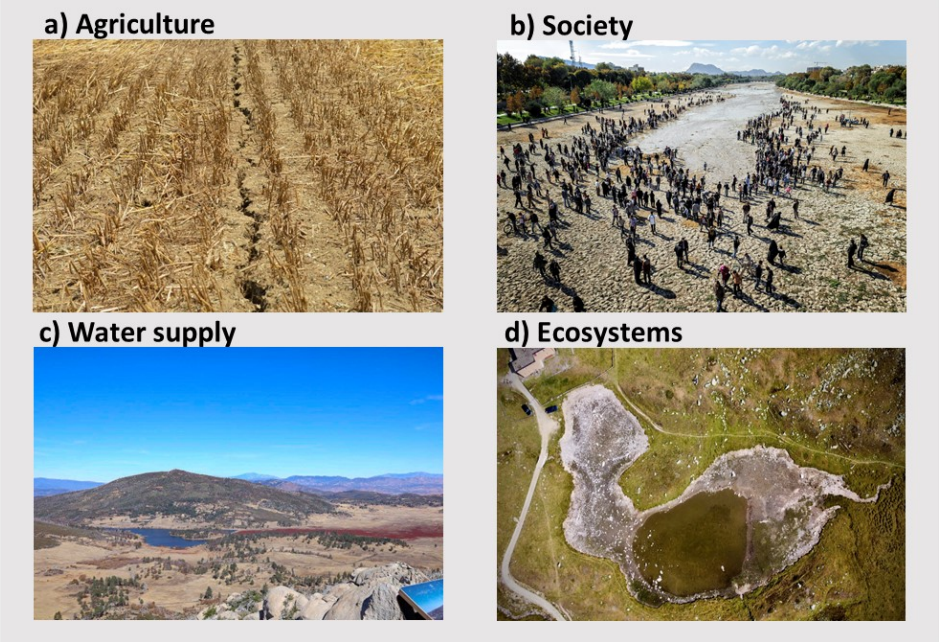

Figure 1.2: Images of sectors affected by droughts: (a) agriculture, 'Climate change and arid soil', Italy, 2017; (b) society, 'Cheers for water recursion', Iran, 2011; (c) water supply, 'Anthropogenic Drought on Cuyamaca Lake', USA, 2017; and (d) ecosystems, 'A ghost lake or a dry snail?', Italian Alps, summer 2022. Credits: Andrea Carri, Arash Modaresi Rad, Alexandre Martinez, and Alessandro Ceppi (distributed via imaggeo.egu.eu).

in northern Italy from 1965 to 2017 [45]. Drought hazard could further increase in the near future due to climate change [46, 47, 48], especially in some areas like the Mediterranean [49]. [50] for instance predicted an increase in the severity of meteorological droughts over northern Italy by the end of the century and [51] showed an expected enhancement of drought impacts across Europe, as a result of climatic and socio-economic projections.

Drought adaptation measures are a pressing challenge today. Like for any natural risk, adaptation measures can be structural, such as the construction of reservoirs and changes in agricultural practices, and non-structural, like drought monitoring tools and water supply forecasting systems for water resources management, and drought risk assessments for policy making. Early warning systems and risk assessments widely rely on hydrological models, which in turn are built upon our understanding of physical phenomena. Hence, we need an in-depth understanding of drought processes to achieve their robust modelling.

1.2 State-of-the-art

My thesis focuses on the understanding of natural processes occurring during droughts and their modelling. Over recent years, drought research received growing attention along four main lines (Figure 1.3): (i) drought characterization or 'How severe is a drought?'; (ii) drought processes understanding or 'How do droughts unfold?'; (iii) drought modelling or 'How well do we simulate droughts?'; and (iv) drought forecasting or 'What will droughts be like in the future?'.

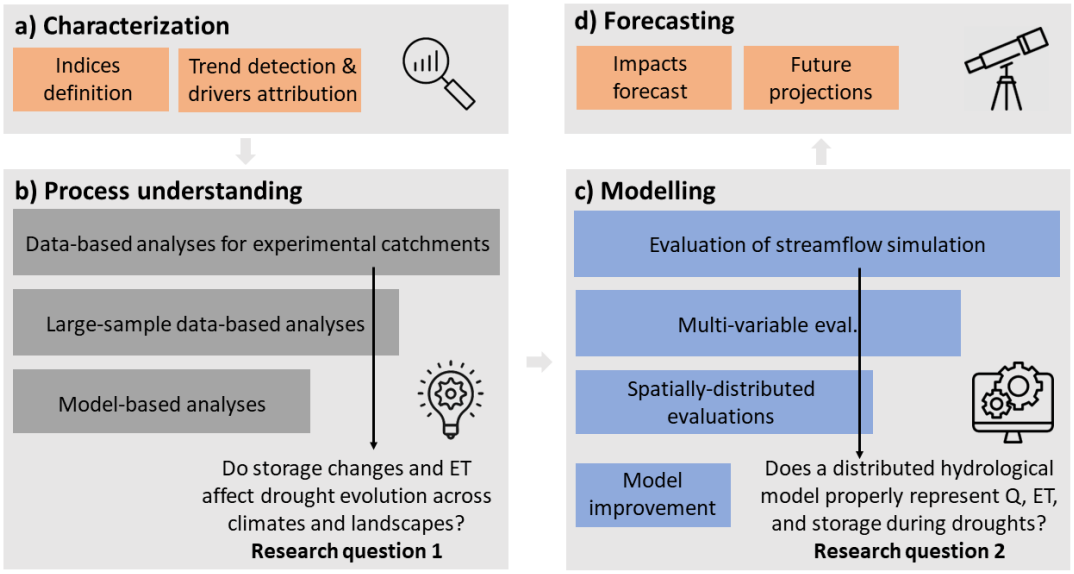

Figure 1.3: Illustration of main lines in drought research: (a) drought characterization, (b) processes understanding, (c) modelling, and (d) forecasting, with their methods and links among them. In (b) and (c) the main research questions addressed in the thesis are reported.

In the following sections I firstly provided an overview of useful hydrological concepts (Section 1.2.1) and then briefly outlined the state of the art for research lines (i) to (iii) (Sections 1.2.2, 1.2.3, 1.2.4). I did not discuss in detail the research on drought forecasting for impact-based forecasts (e.g., [52]) and future projections (e.g., [47, 46, 53]) as this was beyond the scope of the thesis. However, robust hydrological modelling during droughts is essential for drought forecasting and the findings of my thesis can have implications for it (Section 4.4.1).

1.2.1 Preliminary hydrological concepts

The hydrological cycle is the partitioning of precipitation (P) into evapotranspiration (ET), streamflow (or discharge, Q), and changes in the Terrestrial Water Storage (TWSC) in glaciers, snowpack, water bodies, soil, and groundwater. At an annual time scale and for particular catchments

(non-glacierized and unaffected by large water bodies), TWSC are mainly due to changes in the water content of soil and groundwater, i.e., changes in the subsurface storage (ΔS). The water balance equation (Equation 1.1) can mathematically represent the hydrological cycle at the catchment scale:

$$P = Q + ET + TWSC \tag{1.1}$$

Monitoring water balance components across the landscape is challenging, especially with regard to ET and TWSC. ET is the coupling term between the surface water and energy balances, and several methods exist for its monitoring, based on the measurement of either water or energy fluxes [54]. Measurement sites, such as flux towers [55] and lysimeters [56], provide point ET measurements. Yet, they are sparse, and ET is highly variable in space because of its strong dependence on land cover and local climate. Today, remote sensing allows large-scale (near) real-time ET estimates, from remote sensed data (e.g., the Normalized Difference Vegetation Index [57]), and possibly hydrological or energy models. Land surface modelling in retrospective analyses (reanalyses) also provide large-scale ET estimates. However, verification of such ET estimates against point-scale measurements is desirable. Finally, a water balance approach can provide ET estimates from Equation 1.1 and P, Q, and possibly TWSC data [58, 59]. Similarly, the different components of TWS can be measured at point-scale, but in-situ data for them are generally rare and potentially not representative at a catchment scale. A water-balance approach can also provide estimates of storage changes across catchments [60, 13]. Lastly, integrated measures of TWS are now available at large scale through remote sensing from the Gravity Recovery And Climate Experiment (GRACE, Section 4.2.3.2).

Hydrological models are mathematical tools to simulate the hydrological cycle. They can be defined mainly according to their (i) structure (data-driven, conceptual, or physics-based), (ii) spatial distribution (lumped, semi-distributed, or distributed), and (iii) temporal application (event-based or continuous) [61]. Model complexity increases from data-driven (lumped/event-based) to physics-based (distributed/continuous) models. Many hydrological models have a conceptual representation - generally a storage schematization - for physics-based processes and [61] referred to those as hybrid models. Here I used the term process-based (or -oriented) hydrological models, I exclusively focused on, to distinguish them from purely data-driven (statistical [62] or machine learning [63]) models. According to [64], a process-based hydrological model 'explicitly represents and/or incorporates through assimilation approaches the hydrologic state variables and fluxes that are theoretically observable ... at temporal scales characterizing the underlying physical processes'. Further classifications and definitions are available for hydrological models, which are beyond the scope of this brief literature review. Besides, additional modules can be coupled to hydrological models to simulate processes interacting with the hydrological cycle, such as vegetation dynamics and tracers transport in ecohydrological models [65]. Hydrological models generally require a calibration (or training) phase to select suitable values for model parameters and an evaluation (or validation or verification) phase to verify the suitability of calibrated parameters beyond the calibration data. [61] provided a review of common methods for model calibration and evaluation. The increasing availability of hydrometeorological remote

sensing-based data has fostered their application in hydrological modelling over recent years, for calibration [66, 67], evaluation [68], and data assimilation [69]. The integration between remote sensing and hydrological modelling is of key importance in digital twins of the Earth System [70] to monitor and forecast hydrological extremes [69].

Today, human activities, such as water abstractions, reservoirs, land use changes, irrigation, and water transfers, heavily affect the hydrological cycle [71], but properly considering them in large-sample analyses [72] and hydrological modelling [73, 74] is challenging. Here, I focused mostly on natural processes occurring during droughts and I discussed possible human interference in the analyses in Sections 3.4.3, 4.4.2, and 5.2.

1.2.2 Drought identification and characterization

Drought analyses, monitoring, and forecasting require the identification of - past, current, and future - drought events and their characterization through drought indicators. Because of the relevance for drought impacts, main drought characteristics are the (i) frequency, i.e., the number of events in a time span, (ii) duration, i.e., the period from the onset to the termination of an event, (iii) severity, or magnitude, associated to the water deficit during the event, (iv) intensity, i.e., the ratio between severity and duration, and (v) spatial extent, i.e., the number of affected catchments or percentage of affected area over a region [42] (Figure 1.4).

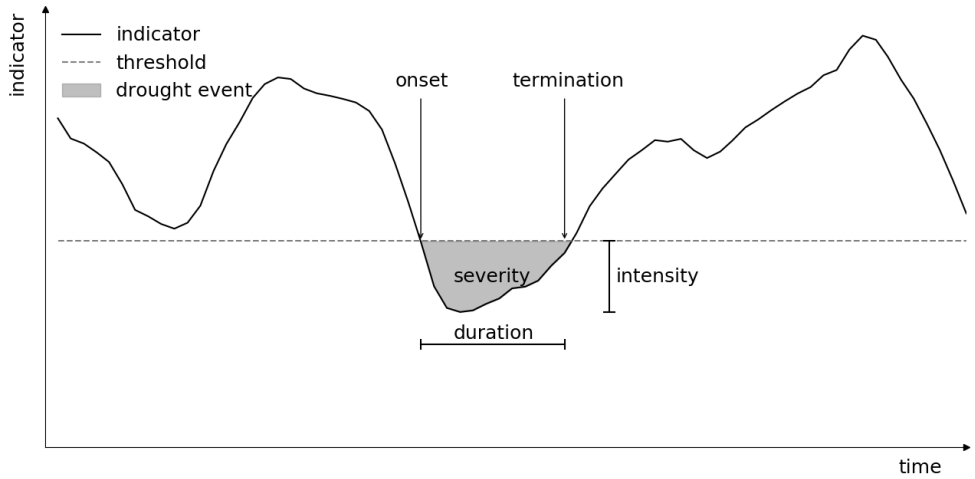

Figure 1.4: Illustration of main drought characteristics.

Drought identification and characterization require long-term hydrometeorological data - ideally more than 30 year-long [75] -, and a standardized [76] or threshold-level approach [77]. The standardized approach originated from the definition of the Standardized Precipitation Index (SPI) by [78]. For any given time step, the SPI is the z-score (or standardized anomaly) of the observed precipitation with respect to a normally distributed probability density (i.e., with zero mean and

unit standard deviation) from the long-term P data [78]. Furthermore, SPI time series allow to define drought events, according to predefined thresholds, and the SPI values within the events allow to derive their characteristics [78] (Figure 1.4). Various studies proposed indices for each hydrological flux and state building on the SPI concept, such as the Standardized Precipitation Evapotranspiration Index [79], the Standardized Streamflow Index [80], the Standardized Soil Moisture Index [81], and the Standardized Groundwater Index [82]. Reviews of drought indices are available for instance in [83] for a general overview, and [84] with regard to the link between indices and impacts. The threshold-level approach relies on the definition of a threshold, generally corresponding to a fixed percentile of the considered variable, and it identifies a drought event when the variable is lower than the threshold (trough-under-threshold). The threshold can be either fixed [77] or variable [85] in time. Drought characteristics descend from the time series itself, after the identification of drought events (Figure 1.4, with a fixed threshold).

Vast literature proposed new drought indicators to account for relevant hydrological processes in specific areas, like snowmelt in snow-dominated catchments [86], or combinations of them for specific applications [87]. A fit-for-all drought indicator cannot exist and its choice should be region- and purpose-dependent [17, 5].

Drought characterization studies further include trend detection and drivers attribution for past events [44], also from a climatological standpoint [4].

1.2.3 Drought processes understanding

Over the last decades, literature investigated the mechanisms generating hydrological droughts, which mainly relate to ET and storage in the catchment [60], and proposed theoretical frameworks for drought propagation, such as streamflow drought typologies [88, 89]. Process understanding has generally been carried out through: (i) data-based analyses for experimental catchments; (ii) large-sample data-based analyses; and (iii) model-based analyses (Figure 1.3b).

Experimental catchments allow us to have long-term data for (most) water balance components (Section 1.2.1). Thus, data from experimental catchments allow to directly track the propagation of the drought signal throughout the hydrological cycle. For instance, [3] analysed P, Q, soil moisture, and ET data from four experimental catchments in Central Europe during the 2003 summer drought. They provided evidence that soil moisture deficits were amplified by an increase in ET, which they called 'drought paradox' to underline the somehow counterintuitiveness of an increased outgoing flux at a time of decreased ingoing flux. [6] examined P, Q, soil moisture, and groundwater levels from a Scottish research catchment throughout the 2018 drought. They found that subsurface storage supported almost entirely Q during drought and the following recovery period. However, storage had not completely replenished during the preceding winters and the two factors - dry antecedent conditions and Q sustainment during drought - resulted in the strongest storage depletion on record. Therefore, data-based analyses from experimental

catchments shed light on hydrological processes occurring during droughts.

To synthesize hydrological knowledge across a variety of catchments and scales, analyses across large samples of catchments - tens to thousands - are warranted today [72]. Existing large-sample (or multi-catchments or comparative) analyses mostly relied on P and Q data to identify and characterize meteorological and hydrological droughts, and on catchment properties or hydrological signatures [90] as proxys for other hydrological processes. This stemmed mainly from the difficulty in collecting water balance datasets for large samples of catchments (Section 1.2.1). For instance, [22] studied the controls on hydrological drought characteristics in 44 Austrian catchments through long-term P and Q time series, and climatic and physiographic characteristics. They found that physiographic characteristics related to storage control drought duration, while a combination of climatic and (storage-related) physiographic characteristics affect drought severity. A valuable example of multi-variable large-sample analysis is [91] that exploited data from observations and reanalyses to study the evolution of P, Q, ET, and soil moisture during droughts over the period 1984 - 2007 for 436 European catchments. They found soil moisture droughts reduced more strongly and faster Q than ET across the study area, similarly to what [3] showed at a catchment- and event-scale.

Model-based analyses overcome the poor availability of long-term water balance data at large scales. [92] provided further evidence of the 'drought paradox' during the 2003 summer drought in the Alps through ecohydrological modelling. However, different hydrological models may result in different conclusions, as argued from a large-sample and multi-model sensitivity analysis in [93], and hydrological models may not properly represent drought processes (Section 1.2.4). Thus, model-based analyses should be used cautiously for process understanding and at least be adequately backed up by specific validation during droughts.

1.2.4 Drought modelling

Hydrological models have usually been designed to reproduce high flows, rather than low flows [94]. Furthermore, the transferability of model parameterizations outside the climatic conditions of the calibration period is often limited [95, 96] and this can hamper model performances during multi-year droughts for instance [97] (Section 1.2.5). For these reasons, properly simulating drought conditions can be challenging [98, 97, 99]. However, drought monitoring systems [100] and risk assessments [101] often use hydrological models to predict droughts in data-scarce or ungauged areas. Therefore, assessing model robustness during droughts is highly relevant today and it is the first step toward possible model improvement (see for instance [102] and [103] as an example of model evaluation and subsequent improvement for multi-year droughts).

Model evaluations during droughts have mostly focused on Q [98, 97, 99], either in a calibration-evaluation approach [97] or by assessing the simulation of streamflow drought events and their characteristics [98, 99]. For example, [97] investigated the ability of 6 lumped conceptual hy-

drological models in reproducing Q during the Millennium drought for 124 catchments in south-eastern Australia. They calibrated the models on pre-drought conditions and then evaluated them during the drought, finding that models underperformed in catchments where the multi-year drought was particularly extreme [11] (Section 1.2.5). [99] instead evaluated the performances of various catchment-scale and global hydrological models in simulating streamflow drought events and their characteristics for 8 large catchments all over the world. They showed that catchment-scale hydrological models, and their ensemble mean, have better performances than global hydrological, and single models, in simulating streamflow drought events, even though they have a generally limited ability in properly simulating their characteristics. [98] quali-quantitatively evaluated the ability of an ensemble mean of large-scale models in simulating drought propagation features, streamflow drought typology and characteristics; they argued that model inability in reproducing drought propagation features and streamflow drought typology can be due to a poor simulation of processes involved in drought propagation, as ET and storage.

Recent studies explicitly showed that models may misrepresent ET [13, 59] and storage dynamics [102] during droughts. [59] revealed that Earth System Models largely underestimated the occurrence of positive ET anomalies during droughts between 2003 and 2020 at the global scale, with 25% of drought months experiencing positive ET anomalies from simulations and 44% from observations. Furthermore, [102] showed that 5 commonly used lumped conceptual hydrological models did not properly simulate the decline in storage that emerged from data for the Millennium drought in south-eastern Australia. These findings emphasize the need for multi-variable evaluations during droughts to explicitly verify model internal consistency.

Increased computational capabilities fostered the use of distributed hydrological models over recent years [64] and remote sensing-based data provide the opportunity to evaluate also simulated spatial patterns [104, 105]. Yet, spatially-distributed multi-variable model evaluations focusing on droughts are rare in the literature.

1.2.5 Multi-year droughts

Prolonged streamflow droughts have different hydrometeorological drivers than shorter droughts [106]. Moreover, multi-year droughts can trigger changes in how catchments respond to precipitation [11], resulting in an exacerbation of streamflow droughts compared to what predicted from the meteorological droughts and typical P-Q relationships. Shifts in P-Q relationships occurred in south-eastern Australia during the Millennium drought [11], in Chile during the 2010-2020 megadrought [12], and in California during the 2012-2016 drought [13]. However, there is no consensus on the causes of these hydrological changes [107] and on what makes some catchments more prone to them [108, 12]. These shifts have serious impacts on modelling capabilities [97]. A warming climate may lead to more severe and long droughts [9, 10], and also to transitions from snow- to rainfall-dominated hydrological regimes that foster multi-year streamflow droughts [109]. Therefore, changes in the hydrological response of catchments during multi-year

droughts challenge future water security [110]. Analyses of ET and storage during multi-year droughts are limited, even thought they can provide insights on the mechanisms occurring during these events and their modelling [13].

1.3 Research questions

From the literature review (Section 1.2), two major gaps emerged in the research on the understanding of drought processes and their modelling (Figure 1.3). Previous studies revealed that catchment storage is a key driver in drought evolution (propagation and recovery), using long-term data from small-sized experimental catchments [6] or storage-related catchment properties in large-sample analyses [22, 76]. Though, data-based analyses explicitly quantifying ET and storage contribution to drought evolution across different hydroclimatological regimes are rare (research gap 1). Moreover, several hydrological models showed declining skills during droughts in simulating Q [97], ET [13], and storage [102]. Yet, multi-variable evaluations of spatially-distributed hydrological models have rarely been performed (research gap 2).

Hence, the PhD thesis aimed to answer two main research questions:

(i) do storage changes and ET affect drought evolution across climates and landscapes? (Section 3);

(ii) does a distributed hydrological model properly represent Q, ET, and storage during droughts? (Section 4).

To answer these questions, I collated ground- and remote sensing-based P, Q, ET, and storage changes data at a national scale (Section 2), I analyzed this large-sample dataset to unravel how they vary during droughts and their recovery across different climates and landscape features (Section 3), and I evaluated the performances of a distributed hydrological model in simulating Q, ET, and storage dynamics during droughts at a regional scale (Section 4). Furthermore, I participated in the analysis of possible hydrological changes during multi-year droughts in European climates and the identification of potential drivers for them (Section 5).

Chapter 2

Overview of study area and data[1]

Italy has an Alpine-to-Mediterranean climate and a complex topography (Section 2.1) that make it an ideal case study for large-scale analyses, and it experienced several droughts recently (Section 2.3). Hence, I used Italy as study area for the data-based large-sample analysis (Section 3) and its major basin - the Po river basin - for model evaluation (Section 4). Specifically, I selected 102 catchments across Italy and 38 sub-catchments within the Po river basin (Section 2.2.6). A large-sample hydrometeorological dataset is currently lacking for the region [111], and for this reason I firstly collected hydrological and meteorological data at Italian scale (Section 2.2).

2.1 Study area

2.1.1 Topography and climate

Italy is characterized by a wide variety of topographic areas and climatic environments that are reflected in catchment types and hydrometeorological regimes. Topography in Italy varies from mountainous along the Alps (in the north) to flat and highly urbanized in the lowlands in the northern regions and then to a predominant steep coastal orography all along the peninsular coastline (Figure 2.1). Consequently, Italy has few large catchments (with an area greater than 10^4 km^2) located in the northern and central part of the country and many small- and medium-size steep catchments (drainage areas ranging from 10^1 to 10^3 km^2) across the country. In the northern and north-eastern alpine and sub-alpine regions, climate is cold and temperate without a dry season [112] (Figure 2.2). While it is temperate with a dry season and arid all along the

[1]Part of this chapter is published as G. Bruno, F. Pignone, F. Silvestro, S. Gabellani, F. Schiavi, N. Rebora, P. Giordano, M. Falzacappa, Performing Hydrological Monitoring at a National Scale by Exploiting Rain-Gauge and Radar Networks: The Italian Case, Atmosphere (2021) 12, 771. https://doi.org/10.3390/atmos12060771

western coast and in the central and southern regions [112] (Figure 2.2), with most of the rainfall in autumn and winter — a typical Mediterranean climate [113].

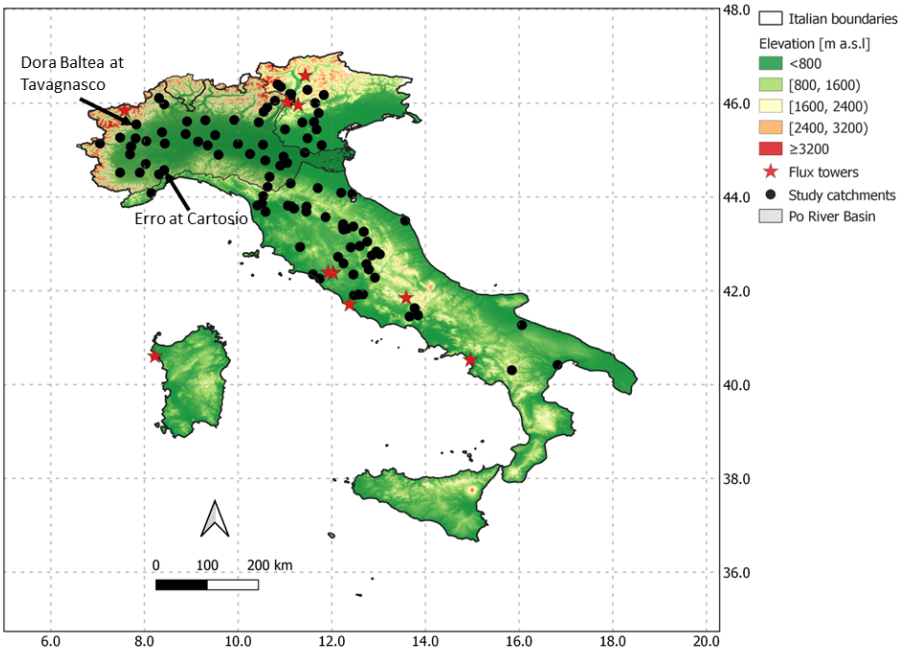

Figure 2.1: Elevation of the study area from [114], with locations of (i) flux towers for evapotranspiration (ET) validation (Section 3.2.2.1), (ii) closure sections of study catchments for the large-sample analysis (Section 3) and example catchments for illustration of hydroclimates (Section 2.2.6), and (iii) the Po river basin for the model evaluation (Section 4).

2.1.2 Land cover

A variety of natural and human-affected land cover types characterize the study region, with forests and semi-natural areas mostly along the mountains, and agricultural areas and artificial surfaces in the lowlands and along the coastline (Figure 2.3). Agricultural areas dominate as land cover type with around 51% of the Italian territory covered by them according to the Corine Land Cover 2018 map (https://land.copernicus.eu/paneuropean/corine-landcover/clc2018, last access on 24 November 2022). Then, forests and semi-natural areas occupy around 42% of the country, urban areas around 5%, and water bodies around 2%.

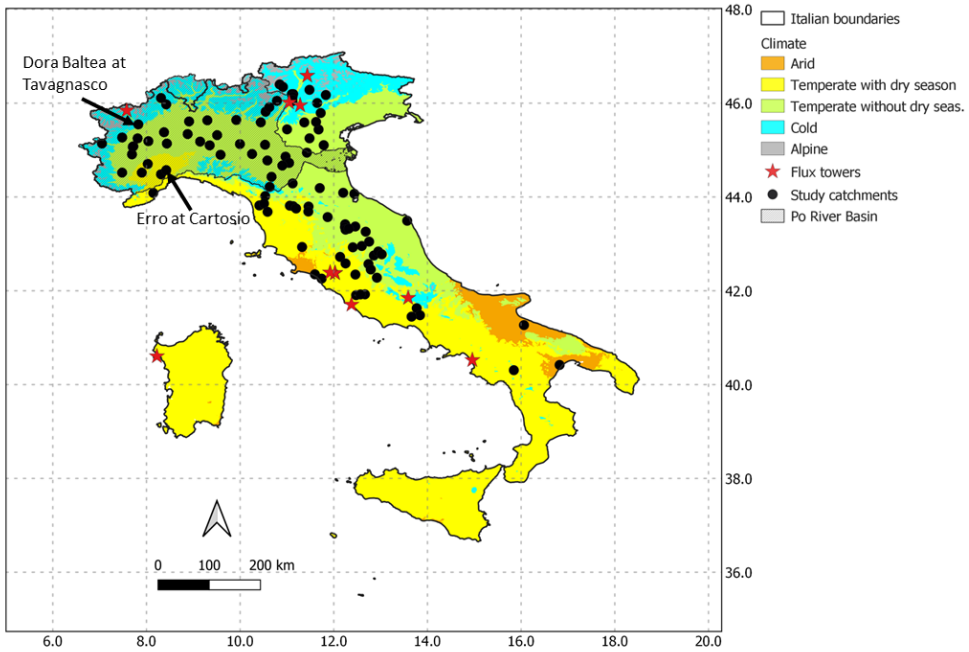

Figure 2.2: Same as Figure 2.1, but for climate from [112].

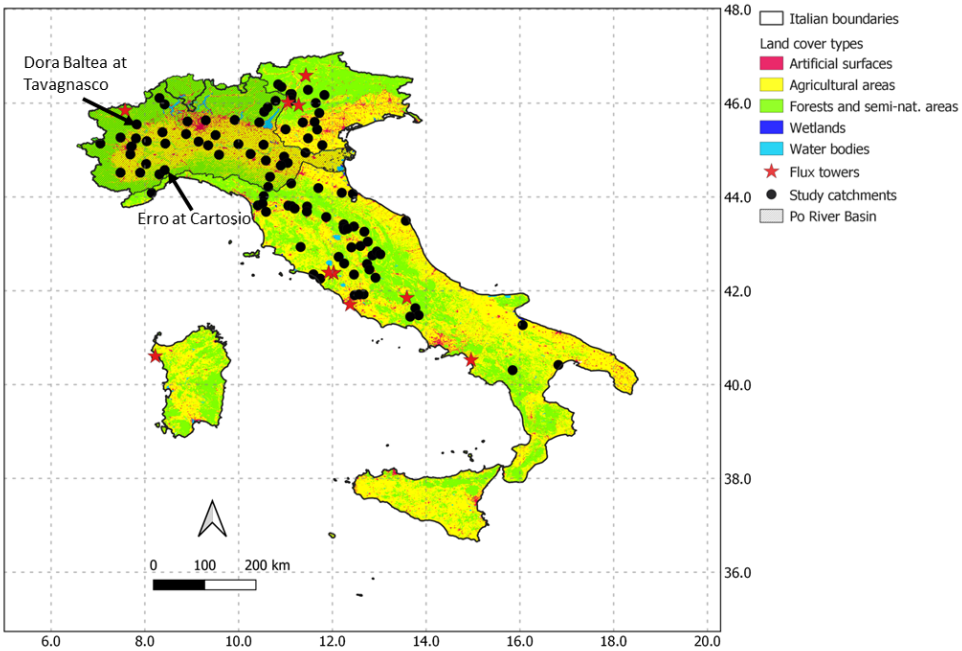

Figure 2.3: Same as Figure 2.1, but for land cover from the Corine Land Cover 2018 map.

2.1.3 Soil and geology

According to [115, 116], the most common soil texture across Italy for both the top- (Figure 2.4) and sub-soil (not shown) layers is medium with low-to-medium percentage of clay and sand, followed by coarse with low percentage of clay and high percentage of sand, and fine with medium-to-high percentage of clay. For topsoil, medium soil texture accounts for around the 68%, coarse for around the 23%, and fine for around the 9%.

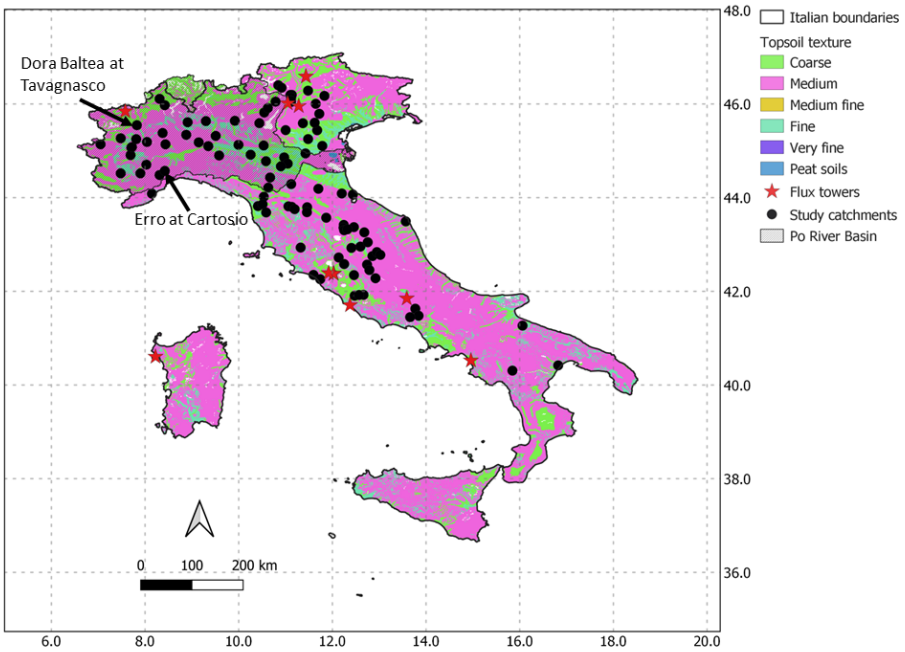

Figure 2.4: Same as Figure 2.1, but for topsoil texture from [115, 116].

Various aquifers characterize the study region basing on the ISPRA hydro-geological complexes map (http://www.sinanet.isprambiente.it/it/sia-ispra/download-mais/complessi-idrogeologici/view8, last access on 02 August 2021). Igneous and metamorphic rocks are mainly in the northwestern Alps, central and southern areas, and the islands; carbonate rocks in the northeastern Alps, Apennines, and southeastern region; silicatic sediment rocks in the Apennines; and unconsolidated aquifers in the northern Po plain and along the coastlines (Figure 2.5).

2.2 A hydrometeorological dataset for Italy

In Italy, regional hydrometeorological offices oversee hydrometerological data collection today. Moreover, the Italian Civil Protection Department (DPC) collects the data at the national scale

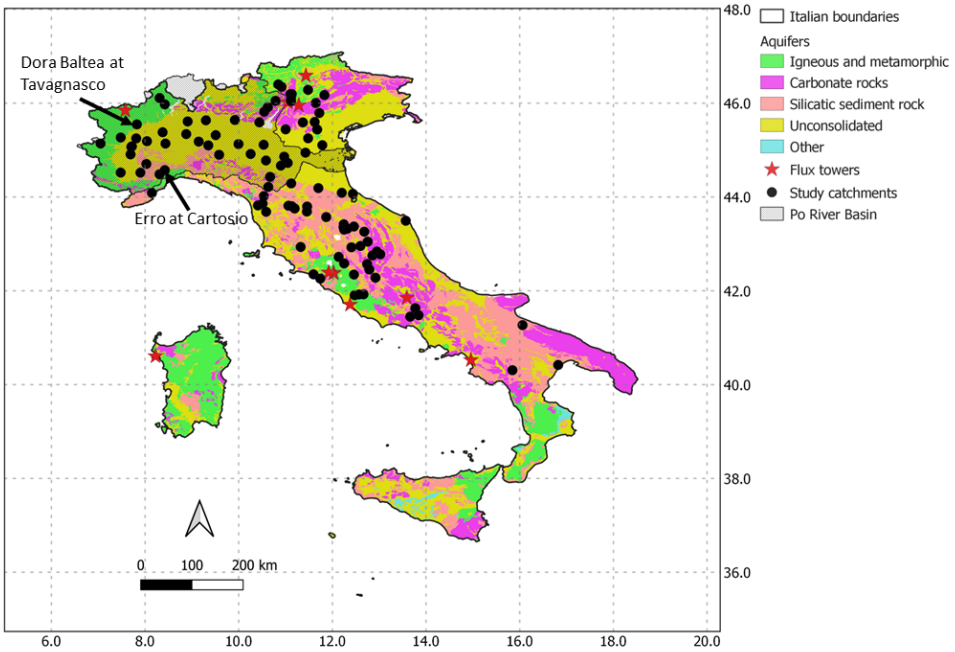

Figure 2.5: Same as Figure 2.1, but for aquifers from the ISPRA hydro-geological complexes map.

from the different regional offices in near real-time for civil protection purposes and hydrometeorological monitoring. CIMA Research Foundation, as DPC Competence Center, has access to its database (hereinafter DPC database). The DPC database was the backbone of the hydrometeorological dataset I collated.

For the large-sample analysis (Section 3), I blended ground- and remote sensing-based data over the hydrological years (h.y.) 2010 - 2019. Further, I extended the dataset up to h.y. 2022 for the Po river basin to include the severe 2022 - ongoing - drought in the model evaluation (Section 4). Throughout the thesis, I considered hydrological years (from September to August, named after the August calendar year) rather than calendar years.

In the following I briefly described data availability for the study region, data I used, and an overview of them.

2.2.1 Precipitation

In Italy, precipitation (P) is monitored by a network of about 4500 gauges and 23 radars today [117]. Therefore, spatial estimates of P for the region can be derived by spatial interpolation of gauges data or the merging of gauge- and radar-data, for instance through the Modified Condi-

tional Merging (MCM) algorithm [117]. I used gridded P data from the DPC database, as well as the gauge-based BIGBANG dataset [118, 119, 120] for drought identification due to its long-term availability (Section 3.2.2.1). Basing on DPC data and the MCM interpolation algorithm [117], mean annual P (2013-2022) varies between less than 600 mm in southern regions and more than 2500 mm in the northeastern Alps and northwestern Apennines (Figure 2.6).

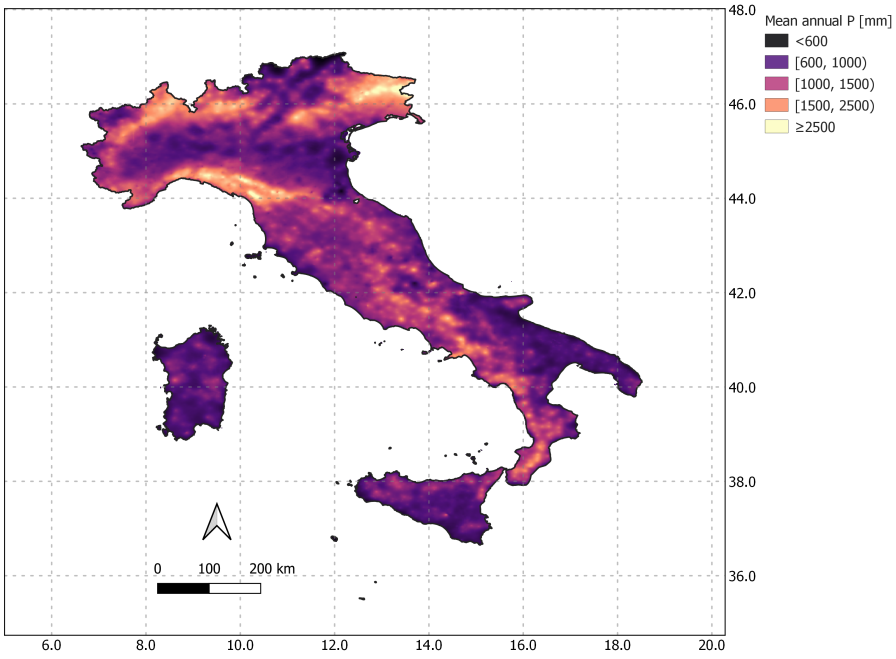

Figure 2.6: Mean annual P (2013-2022) for Italy according to DPC data and the MCM interpolation algorithm [117].

2.2.2 Streamflow

In Italy, water levels are currently monitored by around 1250 gauges, but updated rating curves to convert them to streamflow (Q) data are available for only about 600 of them [121] (Figure 2.7) and long-term Q data for still less. I collated Q data from the DPC database and regional hydrometeorological offices. The DPC database consists of pre-validated Q data from near real-time water levels, whereas some validated Q time series are available online from regional hydrometeorological offices. Thus, I screened the dataset for possible outliers through a semi-automated quality checking procedure (Section 3.2.2.1) and linearly interpolated small gaps before the analyses.

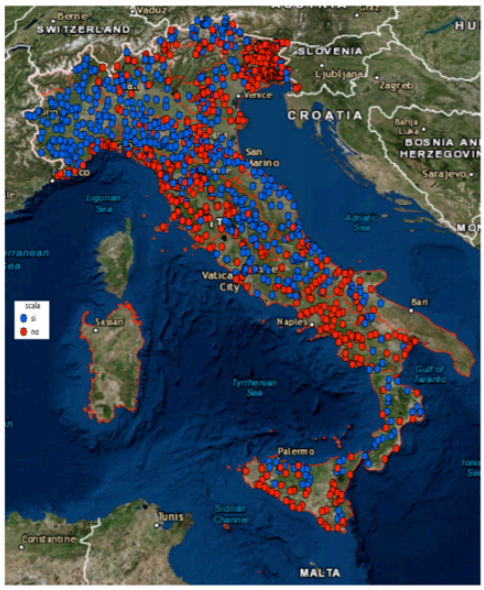

Figure 2.7: Water level gauges across Italy with (blue dots) and without (red dots) updated rating curves as of 2016, from [121].

2.2.3 Evapotranspiration

For evapotranspiration (ET), I exploited the remote sensing-based ET dataset from the Land Surface Analysis of the EUMETSAT Satellite Application Facility (hereafter LSASAF) which I quality-checked for the study region through an in-situ validation at 12 flux towers (location in Figures 2.1 to 2.5) and in a multi-dataset comparison (Section 3.2.2.1). According to the LSASAF product, mean annual ET (2010 - 2022) ranges from less than 200 mm in the Alpine northern regions and coastal areas in southern regions to more than 500 mm in the northern Po plain (Figure 2.8).

2.2.4 Terrestrial Water Storage

To have storage data for a variety of small-to-large catchments, I estimated storage changes as annual residual from the water balance equation (Equation 1.1) for the large-sample analysis, while in the model evaluation I used monthly Terrestrial Water Storage (TWS) data from remote sensing-based GRACE products as independent data at a regional scale (Section 4.2.3.2).

In Section 3.4.2, I discussed the robustness of storage estimates from water balance through a comparison with alternative P and ET datasets, and a correlation analysis with possible morphological and climatic predictors. Furthermore, I compared monthly estimates of storage changes from the observed water balance components and GRACE products for the outlet of the Po river

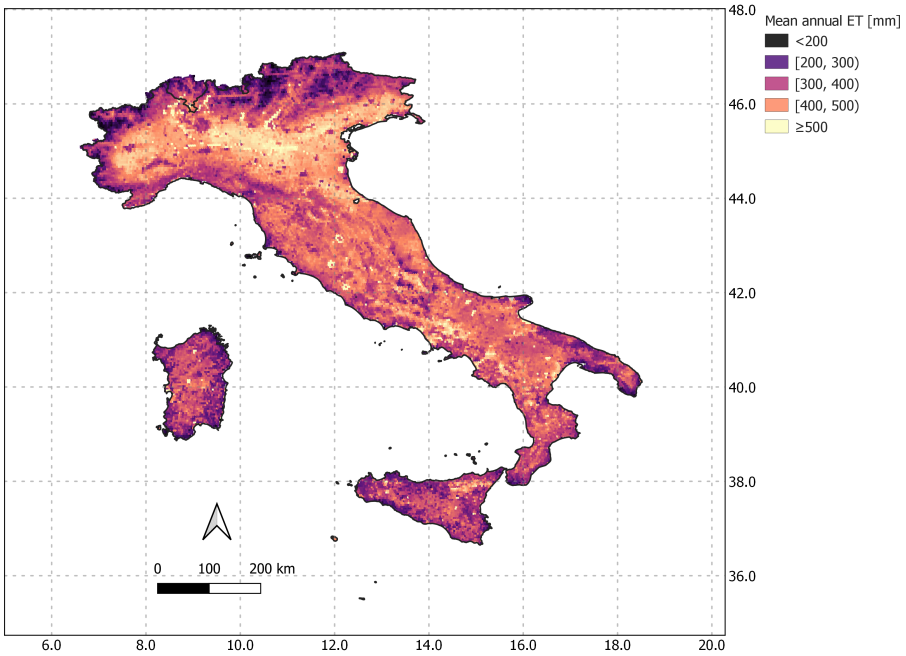

Figure 2.8: Mean annual ET (2010-2022) for Italy according to the LSASAF product [122, 123].

basin following [124]. I obtained a satisfactory agreement between the two estimates of storage changes with Pearson's correlation coefficient (r) equal to 0.73 and Root Mean Square Error (RMSE) equal to 20 mm/month (Figure 2.9).

2.2.5 Meteorological dataset

The Italian official meteorological network currently consists of around 3200 sensors for temperature, 2000 for radiation, 1000 for wind, and 1500 for relative humidity. Here, I used ground-based data from the DPC database to derive (i) catchment-average temperature for climate characterization of the study catchments in the large-sample analysis (Section 3.2.2.2) and (ii) maps of the required meteorological variables for the modelling study (Section 4.2.3.1).

2.2.6 Study catchments and their characteristics

As study catchments, I selected 102 Italian catchments for the large-sample analysis and 38 sub-catchments in the Po river basin for the modelling study, according to data availability and catchment suitability for the analyses (Sections 3.2.1 and 4.2.3.2). For each study catchment I derived a set of characteristics and hydrological signatures (Section 3.2.2.2).

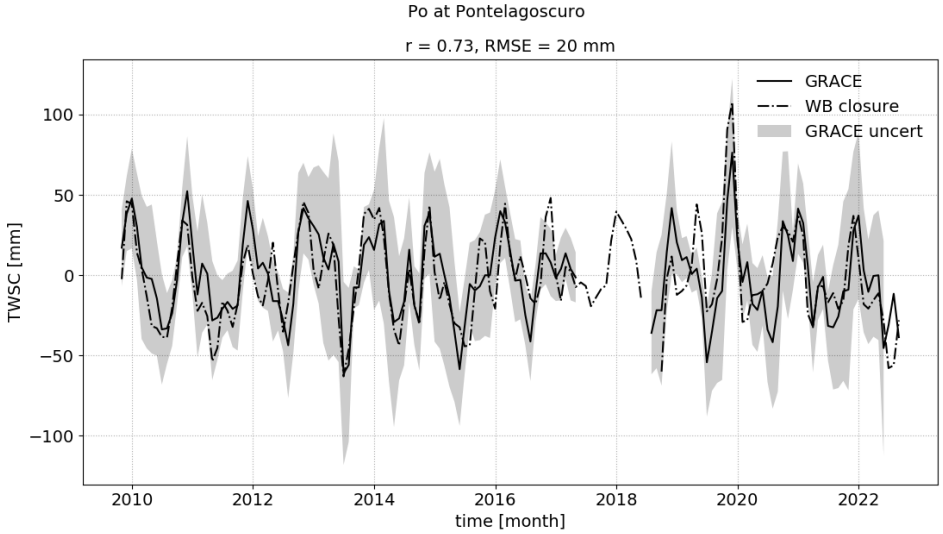

Figure 2.9: Comparison between monthly Terrestrial Water Storage Changes (TWSC) from GRACE data and observed water balance (WB) data for the outlet of the Po river basin. The gray shading corresponds to uncertainty in GRACE data, following [125, 124].

The study catchments span the variety of climates, land covers, and subsurface properties across Italy and the Po river basin (Figures 2.2, 2.3, and 2.5). Furthermore, different hydroclimatological regimes and streamflow generating mechanisms characterize the study catchments, for instance in terms of Asynchronicity Index (ASI) [126], Baseflow Index (BFI), and snow contribution to Q. ASI is a seasonality index with respect to P and ET [126], with 0.36 as the lower threshold to define a Mediterranean climate, that is a P regime highly seasonal and out-of-phase with ET. The ASI shows a clear latitudinal pattern across the study catchments (Figure 2.10), with values < 0.36 in the northern and central-eastern parts of Italy, and values > 0.36 in the (Mediterranean) southern Po river basin, central-western and southern parts of Italy. The study catchments also exhibit rather different BFI values (Figure 2.11), and so a varying degree of baseflow contribution to Q. BFI is the result of geology and climate in the area (Figures 2.5, and 2.10), with low BFI (< 0.4) mostly in Mediterranean areas, medium BFI ($0.4 < \text{BFI} < 0.8$) in non-Mediterranean areas, and high BFI (> 0.8) for carbonate aquifers. Finally, the mean snow contribution to Q is rather variable across the study catchments and exceeds 60% for some alpine catchments [127] (Figure 2.12).

As a consequence, the study catchments show a transition from Mediterranean to Alpine hydroclimates (Figure 2.13). Mediterranean (or rainfall-dominated) catchments exhibit erratic P and Q peaks shortly after rainfall events, mostly during autumn and winter, and a dry summer when ET is the dominant hydrological flux (Figure 2.13a and b). Alpine (or snow-dominated) catchments show an almost year-round P distribution and annual maximum Q in summer, because of snowmelt and rainfall events, in-phase with ET (Figure 2.13c and d).

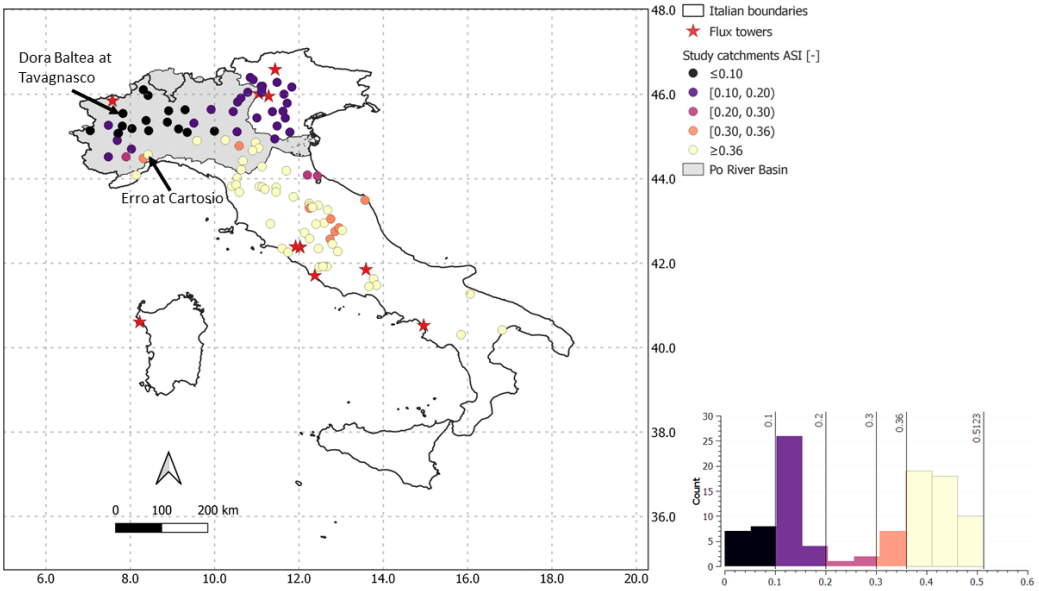

Figure 2.10: Same as Figure 2.1, but for Asynchronicity Index (ASI).

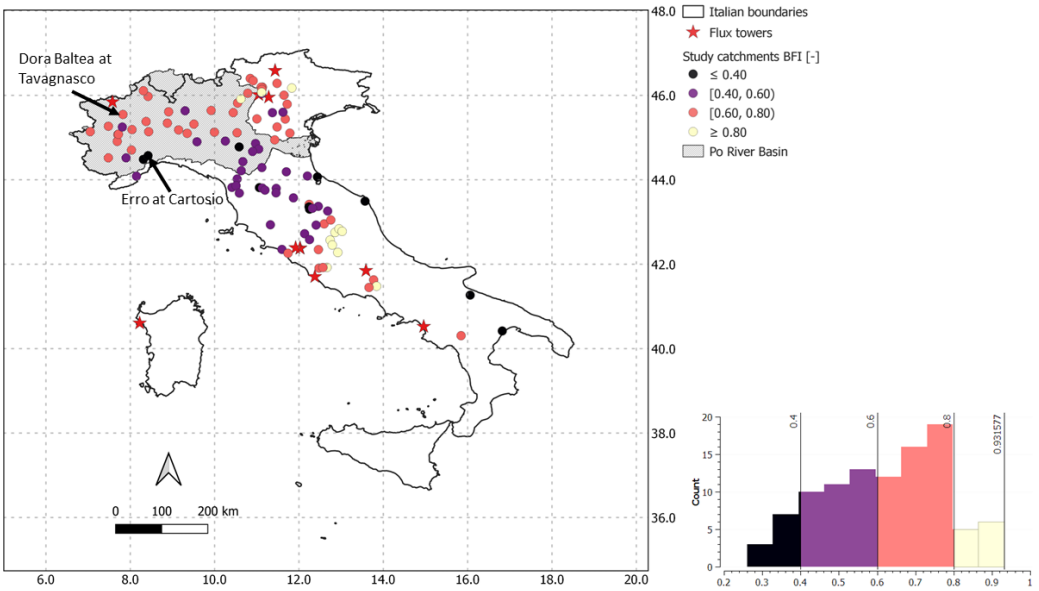

Figure 2.11: Same as Figure 2.2, but for Baseflow Index (BFI).

2.3 Drought characterization

The study region experienced three major droughts during the study period, in 2012, 2017, and 2022 (ongoing), as emerging from [128, 129], reports [130, 131, 132], and indices I computed.

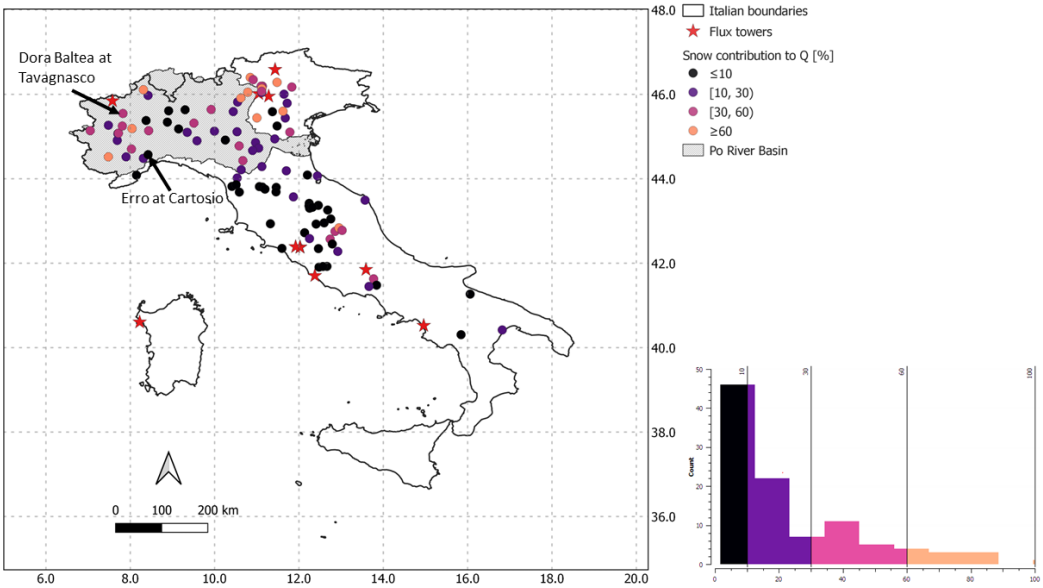

Figure 2.12: Same as Figure 2.1, but for the mean annual ratio [%] between peak Snow Water Equivalent and streamflow (Q) as a measure for snow contribution to Q, from [127].

For a brief characterization of drought events over the study area and period, I identified main drought events for the 38 study sub-catchments in the Po river basin, for which I collected data up to August 2022. For this purpose, I considered the Standardized Precipitation Index [78] with a 12-month aggregation period (SPI12) and the Standardized Streamflow Index [80] with a 1-month aggregation period (SSI1). SPI is strictly speaking a meteorological drought indicator, since it relies on P data only, but it is often used as a hydrological drought indicator with a 12-month aggregation period, as this time scale allows to detect P deficits long enough to generate hydrological droughts [133, 134]. On the other hand, SSI is a purely streamflow drought indicator. [76] proposed to correlate the SSI1 and SPI with various aggregation periods to study drought propagation over a region. This allows to find the most suitable aggregation period to use SPI as a proxy for streamflow droughts. To compute the indices, I used catchment-average monthly cumulative P data from the MCM algorithm [117] (Section 2.2.1) over the period January 2002-August 2022 and monthly mean Q (Section 2.2.2) over the period September 2004-August 2022. Further, I followed [135, 136] for the selection of the probability distribution to fit the data, and I used for both indices a loglogistic distribution.

Both SPI12 and SSI1 showed negative values, i.e., drought conditions, in 2012 (mean SPI12 = -0.56$\pm$0.12 and mean SSI1 = -0.31$\pm$0.21 across the study sub-catchments), 2017 (mean SPI12 = -0.33$\pm$0.11 and mean SSI1 = -0.4$\pm$0.19), and 2022 (mean SPI12 = -0.83$\pm$0.18 and mean SSI1 = -1.16$\pm$0.21), although some differences emerged among the indices and the three events (Figures 2.14 and 2.15). In terms of SPI12, the 2012 drought developed at the beginning of the hydrological year (h.y), and lasted for the whole h.y. for most of the study catchments (Figure

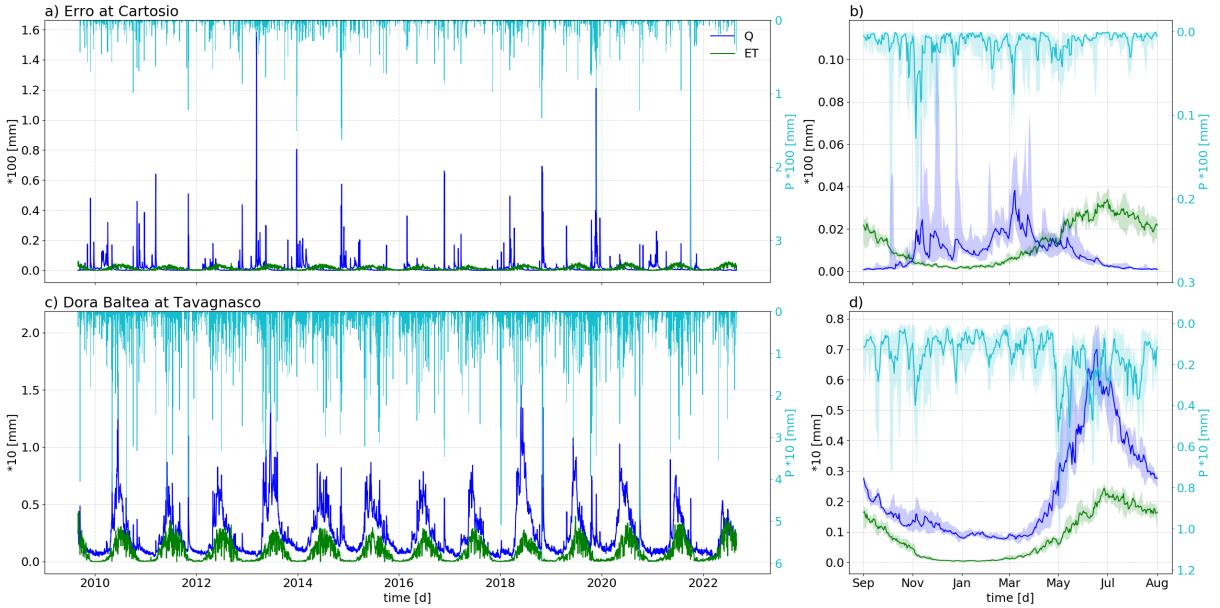

Figure 2.13: Daily time series and climatology of catchment-average precipitation (P), evapotranspiration (ET), and streamflow (Q) for two contrasting example catchments: in (a and b) the Mediterranan Erro at Cartosio with low contribution of storage to Q, while in (c and d) the Alpine Dora Baltea at Tavagnasco with high contribution of storage to Q. In (b and d) the thick lines refer to daily medians and the shading to the interquartile ranges over the study period (2010-2022).

2.14). The 2017 drought followed an already dry year, affected particularly the eastern part of the Po river basin, and lasted over the following year in some cases. Finally, the 2022 drought developed already in 2021 in the western part of the basin, during summer affected most of the basin, and was the most severe drought over the study period for most sub-catchments. The SSI1 showed higher variability in space and time than the SPI12 (Figure 2.15). However, it revealed similar patterns to the SPI12 with severe dry spells in 2012, dry conditions throughout the whole 2017 for the eastern parts of the basin, and throughout the 2022 for most sub-catchments.

The differences between the SPI12 and the SSI1 can be due to several factors, such as local processes, the aggregation period, and the relatively short standardization period. An in-depth analysis would be required to identify the most suitable aggregation periods to analyze streamflow droughts over the study region [76], which was out of the scope of this drought characterization. Furthermore, longer record length would allow to estimate drought indices more robustly and for this reason I used alternative data/methods to identify droughts with hydrological impacts in the following (Sections 3.2.2.3 and 4.2.4.1). However, I concluded that (i) the dataset I collected and analyzed in the thesis was coherent with literature and reports in depicting droughts with hydrological impacts over the study period and area, and (ii) the SPI12 could properly detect them.

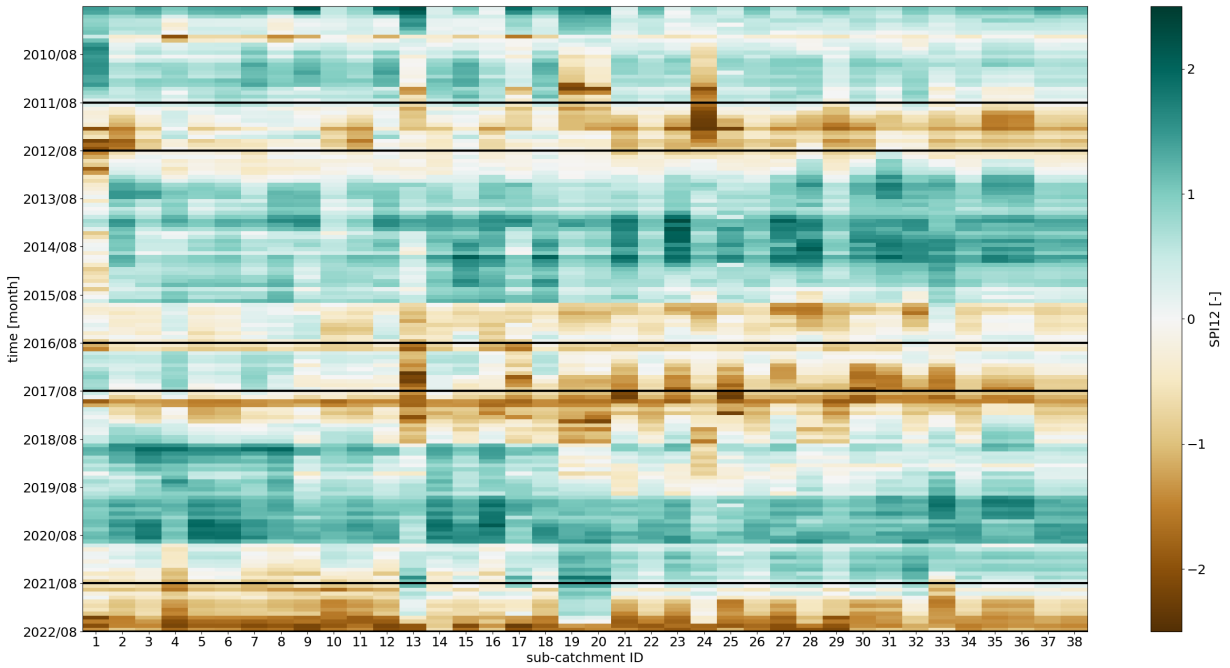

Figure 2.14: Monthly Standardized Precipitation Index with a 12-month aggregation period (SPI12) for study sub-catchments in the Po river basin (Table I.1) over the period h.y. 2010-2022. Catchments are ordered west-to-east according to their outlet. Black edges denote major drought years.

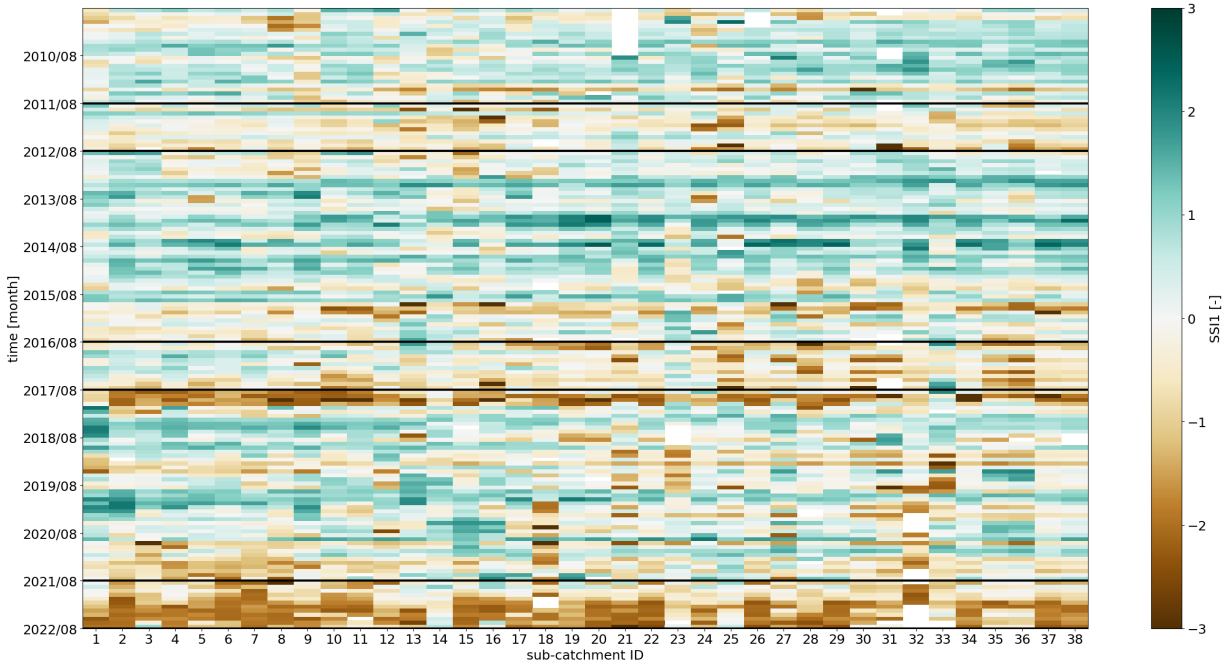

Figure 2.15: Monthly Standardized Streamflow Index with a 1-month aggregation period (SSI1) for study sub-catchments in the Po river basin (Table I.1) over the period h.y. 2010-2022. Catchments are ordered west-to-east according to their outlet. Black edges denote major drought years.

Chapter 3

Disentangling the role of subsurface storage in the propagation of drought through the hydrological cycle[1]

3.1 Introduction

Drought is among the most impactful natural hazards in term of affected people all over the world [43] and has severe and intertwined impacts on environmental, economical, and social aspects, such as terrestrial and freshwater ecosystems, agriculture, water supply, human health, and social stability [137]. Furthermore, drought hazard is expected to increase in frequency, magnitude, and duration in the near future due to climate change [47, 53, 46].

Drought starts from a deficit in precipitation - P -, possibly in combination with an increase in temperature (meteorological drought); a meteorological drought then propagates through the hydrological cycle to generate soil moisture deficits (soil moisture or agricultural drought), as well as discharge - Q - and groundwater deficits (hydrological drought) [17]. Here we use the term hydrological drought to refer to discharge deficits. The process leading from meteorological to hydrological drought, which is known as drought propagation, is governed by local climatic and topographic features [22], along with human influences [23, 138]. Hydrological drought is generally attenuated compared to the corresponding meterological drought [88] by land surface processes, i.e., actual evapotranspiration - ET - and catchment storage. However, prolonged

[1]This chapter is adapted from G. Bruno, F. Avanzi, S. Gabellani, L. Ferraris, E. Cremonese, M. Galvagno, and C. Massari, Disentangling the role of subsurface storage in the propagation of drought through the hydrological cycle, Advances in Water Resources (2022) 104305, https://doi.org/10.1016/j.advwatres.2022.104305

dry periods can also lead to an intensification of hydrological drought [11, 134, 139, 13, 12, 140, 141]. Also the period required to recover from deficit conditions (drought recovery) may vary across the different components of the hydrological cycle [18], and it is also affected by catchment properties [19] and human factors [20, 142]. Thus, quantifying water availability in each hydrological compartment during and after dry periods still remains challenging because of several factors involved in drought propagation and recovery, but it is essential to properly inform water managers.

A growing number of papers studied drought propagation (e.g., [88, 143, 144]) and recovery (e.g., [145]), as well as the influence of climatic [133] and catchment properties [22, 76, 146, 19, 147] on them. Previous works mostly used the threshold level method [22, 146, 19, 147] or standardized indices [76, 133] to identify meteorological and hydrological droughts, and to characterize them in term of drought characteristics (severity and duration). More importantly, they used catchment properties and hydrological signatures to represent the land surface processes involved in drought propagation. For instance, Van Loon and Laaha [22] studied how various physiographic catchment properties control hydrological drought characteristics for 44 Austrian catchments and they found that catchment storage, represented by the Base Flow Index (BFI), affects hydrological drought duration. Further, [76] analyzed drought propagation for 121 catchments in UK, showing that catchment properties related to storage, such as the BFI, the percentage of productive aquifer in the catchment, and the soil wetness, control hydrological drought characteristics, as well as its delay with respect to the meteorological drought.

However, few studies focused on explicitly quantifying each hydrological flux and storage to provide mechanistic understanding of hydrological processes during drought propagation and recovery [3, 60, 6]. [3] showed that ET aggravated soil moisture deficits during the 2003 European summer drought across a set of experimental catchments, while [6] found that subsurface storage sustained Q in an experimental Scottish catchment during the Northern European 2018 drought and the following recovery. Both the processes revealed by [3, 6] lead to a net depletion of subsurface storage during drought [148], which in turn can lead to a reduction of available groundwater for human purposes. Thus, we argue here that considering the whole hydrological cycle is necessary to better understand the hydrological processes occurring during drought propagation and recovery, and to quantify water availability in each hydrological compartment during such periods.

To pursue such an approach, we rely on the water balance model (Equation 3.1) following [60].

$$P = Q + ET + \Delta S \tag{3.1}$$

Here we define ΔS as the subsurface storage change (hereafter subsurface storage) in the whole regolith, either in the soil and in the weathered bedrock. Storage changes could also be due to surface water bodies, snowpack, and glaciers within the catchment. Nonetheless, the annual time scale and the selection of suitable catchments (non-glacierized and not regulated by lakes, for instance) allowed us to minimize snow influence and the effects due to glaciers and surface

water bodies. Therefore, at annual time scale positive annual ΔS values represent an inter-annual carryover in the subsurface storage, while negative values an inter-annual drawdown. The assumption that catchments do not show any inter-annual change in subsurface storage may not hold true [149, 150, 151, 152], due to net intercatchment groundwater flow - that can be part of ΔS - or catchment properties such as large depth of soil and heavily weathered bedrock, for which we expect large subsurface storage changes and variability.

Catchment-scale water balance datasets have historically been challenging to collect, especially for comparative studies across a variety of catchments. Ground-based ET and ΔS (soil moisture and groundwater) data are seldom available and mostly limited to small-sized experimental catchments, while total terrestrial water storage estimates from GRACE satellites can be used only for large-sized catchments, due to their coarse spatial resolution [153]. Consequently, systematic large-sample analyses across a wide range of catchments to quantify ΔS contribution to the allocation of P through the hydrological cycle [154, 148] and to drought propagation and recovery are rare, despite few exceptions [91]. In order to fill this gap, here we hypothesized that blending ground-based and remote-sensed data can provide a consistent, large-scale water balance dataset across different climates and landscapes.

Thus, in this work we aimed at answering three research questions: (i) how much is the inter-annual carryover or drawdown in subsurface storage for a large-set of Italian catchments across different hydroclimatic regimes?, (ii) does this subsurface storage carryover or drawdown affect drought propagation?, and (iii) do ΔS, ET, and Q recover over similar time scales after a deficit in P? To answer these questions, we leveraged the dataset we collected to perform a large-sample analysis of each water balance component for 102 Italian catchments over the period 2010 - 2019 and gain insights into the propagation of meteorological drought through the hydrological cycle for annual drought events in the considered decade.

3.2 Material and methods

We chose Italy as study region because it presents a broad variety of climatic and topographic features, as briefly described in [117]. Moreover, it experienced several drought episodes over the recent years [155, 128, 156], such as the 2012 and 2017 events, and thus it is a suitable study region for the objectives of the work.

Here, we selected the period from hydrological year (h.y.) 2010 to h.y. 2019 as study period, and we considered h.y. as the period from September to August [117].

3.2.1 Study catchments

We collected estimates for each water balance component (Equation 3.1), as well as hydro-meteorological data and catchment properties for 102 partly-nested catchments across Italy (Figure 3.1). We carried out catchment delineation using the Shuttle Radar Topographic Mission (SRTM) Digital Elevation Model (DEM) and we used catchment boundaries from it to derive catchment-scale hydro-meteorological data and properties (see Section 3.2.2 for details about each of them). We selected the study catchments according to some criteria to make them suitable for the analysis: (i) catchment area greater than 100 km^2, as the spatial resolution of the selected satellite-derived ET product is around 4 km x 5 km (Section 3.2.2); (ii) annual runoff ratio less than 1.5, as an arbitrarily chosen threshold to guarantee coherence between the P and Q data, but at the same time to allow for possible import from the subsurface storage; (iii) percentage increase in catchment area greater than the 10% between upstream and downstream nested catchments, to avoid clusters of nested catchments [157] that could bias our general results; (iv) relative difference between the catchment area we obtained from SRTM DEM and the one provided by regional hydrometeorological offices - if available - less than 20%, to exclude errors in our catchment delineation [157]; (v) glacier cover, from the RGIv6.0 glacier outlines [158], less than 10% of catchment area to avoid glacierized catchments [12] and effects in the drought propagation owing to glacier contribution to storage [159].

The resulting study catchments (Figure 3.1 and Table B.1) cover different hydro-climatic regimes - as identified by the aridity index (AI) introduced in Section 3.2.2 -, a steep orographic gradient, and include medium-to-large size catchments. Energy-limited catchments ($AI < 1$) are the 24% of study catchments, while very energy-limited catchments ($AI < 0.75$) are the 53% of them. Further, water-limited catchments ($AI > 1$) are the 17% of study catchments, while very water-limited catchments ($AI > 1.25$) are the remaining 6%, these latter mostly in the central and southern regions of Italy. Catchment elevation has a mean (min/max) value of 1076 (143/2487) m a.s.l., while the mean (min/max) catchment area is 3631 (105/68619) km^2. Moreover, the study catchments are characterized by different dominant soil type, land cover, and geological classes (Table B.1).

3.2.2 Data

3.2.2.1 Water balance dataset

To perform a large-sample analysis across different hydroclimatic regimes, we collected data from multiple sources to close the annual water balance by blending ground-based measurements and remote sensing. We further collected alternative estimates of P and ET, as detailed in the following paragraphs and Table 3.1, for a multi-dataset comparison to verify the consistency of the water balance dataset.

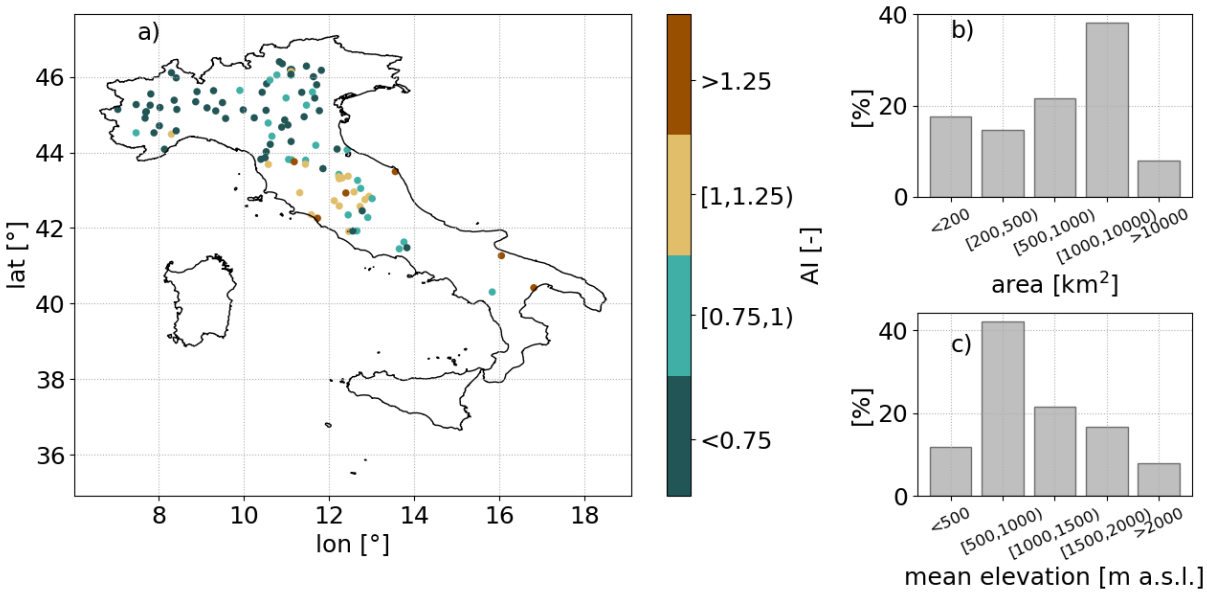

Figure 3.1: Location of the closure section and properties for the study catchments: (a) aridity index, AI for each catchment; (b) frequency distribution of catchment area; (c) frequency distribution of catchment mean elevation.

Table 3.1: Overview of the datasets used in the study

Variable	Dataset	Purpose
T	DPC [117]	PET estimation
P	DPC [117]	Water balance analysis
Q	DPC [117]	Water balance analysis
ET	LSASAF (METv2) [122, 123][1]	Water balance analysis
P	BIGBANGv4.0 [118, 119, 120][2]	Multi-dataset comparison and SPI calculation
ET	BIGBANGv4.0 [118, 119, 120][3]	Multi-dataset comparison
ET	FLUXNET2015 [160][4]	Multi-dataset comparison
ET	GLEAMv3.3a [161]	Multi-dataset comparison
Digital Elevation Model	STRM DEM	Catchment characterization
Glacier outlines	RGIv6.0 [158]	Catchment characterization
Land cover	Corine Land Cover 2018[5]	Catchment characterization
Soil properties	European Soil Database Derived data [115, 116]	Catchment characterization
Geological properties	ISPRA hydro-geological complexes[6]	Catchment characterization

We derived daily catchment-average precipitation from ground-based P data from the Italian regional hydrometeorological offices and the Italian Civil Protection Department (in the following, DPC dataset) [117]. Additionally, we used monthly catchment-average P data from the BIGBANGv4.0 dataset [118, 119, 120]. BIGBANG is a national-scale gridded water balance model, relying on ground-based P and temperature (T) data and parsimonious formulations. It provides estimates of each water balance component (precipitation, actual evapotranspiration, surface flow, change in soil storage, groundwater recharge) along with potential evapotranspiration (PET), at monthly and 1 km resolutions for the Italian territory over the period 1951 - 2019 [118, 119, 120]. We used BIGBANG P data for comparison with P estimates from the DPC dataset and for the calculation of the Standardized Precipitation Index (Section 3.2.2.3) [78], due to its long temporal availability.

For discharge, we relied on data from the DPC dataset [117] and the Italian regional hydrometeorological offices. We further applied some quality checks to the Q dataset to identify and remove possible outliers: (i) a Hampel filter [162], which compares each value with statistics from a surrounding window, and (ii) a filter similar to the one used in [163], comparing each value with statistics for that day of the year over the entire series. The first filter allowed us to detect individual suspicious values, due to temporary malfunctioning in the measurement instrumentation for instance, while the second one enabled us to identify consecutive values outside the climatology for that period of the year, e.g. due to prolonged instrumentation malfunctioning. Thus, we obtained a quality-checked daily mean Q dataset for 102 catchments across Italy (see Figure D.1 for ax example of filtered data). We further underline that Q data for some catchments may be influenced by human activities (e.g., reservoirs and irrigation), but the aim of this study is a large-sample analysis for which a certain degree of anthropogenic influence can be accepted [164] (see Section 3.4.2 for further discussion).

We derived ET maps for the study region from the already validated METv2 product by the Land Surface Analysis of the EUMETSAT Satellite Application Facility (hereafter, LSASAF product) [122, 123]. The LSASAF product provides sub-daily ET estimates at a spatial resolution of 3.1 km x 3.1 km at the nadir (around 4 km x 5 km over Europe), by resolving the surface energy balance from satellite-derived data of radiative forcings, land cover, biophysical parameters, and soil moisture status, along with ancillary meteorological data. Previous works validated it against

[1] `https://landsaf.ipma.pt/en/products/evapotranspiration-energy-flxs/met/` (last access on 24 September 2020)

[2] `https://groupware.sinanet.isprambiente.it/bigbang-data/library/bigbang40/grids` (last access on 27 April 2022)

[3] `https://groupware.sinanet.isprambiente.it/bigbang-data/library/bigbang40/grids` (last access on 27 April 2022)

[4] `https://fluxnet.org/data/fluxnet2015-dataset/` (last access on 20 April 2020)

[5] `https://land.copernicus.eu/pan-european/corine-land-cover/clc2018` (last access on 22 November 2020)

[6] `http://www.sinanet.isprambiente.it/it/sia-ispra/download-mais/complessi-idrogeologici/view` (last access on 02 August 2021)

ground-based flux towers data across Europe [165, 166] and also compared it to the MODIS ET product [165]. Furthermore, it has been used for agricultural drought monitoring [167] and as benchmark for ET simulated by hydrological modelling in European regions [149]. To further verify the reliability of the LSASAF product over the study area and period, we compared ET data at point level against eddy covariance flux tower ET data from the FLUXNET2015 dataset [160]. The FLUXNET2015 dataset collects data from flux tower sites across the globe at a half-hourly time resolution, up to December 2014. For the comparison, we selected the sites with more than 80% of data over the comparison period. We also compared the LSASAF product at catchment-scale against two additional gridded ET products, GLEAMv3.3a and the BIGBANG dataset. GLEAM provides global ET and PET estimates at daily temporal resolution and 0.25° spatial resolution from a physically-based land-surface model and satellite-based data [161, 168].

We assessed ΔS as annual residual from P, Q, and ET data accumulated over the h.y., according to Equation 3.1. For comparison, we also derived catchment-scale ΔS estimates using P and ET from the BIGBANG dataset, and the Q data described above. In Section 3.4.2, we provide a discussion of uncertainties in the data used to close the annual water balance and therefore in ΔS assessment. Moreover, we performed a correlation analysis (Pearson correlation coefficients, r and significance level equal to 0.05) between annual ΔS statistics (mean and standard deviation over the study period) and catchment properties (Section 3.2.2.2) to test if ΔS variability among the study catchments can be explained by such factors.

3.2.2.2 Catchment characteristics

To study drought propagation across multiple climatic and morphologic features, we compiled a set of catchment properties to characterize the study catchments in terms of climatic, topographic, land use, pedological, and geological properties.

For climate characterization, we firstly evaluated catchment-average PET through the temperature-based Hamon method [169] and ground-based T data from the DPC dataset [117]. The Hamon method is based on temperature data only, but we preferred it to alternative formulations considering also radiation and other meteorological variables in order not to propagate uncertainties related to the spatial interpolation of sparse data as meteorological data can be at a large scale. Further, in this study PET was only used for climate characterization of the study catchments and the drought events, while actual evapotranspiration estimates from the LSASAF product were exploited to study drought evolution across the water balance components. We indeed used PET data to derive the aridity index (AI, Equation 3.2 [140]) and so, to characterize the hydro-climatic regime of each catchment (water-limited if AI < 1 or energy-limited if AI > 1).

$$AI = \frac{PET}{P - \Delta S} \tag{3.2}$$

Moreover, we estimated the Asynchronicity Index (ASI) between P and PET [126] (Equations A.1 to A.7) as a seasonality index and as an indicator of dry catchments. ASI is an information

theory-based and non-parametric index that quantifies the difference in relative magnitude and phase between the P and PET signals [126]. ASI varies between 0 and 1, and values greater than 0.36 represent Mediterranean regions with de-synchronized annual cycles of P and PET, both in term of relative magnitude and phase shift [126]. We chose this metric instead of other seasonality indices as it does not require the sinusoidaility assumption for P, which could not hold true for study catchments in the alpine region [170].

As topographic properties, we computed catchment area, and mean catchment latitude and elevation from the SRTM DEM. We also estimated the dominant land cover class and the percentage of urban, crop, shrub, forest, grass, bare soil, and water bodies from the Corine Land Cover 2018. Additionally, we derived the dominant subsoil and topsoil texture, and the catchment-average percentage of silt, sand, clay, organic carbon, and gravel from the European Soil Database Derived data product [115, 116]. We then retrieved the dominant geological class and the percentage of carbonate aquifers, as a proxy for karstic systems in the catchment [150], from a national-scale map of hydro-geological complexes.

Finally, we quantified the BFI and the recession coefficient using [171] which are often used as indicators for catchment memory and groundwater contribution to the discharge [22, 172], as well as the discharge sensitivity to storage as the ratio between the standard deviations of baseflow and hydraulic storage [146]. To derive baseflow, we used the standard method proposed by [173] for baseflow separation, basing on a three-passes digital recursive filter applied to the daily Q data. Furthermore, we computed hydraulic storage via recession analysis following [174] and [151], from daily Q and ET data.

3.2.2.3 Drought propagation analysis

We based our analysis of drought propagation on two steps: (i) drought identification and (ii) drought characterization, as depicted in Figure 3.2.

Firstly, for each catchment we identified the drought years for the following analysis (drought identification, Figure 3.2a). For this purpose, we computed the Standardized Precipitation Index (SPI) [78], based on monthly catchment-average P data over the period 1951 - 2019 from the BIGBANG P product. SPI is a widely used drought index which only needs long-term ($>$ 30 years) monthly P data and provides the probability of a given P anomaly, as deviation from the long-term mean [78]. In the SPI calculation, historical monthly P data are accumulated over different time scales of interest for drought monitoring (usually from 1 to 48 months) and a parametric statistical distribution is fitted to them; the probabilities obtained from the distribution are then transformed into a normal distribution with mean equal to 0 and standard deviation equal to 1 [78]. A drought event is defined as a period with SPI values less than -1 and identified by the first and the last time steps with consecutive negative values [78]. Here we chose an accumulation period of 12 months for the SPI calculation (hereafter SPI12), as we focused on the propagation from meteorological to hydrological drought and SPI12 allows the detection of

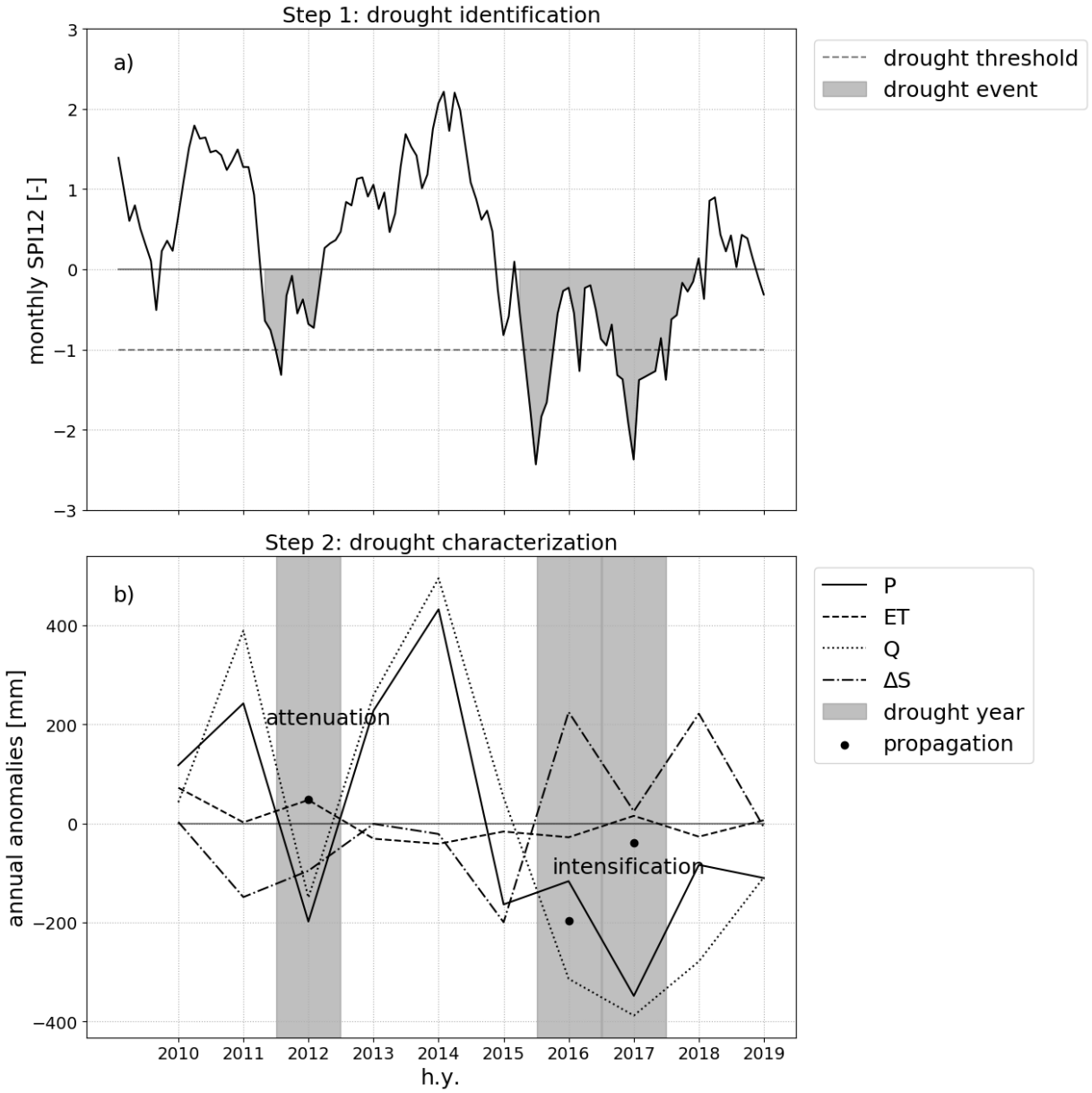

Figure 3.2: Illustration of working steps for drought propagation analysis: 1) calculation of the monthly Standardized Precipitation Index with an accumulation period of 12 months (SPI12) for drought identification (a); 2) computation of annual anomalies in precipitation (P), actual evapotranspiration (ET), discharge (Q), and subsurface storage (ΔS) and quantification of drought propagation as difference between Q and P anomalies for drought characterization (b).

long periods of P deficit that could lead to hydrological drought [133, 134, 139]. Following [135], we hypothesized a number of candidate distributions for the SPI12 calculation and verified the normality for the resulting values through a Shapiro-Wilk test (p-value < 0.05). Thus, we used the Gamma distribution as the one from which we obtained the lower Shapiro-Wilk rejection frequency across the study catchments (Table C.1). We considered hydrological years as drought years if two criteria were met: (i) SPI12 of the last month of the h.y. following a drought event as defined above and (ii) negative P annual anomaly, as defined later, according to the P data from the DPC dataset. The latter criteria allowed us to verify the consistency between the two P datasets used in the study (i.e., the DPC dataset for the analyses and the BIGBANG dataset for drought identification).

Secondly, we characterized drought years in terms of drought severity and attenuation or intensification of the hydrological drought (drought characterization, Figure 3.2b). Thus, we computed P, Q, ET, and ΔS annual anomalies, as departure from mean annual values. Throughout the study, we considered P anomaly as a metric for the severity of the meteorological drought, while Q anomaly for the severity of the hydrological one. Further, we defined a drought propagation measure, as the difference between Q and P annual anomalies, similarly to [12]. A positive drought propagation value stands for an attenuation of the hydrological drought compared to the meteorological, while a negative drought propagation value for an intensification.

3.3 Results

3.3.1 Annual water balance components

Catchment-average mean annual P ranges from 717 mm to 1764 mm and annual P standard deviation from 60 mm to 353 mm. Their variability across the study area reflects climate and orography (Figure 3.3a). For instance, some energy-limited catchments at around 44° latitude - corresponding to catchments along the northern-western coast of Italy in the upper Tuscany region - are characterized by higher annual P amounts than the surrounding energy-limited catchments, due to the complex orography in that area [170].

Catchment-average mean annual ET spans from 206 mm to 637 mm (Figure 3.3b) and annual ET standard deviation from 16 mm to 90 mm. ET shows higher mean values and inter-annual variability in the water-limited central and southern catchments than in the energy-limited northern catchments. On average mean annual ET consists in 41% of P across the study catchments (17% - 77% of P, as minimum and maximum).

Mean annual Q varies from 74 mm to 1503 mm and annual Q standard deviation from 23 mm to 428 mm (Figure 3.3c). Q has a contrasting behaviour compared to ET, with higher mean annual values and inter-annual variability in the northern energy-limited catchments. Mean annual Q

average contribution to P across the study catchments is 48%.

The mean annual ΔS ranges from -534 mm to 747 mm (Figure 3.3d) and annual ΔS standard deviation from 52 mm to 274 mm. Mean annual ΔS thus is on average (min/max) 11% (-41% - 50%) of the corresponding P across all catchments (Figure 3.4). Furthermore, the maximum standard deviation of annual ΔS corresponds to 24% of P, while maximum standard deviations of annual ET and Q are 20% of P and 23% of P. Thus, ΔS shows a slightly higher variability than the other water balance components, when compared to P.

The correlation analysis between ΔS statistics over the study period and possible predictors revealed that catchment properties can partly explain the differences in ΔS behaviour across the study catchments (Table 3.2). Catchment properties showing a significant correlation with mean annual ΔS can be thought as predictors for the tendency of the catchment to have an inter-annual subsurface storage carryover or drawdown, whereas the properties showing a significant correlation with the standard deviation of annual ΔS can be predictors for its inter-annual variability. While catchment properties show somewhat low correlations with ΔS statistics ($-0.35 < r < 0.59$), several correlations are consistent with what expected and with previous works (e.g., [149, 150, 151, 152]), as discussed in Section 3.4.1; this increases confidence in our estimates. For example, catchments with a higher percentage of carbonate aquifers and silty soils, and so a higher storage capacity, have higher mean annual ΔS (r = 0.23 and r = 0.18, respectively). Catchments with higher ASI index, and so a marked dry season and a Mediterranean-type climate, have higher mean annual ΔS (r = 0.28) and higher standard deviation of annual ΔS (r = 0.37). Also, the standard deviation of annual ΔS is negatively correlated with catchment mean latitude (r = -0.35) and positively correlated with the percentage of forest, silt, and carbonate aquifers in the catchment (r = 0.33, r = 0.37, and r = 0.59, respectively), along with the recession coefficient we computed from Q data (r = 0.23, not shown in Table 3.2). This suggests that catchments at a higher latitude have a smaller variability in inter-annual ΔS, while catchments with a higher percentage of forests and silty soils, a drier climate, a higher percentage of carbonate aquifers, and a higher groundwater contribution to the discharge have a higher variability of ΔS.

Table 3.2: Pearson correlation coefficients between change in subsurface storage (ΔS) statistics (mean and standard deviation) and catchment properties (mean catchment latitude, mean catchment elevation, catchment area, percentage of shrub in the catchment, percentage of forest in the catchment, percentage of bare soil in the catchment, percentage of silty soil in the catchment, percentage of carbonate aquifer in the catchment, Asynchronicity Index). Sources and details about each property are provided in Section 3.2.2.2. Significant coefficients (p-value < 0.05) are reported in bold.

	Lat	Elev	Area	Shrub	Forest	Bare	Silt	Carbonate	ASI
mean annual ΔS	-0.18	**-0.2**	-0.12	**-0.31**	0.13	**-0.21**	0.18	**0.23**	**0.28**
std annual ΔS	**-0.35**	-0.19	**-0.3**	-0.16	**0.33**	**-0.27**	**0.37**	**0.59**	**0.37**

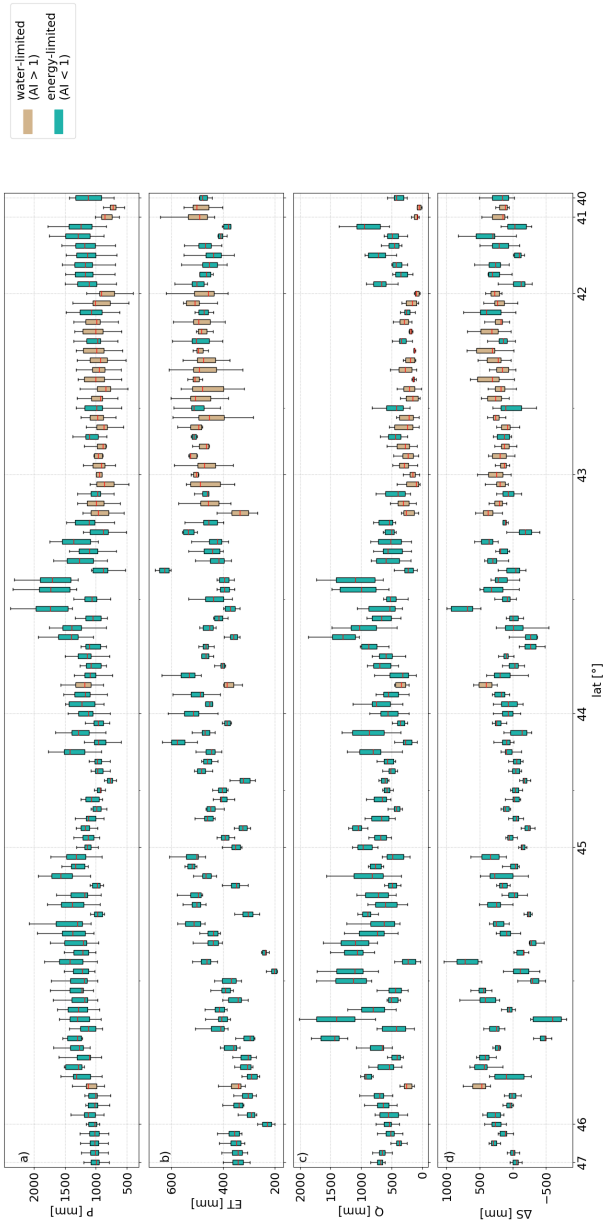

Figure 3.3: Boxplot of each annual water balance component over the study period for each catchment (north to south ordered, from the left to the right hand side): (a) precipitation, P; (b) actual evapotranspiration, ET; (c) change in subsurface storage, ΔS; (d) discharge, Q. Each boxplot is colour coded according to the catchment aridity index, AI.

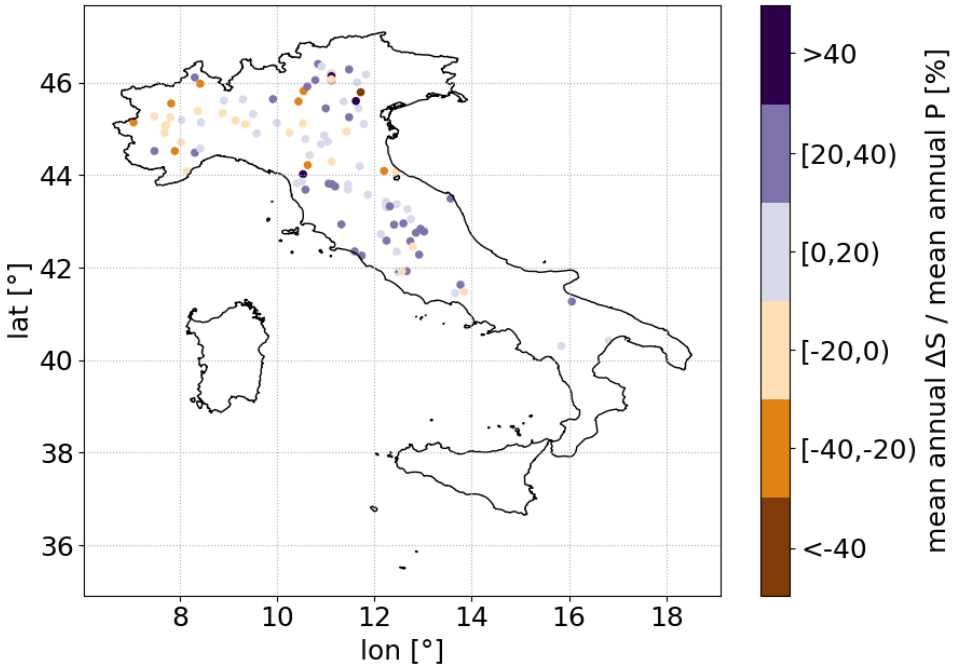

Figure 3.4: Mean annual change in subsurface storage (ΔS) for each study catchment.

3.3.2 Water balance response to drought

During the study period, wet and dry years alternated across Italy: h.y. 2012 and 2017 (2013 and 2014) were dry (wet) periods for the whole study area, according to P anomalies (Figure 3.5a). Several other dry events occurred across the study catchments, but they were geographically less extensive (e.g., during h.y. 2018, northern catchments experienced negative P anomalies, while the central and southern ones had positive P anomalies). According to SPI12, 178 years across 79 catchments were identified as drought years and major drought events in terms of affected catchments were h.y. 2012 and 2017, in agreement with the literature [155, 128, 156] and drought reports [130, 131].

Drought years mostly corresponded to dry-warm periods experiencing concurrent P anomalies and positive PET anomalies (median annual P anomaly equal to -303 mm and median annual PET anomaly equal to 31 mm, Figure 3.5). During such years, annual anomalies of the four water balance components showed contrasting behaviours across the study catchments (Figure 3.5). For both the 2012 and 2017 droughts, ET anomalies were positive for catchments located at latitudes greater than 45° and negative for southern catchments (Figure 3.5b); this spatial pattern could reflect the climate and the dominant land cover type in the catchments, as at latitudes greater than 45° catchments are energy-limited, non-Mediterranean, and coniferous-dominated (Table B.1). ΔS and Q anomalies did not show clear distinction between positive and negative values across different hydro-climatological regions in the study area (Figure 3.5). During

drought years, ΔS anomalies were generally negative (median annual anomaly -77 mm, Figure 3.5i) and Q anomalies were generally attenuated compared to P anomalies (median annual P anomaly equal to -303 mm and Q anomaly equal to -178 mm, Figure 3.5f and Figure 3.5h) across the study catchments.

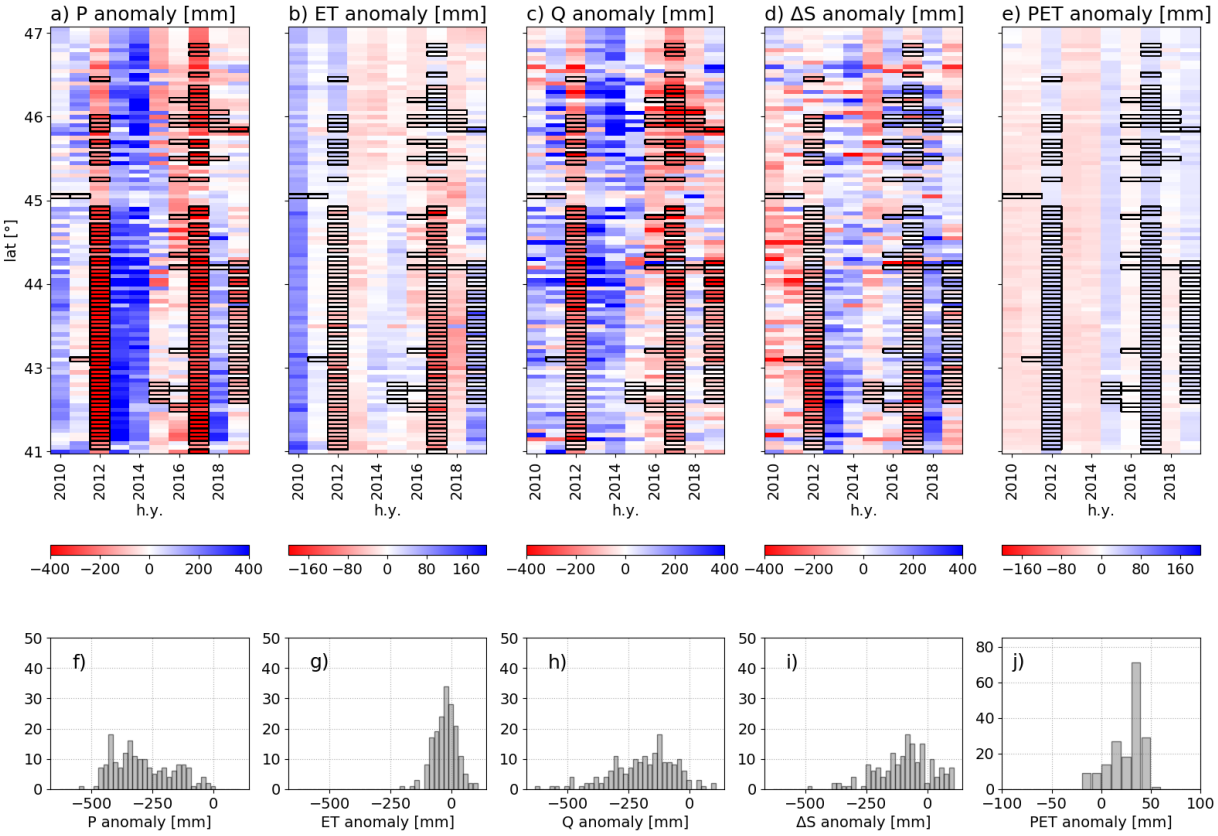

Figure 3.5: Annual anomalies for: (a) precipitation, P; (b) actual evapotranspiration, ET; (c) discharge, Q; (d) change in subsurface storage, ΔS; and (e) potential evapotranspiration, PET over the study period and catchments. Black edges correspond to drought years. Frequency distribution of annual (f) P, (g) ET, (h) Q, (i) ΔS, and (j) PET anomalies during drought years.

Focusing on ET, ΔS, and the drought propagation measure, i.e., the difference between Q and P anomalies, negative ΔS anomalies lead to positive propagation values and thus to an attenuation of the hydrological drought (greyish dots in Figure 3.6a), while positive ΔS anomalies lead to negative propagation values and so to an intesification of the hydrological drought (reddish dots in Figure 3.6a) across the study catchments experiencing drought years over the study period. On the contrary, positive and negative ET anomalies lead to both an attenuation or an intensification of the hydrological drought (Figure 3.6a). Thus, ΔS emerges as the key driver of drought propagation through the hydrological cycle.

The drought propagation measure showed statistically different (two-sample Kolmogorov-Smirnov

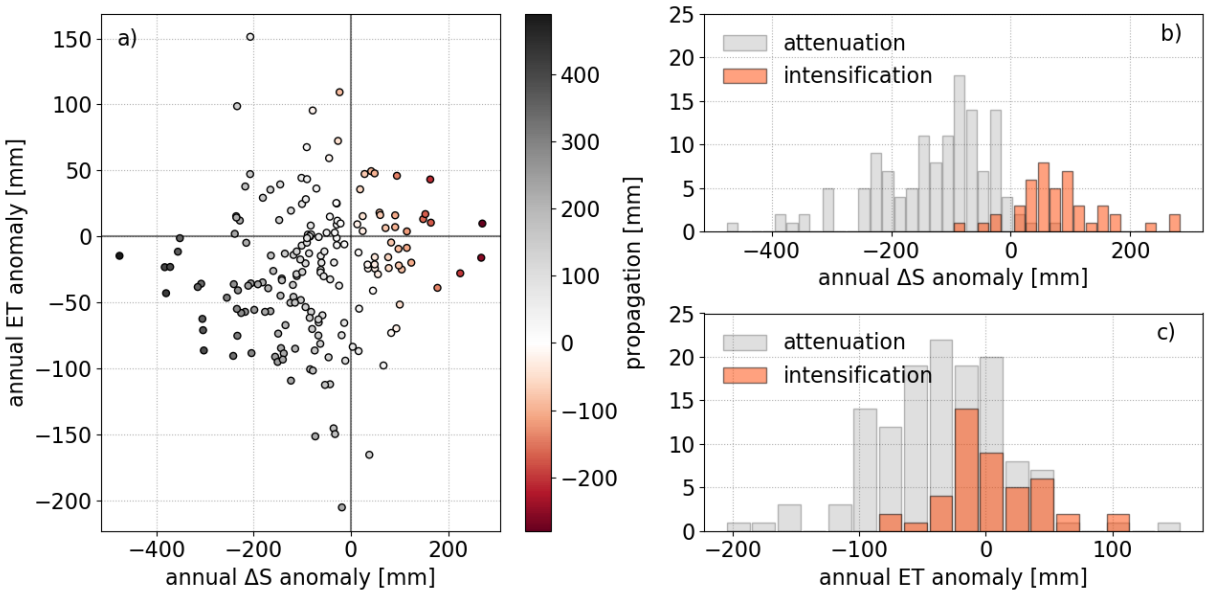

Figure 3.6: (a) Scatterplot between annual subsurface storage, ΔS and evapotranspiration, ET anomalies during drought years; dots are coloured according to the propagation measure (difference between discharge and precipitation anomalies). Catchments attenuating the Q anomaly have greyish colour, while catchments intensifying the Q anomaly reddish. Frequency distributions of annual (b) ΔS and (d) ET anomalies for catchments attenuating (grey) and intensifying the Q anomaly (orange) during drought years.

test, p-value < 0.05) distributions between catchments with contrasting storage-related properties, namely (i) a positive or negative mean annual ΔS (Figure 3.7a) and (ii) a positive or negative annual ΔS in the year preceding the drought (Figure 3.7b). Distributions are partly overlapping, but catchments with a positive mean annual ΔS had a positive median propagation, and so an attenuation of the hydrological drought, whereas catchments with a negative mean annual ΔS had a slightly negative median propagation, i.e., an intensification of the hydrological drought. Similarly, catchments that in the year preceding the drought had a carryover in subsurface storage ($\Delta S > 0$) had a higher median propagation than catchments that had a drawdown ($\Delta S < 0$). Both these findings indicate that catchments replenishing the subsurface storage, as long-term average characteristic or in the year preceding a drought, can attenuate the hydrological drought.

We also investigated the relationship between the tendency of catchments to attenuate or intensify the drought, quantified via the mean propagation measure during drought years, and climatic and morphological properties of the catchments, such as the ASI and the discharge sensitivity to storage (see Section 3.2.2.2 for a description of them). A moderate positive linear correlation was found between mean propagation and ASI (Pearson correlation coefficient, r = 0.43, pvalue < 0.05, Figure 3.8a), while no significant linear correlation was detected between mean propagation and the discharge sensitivity to storage (Figure 3.8b). Also the non-linear correlation

between mean propagation and the discharge sensitivity to storage was sowehow low (Spearman correlation coefficient, ρ = -0.39).

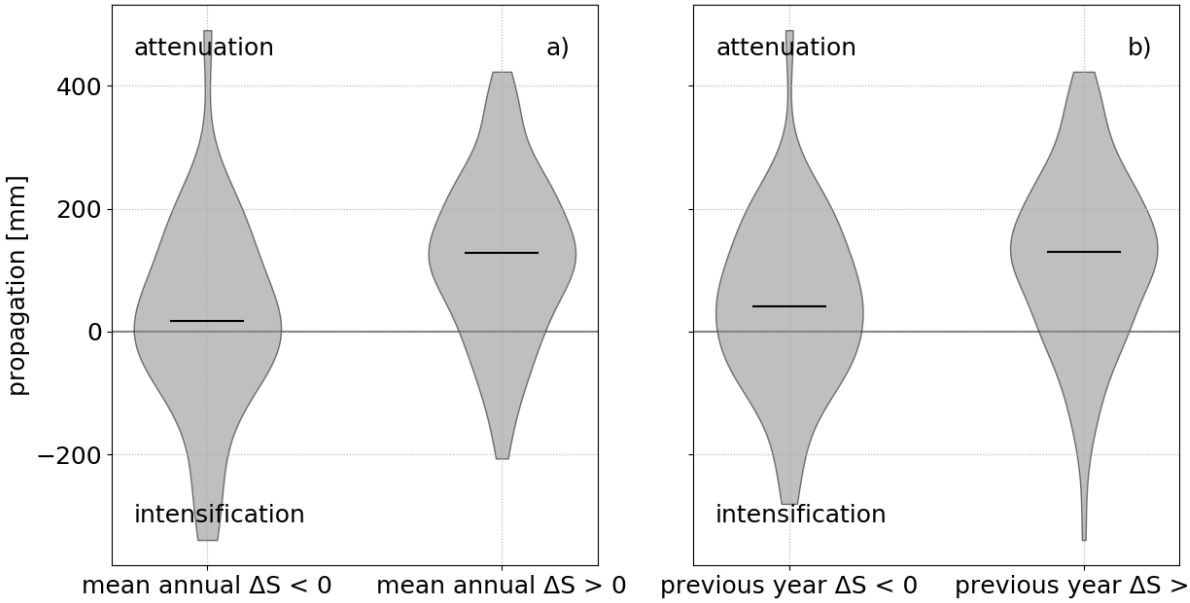

Figure 3.7: Distributions of the propagation measure for: (a) catchments with a positive and negative mean annual change in subsurface storage, ΔS and (b) for catchments with a positive and negative ΔS in the year preceding the drought.

3.3.3 Water balance recovery from drought

The average temporal evolution of P, ET, ΔS, and Q across 55 catchments, which experienced both the 2012 and 2017 droughts, and non-drought conditions in the following h.y., revealed different features in the recovery from drought events for the different water balance components. P, Q, and ΔS had a similar timing, both in wet and dry years, while ET was out-of-phase with the P input (Figure 3.9). Furthermore, the year following a drought event presented an increase in P, Q, and ΔS values, but still low ET values, even decreasing after the 2012 drought for energy-limited catchments. So, ΔS sustains Q not only during drought, but also during the following recovery period. This sustainment is likely more relevant for gaining rivers [175], which are highly dependent on the groundwater storage.

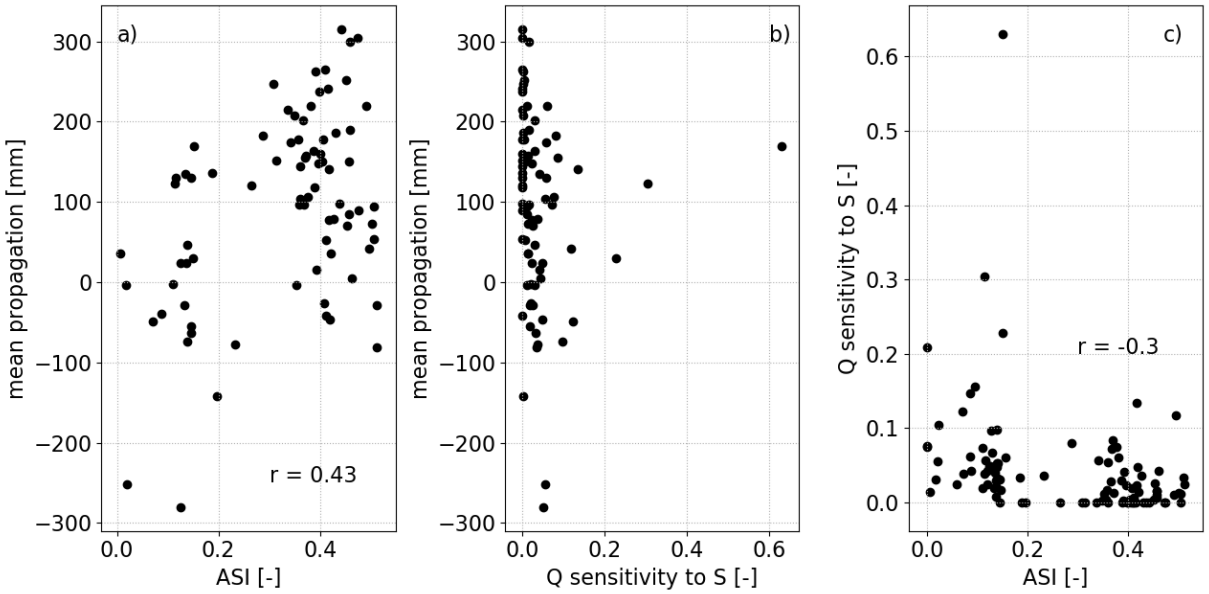

Figure 3.8: Scatterplot between: (a) the Asynchronicity Index (ASI) and mean drought propagation; (b) the discharge (Q) sensitivity to storage (S) and mean drought propagation; (c) the ASI and Q sensitivity to S for each catchment experiencing drought years during the study period.

3.4 Discussion

In this study we closed the annual water balance for 102 catchments across Italy and 10 hydrological years, and we exploited the dataset to perform a large-sample analysis of the response of each water balance component to drought across different hydro-climatological regimes.

3.4.1 Main findings

Quantifying catchment-scale water balance is one of the most recurring open questions in hydrology to assess surface and subsurface water availability for vegetation, river ecosystems, and human supply [176]. Despite advancements in measurement techniques over the last decades, closing the water balance at catchment-scale still remains elusive, mainly because of the paucity of ΔS and ET data, uncertainties in measurements, and spatial heterogeneity within catchments [176]. Today, observatories and experimental catchments provide valuable opportunities to assess temporal and spatial scales for which water balance closure is realistic [148], and remote sensing and hydrological models allow to assess water balance components at large scales, even in data-scarse regions [177].

Assessing water availability across the hydrological compartments during droughts is increasingly important in a warming climate. A water balance perspective can shed light on drought

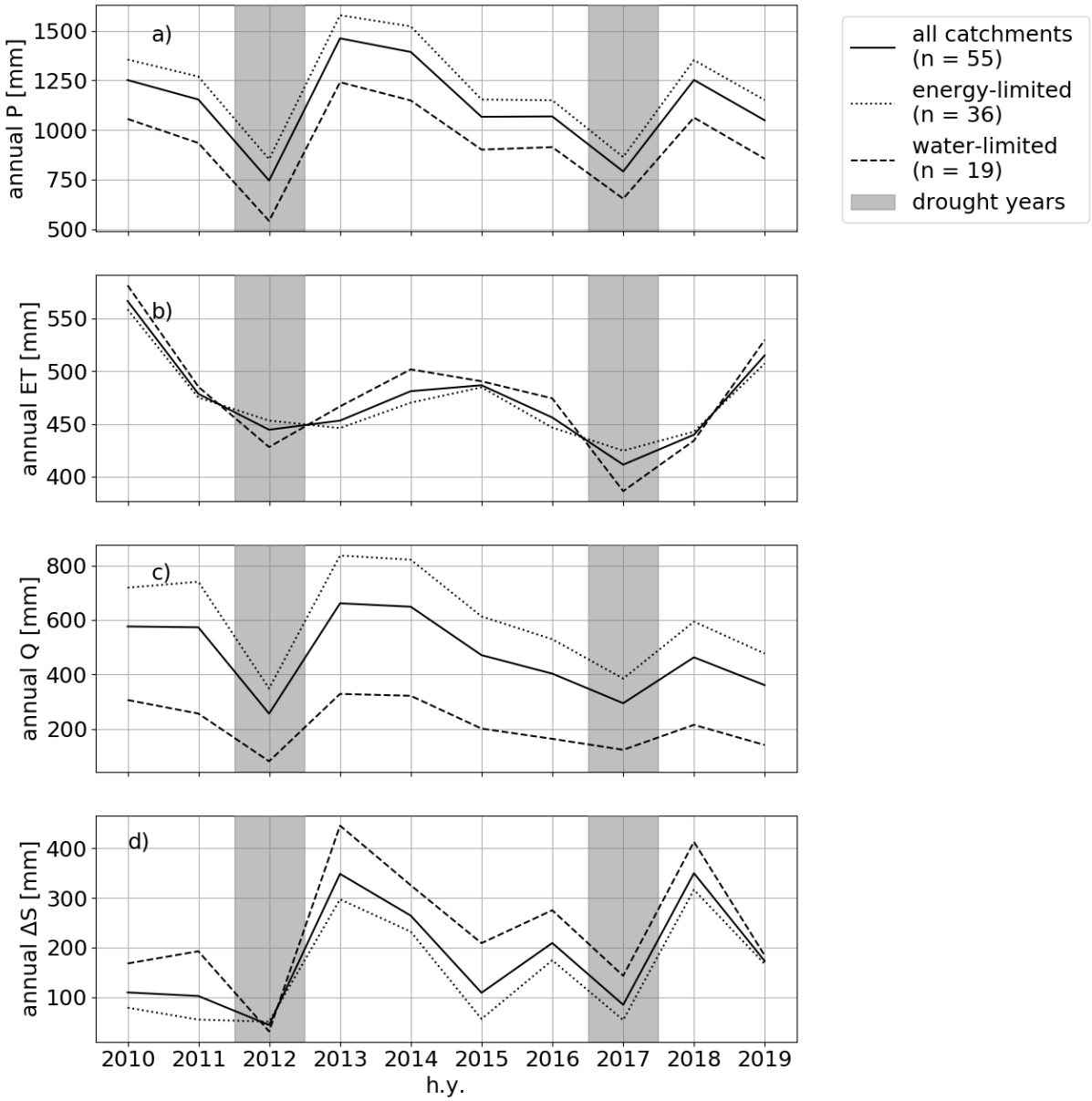

Figure 3.9: Time series of annual (a) precipitation, P, (b) evapotranspiration, ET, (c) change in subsurface storage, ΔS, and (d) discharge, Q averaged across all catchments that experienced both the 2012 and 2017 droughts and non-drought conditions in the post-drought years (solid line, n = 55 catchments), water-limited (dashed line, n = 19 catchments) and energy-limited (dotted line, n = 36 catchments) catchments in the subset.

propagation through the hydrological cycle [3, 60, 91, 6]. Here, we showed that blending ground-based and remote-sensed data can provide a consistent water balance dataset, even at a national

scale, to study drought propagation across different climates and landscapes. In this regard, our main findings were three.

First, we provided further empirical evidence that ΔS contribution to the annual catchment-scale water balance can not be neglected [152]. The average contribution of mean annual ΔS to the long-term water balance is 11% of mean annual P across a large set of temperate catchments (Figure 3.3), coherently with previous results for the study region from different approaches (for example [178] obtained annual ΔS values ranging from -19% to 5% of P for a prealpine Italian catchment through hydrological modelling). We further showed that ΔS contribution can partly be explained by climate and catchment properties, in agreement with previous studies (e.g., [149, 150, 151, 152]). For instance, net intercatchment groundwater flow, which can be part of ΔS, was demonstrated to be more significant in small catchments with productive aquifers, such as karstified rocks, within the Meuse river basin [149], while catchments with an arid climate were found to require a longer time to reach a steady state and thus a neglectable contribution of ΔS in the water balance in a large-sample analysis [152]. We indeed found that mean annual ΔS positively correlates with the percentage of carbonate aquifers in the catchment and the Asynchronicity Index (ASI) between P and PET (Table 3.2). Moreover, the standard deviation of ΔS negatively correlates with catchment area and positively correlates with ASI (Table 3.2). These findings illustrate that catchments with a high percentage of carbonate aquifer and a high ASI (i.e., with a dry and Mediterranean-like climate) have a high mean annual carryover in the subsurface storage (or net groundwater export), while catchments characterized by small area and high ASI have a higher variability in annual ΔS than catchments with large area and low ASI values.

Second, we found that the subsurface storage is the key driver in drought propagation across different climates and landscape features, as already revealed for instance by [22, 76, 146] taking advantange of storage-related catchment properties and by [6] for an experimental small-sized catchment. Across the study catchments, hydrological drought is characterized by concurrent negative P anomalies and positive PET anomalies, as shown for low flows in Switzerland by [179], and generally attenuated compared to the corresponding meteorological drought by land surface processes (ET and ΔS), in agreement with [88] (Figure 3.5). Further, we showed that the storage-ET relationship during droughts is highly complex across a wide range of catchment types (Figure 3.6a), depending on subsurface and vegetation properties [92]. However, we argue that the storage behaviour, rather than that of ET only, drives the attenuation or intensification of Q anomalies compared to the P anomalies. In fact, catchments attenuating the hydrological drought generally experience concurrent negative ΔS anomalies (median ΔS anomaly = -112 mm for catchments attenuating the hydrological drought and = 81 mm for catchments intensifying it, Figure 3.6b), while they can experience both positive and negative ET anomalies (median ΔS anomaly = -27 mm for catchments attenuating the hydrological drought and = 4 mm for catchments intensifying it, Figure 3.6c). We argue that this is due to the different vegetation types in the catchments, their different ecophysiological properties and response to drought [180]. Moreover, we found that catchments with contrasting subsurface storage-related proper-

ties show different behaviours in term of drought propagation (Figure 3.7). This further suggests that catchments characterized by an inter-annual carryover of subsurface storage (as long-term mean or in the year preceding the drought) can attenuate the hydrological drought.

In a modelling experiment across the US [146] found intensity and duration of hydrological droughts to be controlled by climatic properties, as well as the discharge sensitivity to storage, which they quantified from modelled baseflow and deep storage. Here we found that ASI can be thought as a predictor for the tendency of a catchment to attenuate or intensify the hydrological drought, quantified through the mean propagation (Figure 3.8a), while we did not find a significant correlation between discharge sensitivity to storage and mean propagation (Figure 3.8b). The difference we found with respect to [146] may be due to the broader variety of discharge sensitivity to storage values across the catchments analyzed in our study, as a result of the complex interplays among subsurface and climatic properties that determine the discharge sensitivity to storage of a catchment [151] (Figure 3.8c). Furthermore, the quantification of discharge sensitivity to storage from recession data, as done here, relies on the assumption that catchments behave as simple first-order nonlinear dynamical systems [174], which unavoidably may lead to a certain degree of uncertainty across a large-sample of catchments.

Third, we showed that Q recovery from P deficits takes place over similar time scales as ΔS, while ET has a buffered response (Figure 3.9). Large-scale studies found a higher correlation between monthly Q and soil moisture - which is part of ΔS - rather than between other pairs of hydrometeorological variables at a continental and global scale [181, 182], and a delayed response of ET to soil moisture deficits across Europe [91]. Vegetation can have a delayed response to drought [13], because of biochemical and physiological processes [180]. Most of the catchments we considered in the drought recovery analysis is dominated by two land cover types only (broad-leaved forest and crop), therefore we preferred to focus the analysis on water-limited versus energy-limited catchments, rather than on the dominant land cover type. However, different land cover types can be found within the study catchments, due to their generally relatively large scale. Thus, water-limited catchments can be thought as typical of Mediterranean ecosystems, while the energy-limited ones of temperate and mountainous ecosystems (Table B.1), which can have different responses to dry periods because of different water use strategies [180]. We indeed see a slight difference in ET response to drought between water- and energy-limited catchments: water-limited catchments have more pronounced ET variations during and after drought year compared to energy-limited catchments. We further hypothesize that the buffered response of ET to droughts can have more profound impacts on Q deficits in case of prolonged dry periods, and not just annual droughts as those analyzed in this work. Some recent studies showed indeed that ET has a fundamental role in intensifying Q deficits compared to P deficits during multi-year droughts [13, 141].

3.4.2 Data uncertainty

In this paper, we based our analyses on data products rather than on hydrological modelling, as hydrological models can miscapture the water balance during drought [13, 102]. However, ET direct observation is not feasible at large scale and here we relied on an ET model forced by remote-sensed data, the LSASAF product (Section 3.2.2). To verify its suitability across the study region and during drought, we performed a multi-dataset comparison at flux tower- and catchment-scale (see Section 3.2.2 for a description of the ET products used for comparison). Monthly root mean square errors (RMSE) between LSASAF and FLUXNET2015 data over the comparison period (September 2009 - December 2014) are below 30 mm (Figure E.1a) and daily RMSE for the 2012 drought year below 1.5 mm (Figure E.1c) across the selected flux towers, in agreement with previous validation exercises in Europe [165]. Monthly catchment-scale ET data from LSASAF and alternative gridded products are highly correlated, for both the whole comparison period and drought months identified by the SPI12 (r = 0.88 for both the whole period and drought months between LSASAF and GLEAM, r = 0.87 for the whole period, and r = 0.84 for drought months between LSASAF and BIGBANG, Figure E.1b and d). Hence, ET estimates from the selected remote-sensed product can be considered robust across the study catchments, over the whole spectrum of climatic conditions in the study period.

Since we assessed ΔS as annual residual from the water balance model (Equation 3.1), ΔS estimates could reflect uncertainties in P, Q, and ET data [176]. See [176] for a brief review about sources and magnitude of errors in the assessment of water balance components. Yet, we obtained comparable results in term of ΔS estimates using alternative P and ET data from the BIGBANG dataset (r = 0.89, Figure F.1). Moreover, results from the correlation analysis between ΔS and catchment properties agree with previous literature (Section 3.4.1). Therefore, our ΔS estimates can be assumed as consistent and our general findings not dataset-dependent.

3.4.3 Future developments

In this work, we gained a consistent picture of the non-negligible annual change in subsurface storage, the attenuation of hydrological droughts due to subsurface storage depletion, and the similar time scale of discharge and subsurface storage recovery from drought conditions for 102 Italian catchments, regardless of the catchment and climatic properties. However, some study limitations pave the way for future research building on these results.

As a trade-off between data availability and variety in the characteristics of the considered catchments, we based our large-sample analysis on a 10-year time span. A longer record length would be desirable to include in the analysis additional drought events, potentially with different characteristics. Further, it would allow to use alternative methodologies to study drought propagation, as the threshold level method [88] or a standardized approach [76] through the quantification of indices for each hydrological compartment, such as the Standardized Precipitation Evapotran-

spiration Index (SPEI) [79], the Palmer Drought Severity Index (PDSI) [183], the Standardized Streamflow Index (SSI) [80], the Standardized Soil Moisture Index (SSMI) [81], and the Standardized Groundwater Index (SGI) [82].

Moreover, we estimated ΔS as annual water balance closure, whereas long-term soil moisture and groundwater data would allow to directly track storage changes either in the soil and in the aquifers, and thus to investigate their different role in drought evolution [3], as well as to quantify the memory effect in groundwater levels [184] and its relationship with drought propagation [82] in the study region.

Finally, we did not consider anthropogenic activities (e.g., surface- and ground-water abstractions, reservoir infrastructures, land use changes, and water transfers) that may occur in the study catchments and may affect their response to drought [23, 142, 20, 138]. [138] showed that human activities aggravated hydrological drought characteristics compared to natural conditions in 28 human-altered catchments across the world, regardless of the typology and purpose of these activities. Given the consistent variation observed in hydrological drought charactertistics due to various human activities [138], we argue that the neglection of possible anthropogenic disturbances in the study catchments does not affect our findings. However, detailed information about human activities in the study catchments would be beneficial to test for instance if the intensification of the hydrological drought we observed in some catchments can be related to anthropogenic influences, which was beyond the scope of the present work.

3.5 Conclusions

Hydrological drought is shaped by several factors, including the interaction between meteorological drought, i.e., precipitation deficits and possibly increases in temperature and potential evapotranspiration, and land surface processes, e.g., actual evapotranspiration and storage in the soil and weathered bedrock. Nevertheless, systematic data-based analyses of the response of each water balance component (precipitation, discharge, evapotranspiration, and subsurface storage change) to drought across different climates and catchment types are rare. Here, we revealed that such analyses are feasible blending ground-based and remote-sensed data. Specifically, we showed that long-term mean annual subsurface storage change is on average 11% of mean annual precipitation across 102 Italian catchments along a steep climatic and topographic gradient (Figure 3.3). Thus, neglecting subsurface storage change could bias water balance assessments at annual scale. Furthermore, we pointed out that hydrological drought is generally attenuated compared to meteorological drought (Figure 3.5) and this is mainly due to a net depletion of subsurface storage (Figure 3.6 and 3.7) across a large set of catchments with different morphological properties and in different hydroclimatic regimes. Finally, we showed that across the study catchments subsurface storage and discharge have a similar timing in recovery from precipitation deficit, while evapotranspiration has a buffered response to dry periods (Figure

3.9). Our results reveal the usefulness of explicitly considering subsurface storage changes to disentangle hydrological processes during drought and provide opportunities to properly inform water managers about water availability in the different hydrological compartments during such periods.

Chapter 4

Parameter transferability of a distributed hydrological model to droughts[1]

4.1 Introduction

Droughts affect all components of hydrological systems as they propagate from precipitation deficits (meteorological droughts) to streamflow deficits (streamflow droughts [22]). Droughts have severe and multifaceted impacts on the environment, societies, and economies [26] and these impacts will likely increase in a warming climate with an increase in the frequency and severity of streamflow droughts [51]. Therefore, robust modelling of water availability throughout the whole hydrological cycle during droughts is essential to inform water management, disaster risk reduction, and climate change adaptation strategies.

Distributed process-based hydrological models allow spatial estimates of hydrological fluxes and states [64], even at large scales and hyper-resolutions ($<$ 1 km [185]). Climate impact assessments [186, 187, 48], drought monitoring [188, 53, 100] and forecasting systems [189, 190, 191], and drought studies in general [92, 8, 9] widely use these models today. Some studies revealed poor model performances when simulating streamflow droughts [99] and their generating processes [88, 13]. Further, human activities can heavily modify the hydrological cycle [192] and streamflow droughts in particular [138], but their representation in hydrological models remains challenging [73].

More broadly, many hydrological models have decreases in streamflow (Q) performance during

[1]This chapter is adapted from G. Bruno, D. Duethmann, F. Avanzi, L. Alfieri, A. Libertino, and S. Gabellani, Parameter transferability of a distributed hydrological model to droughts, Hydrol. Earth Syst. Sci. Discuss. [preprint], 2022, https://doi.org/10.5194/hess-2022-416, in review

climatic conditions that differ from those during the calibration period [193, 194, 96]. Such issues in the transferability of model parameterizations (hereinafter model transferability) can pose challenges in simulating correctly Q during droughts [97]. While some studies showed the ability of distributed process-based hydrological models in reproducing drought conditions [8], research on model transferability to severe droughts is still limited with specific regard to distributed hydrological models [195].

Previous studies revealed that decreased model performances in Q simulation during severe droughts may be related to poor simulation of actual evapotranspiration (ET, [13]) or Terrestrial Water Storage (TWS, [196, 102]). For instance, [13] showed that a semi-distributed hydrological model had statistically significant decreases in Q and ET simulation during the 2012-2016 drought over a Californian river basin, but not in the simulation of subsurface storage; thus, they argued that the poor representation of ET, and its climate elasticity in particular, drove the deterioration in Q modelling skills. [102] found that in Australian catchments where common lumped conceptual models simulated Q poorly during the Millennium drought, the models also failed in reproducing long-term decline in storage. This indicates that evaluating hydrological models against multiple hydrological fluxes and states represents a way to analyze causes of poor model transferability, evaluate model internal consistency and hence move towards more robust modelling [197]. Especially for distributed models, ET and TWS remote sensing-based products can be particularly useful for model evaluation [104, 68, 105] as they allow to check also their spatial representativeness. Nonetheless, assessment of model transferability to severe droughts using independent and spatially distributed ET and TWS remote sensing-based products is still rare.

Furthermore, some studies suggested that including dry periods in the calibration improves Q simulation during droughts [194, 8], but contrasting results were shown when transferring to severe droughts [13].

To contribute to filling these knowledge gaps, we aimed to answer three research questions: (i) is the Q simulation performance of a distributed hydrological model sensitive to drought severity?; (ii) if so, what are the causes for the expected decrease in Q simulation performance during severe droughts, with regard to ET and TWS?; (iii) does including a moderate drought in the calibration period improve model transferability to severe droughts?

For this purpose, we analysed the performance of the distributed hydrological model Continuum [198] over the Po river basin in northern Italy during the flood- and drought-rich period September 2009–August 2022. We calibrated the model against Q data and evaluated the model capability in reproducing the temporal and spatial variability of Q, ET, and TWS for the whole river basin and 38 sub-catchments in it during wet years and droughts of varying severity, using independent ground- and remote sensing-based datasets as benchmarks.

4.2 Data and methods

4.2.1 Study area

For this study, we selected the Po river basin, as a drought-prone area [199, 129, 200, 2], and major catchment in Italy regarding drainage area (around 74000 km^2) and socio-economic relevance with 27% of Italian population, 35% of agricultural production, and 37% of industrial production [201].

The Po river basin lies in northern Italy and part of the Swiss Canton Ticino region (Figure 4.1). The Alps border the basin in the west and north, and the Apennines in the south, while the Po plain characterize its central part. Consequently, the basin shows a steep orographic gradient and elevations range from sea level to about 4800 m above sea level [114] (Figure 4.1a).

The climate in the region transitions from alpine and cold, with a bimodal annual precipitation cycle and peaks in autumn and spring, to temperate with a dry season and most of the precipitation in winter [112, 170] (Figure 4.1b). Snow contribution to streamflow generation is relevant especially at high elevations in the northern and western part of the catchment, where the mean annual ratio between peak snow water equivalent and annual streamflow can exceed 60% [127]. Subsequently, streamflow has usually two peaks, one in autumn for heavy rainfall events and one in spring for rainfall events and snowmelt, and a low-flow period during summer.

As a result of topographic and climatic characteristics, a variety of land cover types characterize the basin (Figure 4.1c): transitions between bare soil, grassland, and forests following the elevational gradient in the mountainous parts, shrubland in the temperate and dry areas in the southwestern part, and cultivated and urban areas in the central lowlands [202]. In addition to three major lakes, around 180 multi-purpose reservoirs influence the hydrographic system in the basin [201]. Further, anthropogenic water withdrawals for irrigation, industrial, and drinking water uses affect heavily the hydrological cycle in the area. Irrigation accounts the most among the water uses (60%), responsible for water withdrawals of around $17*10^9$ $m^3 year\_1$ (i.e., 5% of mean annual precipitation), with further increases by up to 15% during droughts [201].

4.2.2 Hydrological modelling

The hydrological model Continuum [198] is an open-source continuous grid-based hydrological model (available at `https://github.com/c-hydro`). It simulates the main hydrological processes in a process-oriented but parsimonious way, with only few calibration parameters, by solving the mass and energy balances [198]. The model can also include optional modules to simulate lakes, dams, and hydraulic infrastructures, such as point water withdrawals and releases. We refer the reader to [198] for a description of the model, [203] for specifics on the snow module, and [204] for specifics on the surface flow routing scheme.

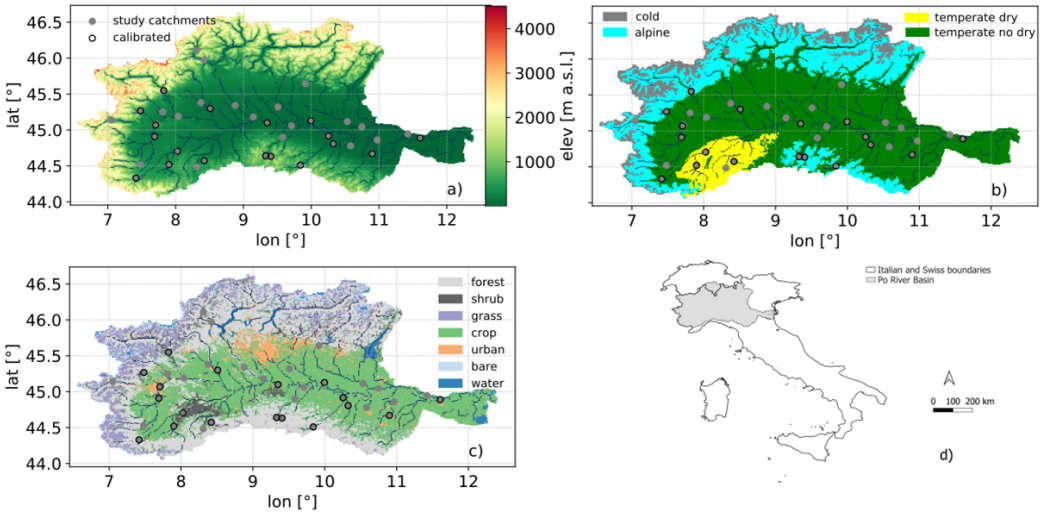

Figure 4.1: Maps with (a) elevation, (b) climates, (c) land cover types, and (d) location of the model domain, modelled river network (black line), and study sub-catchments (grey dots and black edge if calibrated). For data sources please refer to Table H.1.

Here we used six modules (namely, the snow, vegetation, energy balance, soil, groundwater, and surface water modules) to simulate snow dynamics, vegetation interception, energy fluxes, evaporation from the canopy layer, ET, soil moisture and groundwater dynamics, the dynamics of major lakes and dams in the region, and streamflow generation (Figure G.1). In Figure G.1 we provided a scheme of the model configuration, along with model fluxes and states.

In this work, we run Continuum at a 0.009° (around 1 km) spatial resolution and 1 hour temporal resolution [69] over the hydrological years 2009-2022, with the first year as warm-up period. Please note that throughout the manuscript we referred to hydrological years, spanning from August to September, rather than calendar years.

4.2.3 Data

4.2.3.1 Model input data

In this work, we used the model setup and the required datasets, regarding topography, soil properties, land cover, dams, lakes, and glacier cover, presented in [69]. We summarized the input data in Table H.1.

Further, the model needs dynamic maps of precipitation (P), air temperature, relative humidity,

wind speed, and shortwave solar radiation as forcing data. For P we used maps interpolated from 1377 gauges and radar data from the Italian Civil Protection Department (DPC), computed with the Modified Conditional Merging algorithm [117]. This product outperformed gauge-only interpolation [117] and satellite products for hydrological modelling over the study area [69]. For other meteorological variables we used maps interpolated from ground-based data provided by DPC (see [69] for details).

4.2.3.2 Data for model calibration and evaluation

For model calibration and evaluation, we exploited a set of independent ground- and remote sensing-based datasets (Table H.1). For Q, we used quality-checked daily mean Q time series for 38 sub-catchments in the Po river basin (Figure 4.1) from DPC and Italian regional hydrometeorological offices [69, 205]. We selected the study sub-catchments according to data availability (maximum 6 months of missing data). These sub-catchments reflect the variety of topographic, climatic, and land cover characteristics in the study area (Table I.1).

For ET, we applied the METv2 product by the Land Surface Analysis of the EUMETSAT Satellite Application Facility, in the following LSASAF product [122, 123]. The LSASAF product provides gridded ET estimates by exploiting data from the Meteosat Second Generation satellite at a spatial resolution of 3.1 km at the sub-satellite point and at a temporal resolution of 1 hour. It derives ET estimates from a surface energy model, based on the Soil-Vegetation-Atmosphere-Transfer scheme described in [122], and remote-sensed data. This product showed reasonable agreement with alternative gridded ET products and eddy-covariance data over Italy [205]. We used the LSASAF product as benchmark of simulated ET for both catchment-scale and spatial patterns analyses.

Finally, we employed TWS data from the Gravity Recovery And Climate Experiment (GRACE) and GRACE Follow-On (GRACE-FO) missions, henceforth GRACE data. GRACE launch was in April 2002 and its dismissal in Jun 2017, whereas GRACE-FO is operational since May 2018. These satellite missions consist of two twin satellites measuring variations in distance between them and, thus, in the Earth's gravity field. Consequently, GRACE data provide estimates of changes in mass over a certain area that mainly correspond to variations in TWS, i.e., in the groundwater, soil moisture, surface water bodies, snow, and ice storages. As GRACE data, we used the recently developed mass concentration (MASCON) solution, as it is particularly suited for hydrological applications compared to the traditional spherical harmonics solution [206]. MASCON does not require any significant postprocessing, while minimizing errors due to the leakage of the signal from land to oceans. We processed the latest products of GRACE MASCONS (release 06) from the Center for Space Research at the University of Texas (CSR) [207, 208], the NASA Jet Propulsion Laboratory (JPL) [209, 210], and the NASA Geodesy and Geophysics Research Laboratory (GSFC) [211] at monthly temporal resolution, and spatial resolutions of 1° for CSR and GSFC products and 0.5° for the JPL product. We regridded, using a

nearest neighbour approach, the three products to a common grid of 0.5° spatial resolution. Then, we considered the mean among them to reduce the uncertainties associated with specific GRACE products [125]. GRACE data provide anomalies regarding the period 2004–2009, therefore we converted them to anomalies over the study period by subtracting their long-term means [125]. Due to the coarse spatial resolution of GRACE data and the relatively small drainage area for most of the study sub-catchments (Table I.1), we used GRACE data only for the catchment-scale analysis and at the outlet section of the basin (drainage area = 72545 km^2).

4.2.4 Analyses

4.2.4.1 Experimental design

We performed two calibration experiments to evaluate whether model performances decreased during droughts of different severity, as expected, and whether including a moderate drought improved model transferability to severe droughts (Table 4.1). For each calibration experiment, we evaluated model performances during the whole study period and periods with contrasting climate.

For each study sub-catchment, we characterized the climatic conditions in terms of annual P standardized anomalies according to Equation 4.1:

$$P_{anom}(t) = \frac{P(t) - \overline{P}}{\sigma_P} \tag{4.1}$$

where $\overline{P}$ is the mean and σ_P the standard deviation of annual P over the study period. We defined wet (or dry) years as those years with positive (or negative) annual P standardized anomalies for most of the study sub-catchments (Figure J.1). Further, we referred to dry years as droughts, and we defined them as moderate or severe in terms of decreasing annual P standardized anomalies (Table 4.1).

Table 4.1: Calibration and evaluation periods, and their climatic characteristics in terms of annual P standardized anomalies across the study sub-catchments (mean ± one standard deviation).

Purpose	Climatic conditions	Period	Annual P standardized anomalies [-]
Calibration experiment 1	”normal” years	2018-2019	0.34±0.42
Calibration experiment 2	including a moderate drought	2016-2017	-0.85±0.61
Evaluation	wet years	2014 and 2020	1.14±0.65 and 1.48±0.34
Evaluation	moderate droughts	2012 and 2017	-0.8±0.39 and -0.85±0.61
Evaluation	severe drought	2022	-1.68±0.43

We first calibrated the model during the “normal” years 2018 and 2019 which represented average conditions regarding annual P, and we evaluated model performances in independent periods

with contrasting climate conditions (Figure 4.2): the wet years 2014 and 2020, the moderate droughts 2012 and 2017, and the severe drought 2022 (Sections 4.3.2 and 4.3.3). Then, we calibrated the model during a moderate drought (Figure 4.2, years 2016 and 2017) and we evaluated whether this improved model transferability to the severe drought (Section 4.3.4).

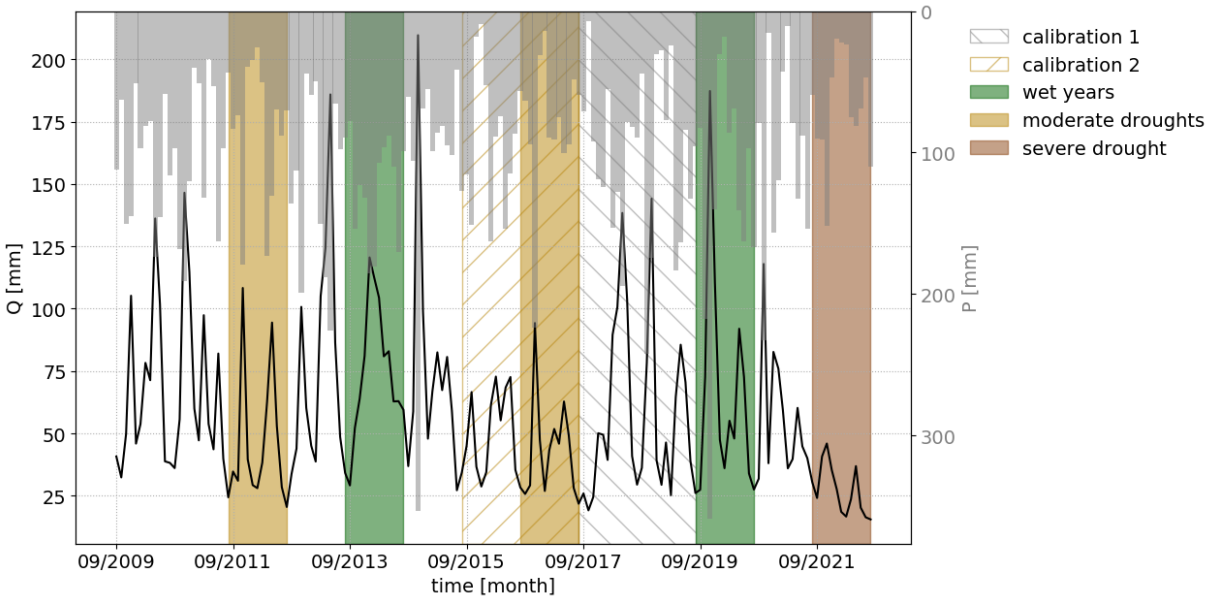

Figure 4.2: Monthly observed precipitation (P) and streamflow (Q) during the study period averaged across the study sub-catchments, with sub-periods used for model calibration (hatched areas) and evaluation (shaded).

4.2.4.2 Model calibration

We deployed a multi-site calibration procedure to calibrate the model against Q data, following [69] for the calibration approach and the selection of calibration sub-catchments. Therefore, we used 18 sub-catchments over a 2-year period, with a warm-up period restricted to 6 months during the calibration runs for computational reasons. We calibrated four model parameters (Figure G.1): the Curve Number (CN), the field capacity (c_t), the infiltration velocity at saturation (c_f), and a parameter regulating the baseflow from the groundwater storage (w_s). CN, c_t, and c_f are spatially distributed parameters, while w_s is lumped for the whole model domain. We set the first guess parameters from (i) global maps of soil characteristics [212] and land cover [202] for CN, c_t, and c_f, and (ii) expert knowledge for w_s. Then we used an iterative parallel search algorithm to rescale the first guess parameters until the minimization of the cost function, with convergence set as an improvement $< 1\%$ compared to the previous iteration. This allowed to preserve the spatial patterns from the first guess parameters while minimizing the cost function. We based the cost function on a sum of Kling-Gupta Efficiency (KGE [213]) on the daily Q of

each calibration sub-catchment, weighted with the logarithm of the sub-catchment area, to give more emphasis to the downstream sub-catchments [69]. The KGE is an aggregated measure of the agreement in timing, magnitude, and variability between simulations and observations, according to Equation 4.2:

$$KGE = 1 - \sqrt{(r-1)^2 + (\beta-1)^2 + (\gamma-1)^2} \tag{4.2}$$

where r is the Pearson's correlation coefficient, β is the ratio between simulated and observed mean as a measure of bias, and γ is the ratio between the simulated and observed coefficient of variation (KGE $\in$ (-∞, 1], optimal value = 1, no-skill threshold over mean flow as predictor = -0.41 [214]). We used the KGE, instead of other metrics tailored specifically to low-flows [215], because we intended to evaluate a model for general hydrological applications, such as climate impact assessments, and not to optimize the low flows at the expense of other streamflow regimes. We reported the KGE from the two calibration experiments in Table K.1.

4.2.4.3 Model evaluation

We evaluated model performances in reproducing Q, ET, and TWS temporal variability at monthly time scale which is the temporal resolution of GRACE data. To evaluate model skills for TWS, we reconstructed the simulated states in model stores, i.e., from the water volumes in the snow, vegetation, surface water, soil, and groundwater stores (Figure G.1). We then computed the TWS anomalies from the long-term mean for the simulation period. We used catchment-average ET and TWS time series for this catchment-scale analysis. Additionally, we evaluated model performances in simulating monthly ET spatial patterns, by computing pixel-wise deviations. Since hydrological processes in the region are highly seasonal, we evaluated model capability in simulating seasonality (i.e., monthly mean values), deviations from it (i.e., monthly standardized anomalies), and long-term changes. We evaluated the model capability in simulating long-term changes only qualitatively, as we considered the study period too short for trend detection.

We computed the monthly standardized anomalies, z_{anom} as the anomalies relative to the monthly climatology according to Equation 4.3:

$$z_{anom}(t_i) = \frac{z(t_i) - \overline{z_i}}{\sigma_{z_i}} \tag{4.3}$$

where z is the value at each time step, $\overline{z}_i$ and σ_{z_i} are the long-term mean and standard deviation for month i.

As performance metrics for model evaluation, we used the KGE (Section 4.2.4.2), the Pearson's correlation coefficient (r, with r $\in$ [-1, 1] and 1 as optimal value), and the normalized Root Mean

Square Error (nRMSE) with nRMSE $\in$ [0, +∞) and 0 as optimal value [216]), according to Equation 4.4:

$$nRMSE = \frac{\sqrt{\frac{1}{N}\sum_{i=1}^{N}(X_{sim,i} - X_{obs,i})^2}}{\sigma_{X_{obs}}} \tag{4.4}$$

where $X_{sim,i}$ is the simulated variable at time step i, $X_{obs,i}$ the observed, $\sigma_{X_{obs}}$ the observed standard deviation, and N the number of time steps. r is a measure of the agreement in timing, while nRMSE measures the general agreement between simulations and benchmark. We normalized the RMSE to allow a fair comparison among sub-catchments/grid cells that may have different observed ranges. For normalizations, we used the standard deviation rather than the widely used mean to avoid numerical issues when the mean is close to zero as in the case of TWS.

To identify statistically significant differences across the evaluation periods, we used a two-sample t-test for the mean across the study sub-catchments (pvalue < 0.01).

4.3 Results

4.3.1 Hydroclimatological conditions during droughts

Three droughts occurred in the region during the study period, namely in 2012, 2017, and 2022 - ongoing - as depicted by annual P standardized anomalies (Table 4.1 and Figure J.1) and reported by [199, 129, 200, 2]. Low winter P characterized the three events (Figure 4.3a). However, duration and severity of low P values differed among the events, with moderate annual P standardized anomalies in 2012 and 2017, and severe in 2022 (Table 4.1). Furthermore, during the three events P deficits propagated rather differently through the hydrological cycle (Figure 4.3). For 2012 and 2017, the LSASAF product showed higher-than-usual ET during spring (Figure 4.3b), but lower-than-usual ET during summer (August ET = 52 mm month^{-1} in 2012 and 46 mm month^{-1} in 2017 compared to a climatology of 71±15 mm month^{-1}, with climatology expressed as the mean ± standard deviation of August ET over the study period 2010-2022). On the contrary, the ET product showed higher-than-usual values during the 2022 drought (Figure 4.3b, July ET = 124 mm month^{-1} compared to a climatology of 87±18 mm month^{-1}). Further, TWS was within the climatology in 2012 and 2017, whereas it was already low at the beginning of 2022 (Figure 4.3c, September TWS anomaly = -92 mm compared to a climatology of -58±37 mm) and during summer it reached the minimum value over the whole study period (August TWS anomaly = -158 mm compared to a climatology of-54±56 mm, Figure 4.3c). As a result, Q showed moderately low values throughout 2012 and 2017 (Figure 4.3d, July Q = 18 mm month^{-1} in 2012 and 25 mm month^{-1} in 2017, compared to a climatology of 30±13 mm month^{-1}), while it experienced lower-than-usual values during most of 2022 (July Q = 9 mm month^{-1}).

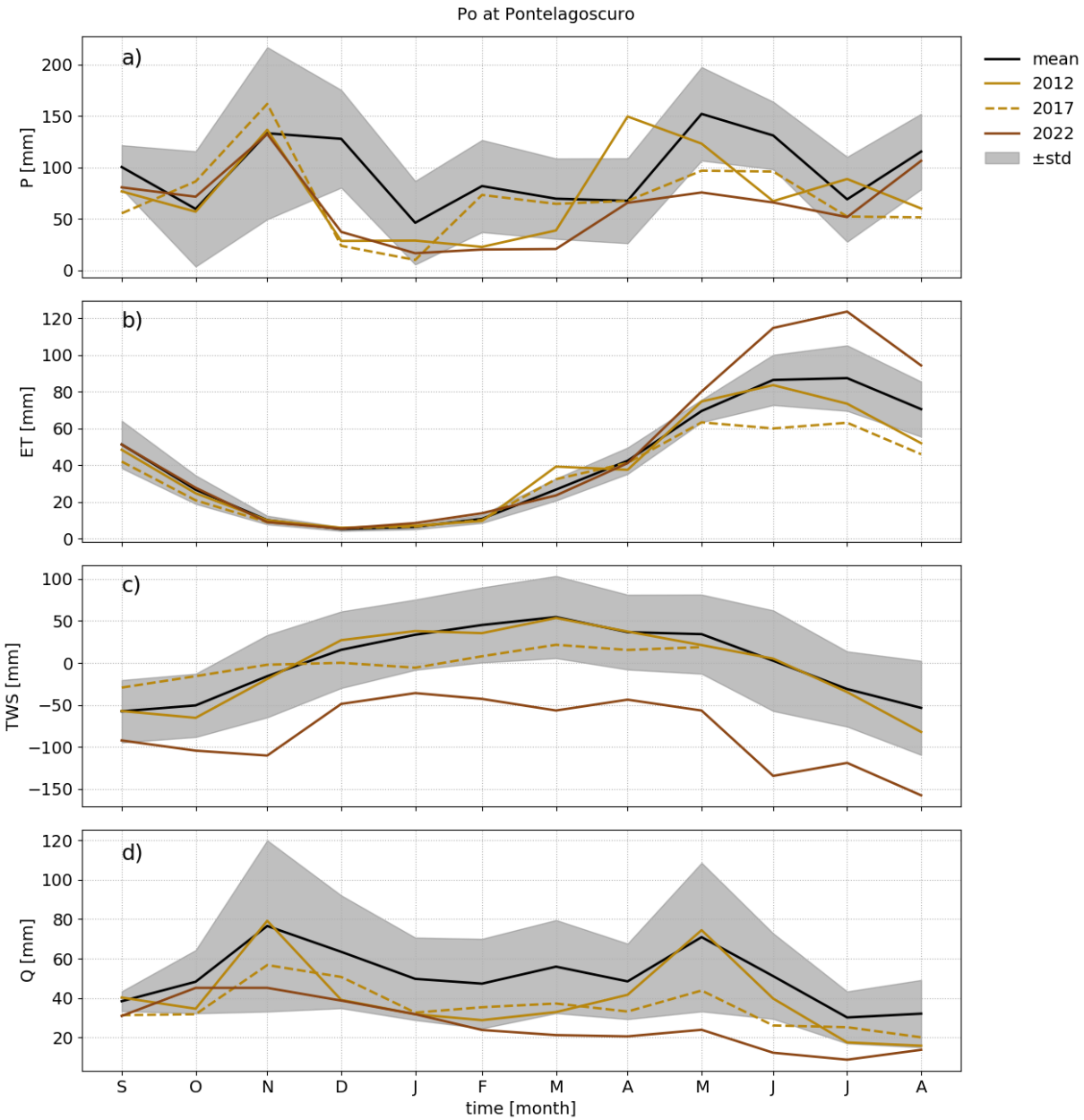

Figure 4.3: P (a), ET (b), TWS (c), and Q (d) observed monthly climatology (mean and standard deviations over 2010-2022) and monthly values during drought years, for the basin outlet.

4.3.2 Model evaluation for streamflow during droughts of different severity

Model performances for Q were comparable during wet years, moderate droughts (Figure 4.4a, b, and d), and the whole study period (Table K.1) for the model calibrated during "normal" climatic conditions (Section 4.2.4.2). Across the sub-catchments, mean KGE (± 1 standard deviation) was equal to 0.59(±0.32) during the wet years, 0.55(±0.25) for moderate droughts, and 0.7(±0.19) over the whole study period. At the basin outlet, the model represented properly the slight decline in Q since autumn 2019 (as visualized by the 24-month running means in Figure 4.5a), Q seasonality (Figure 4.5b), and also Q monthly values during the severe 2022 drought (KGE = 0.82).

Nonetheless, model performances across the study sub-catchments showed a decrease during the severe 2022 drought (mean KGE = 0.18±0.69, Figure 4.4c and d). Even though the model preserved some skills over a climatological mean [214], performances were low especially in the evaluation catchments and in terms of bias with a general overestimation of Q (Figure L.1, mean β = 1.37±0.75). The other components of KGE (r and γ) did not change significantly between moderate droughts and the severe drought (Figures M.1 and N.1). In the following we investigated the simulation of ET and TWS, and the uncertainty in observed data as possible culprits for Q overestimation during 2022 (Section 4.3.3).

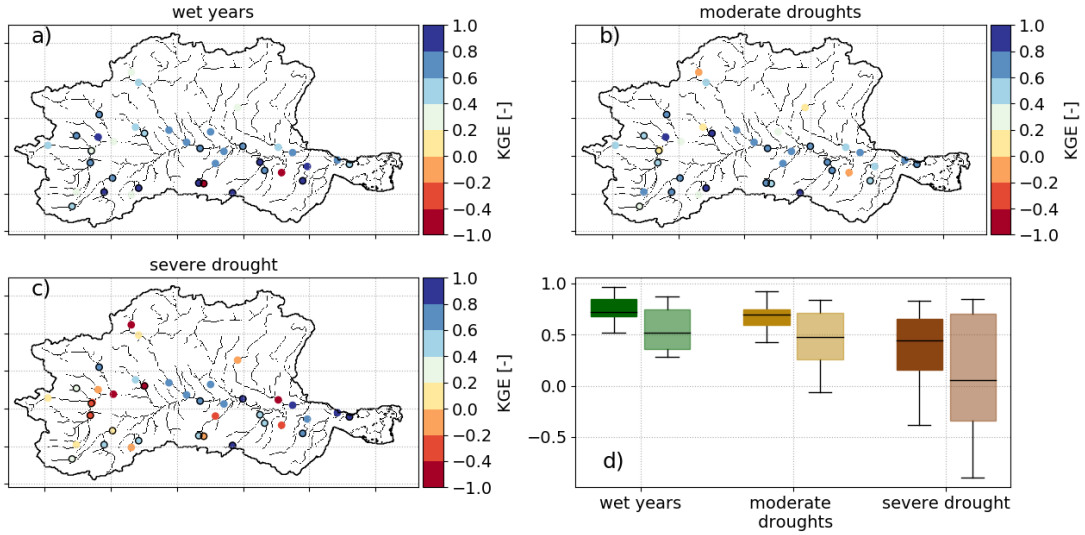

Figure 4.4: KGE values on monthly Q during wet years (a), moderate droughts (b), and the severe drought (c) for each study sub-catchment, and their distributions as boxplots (d) grouped by calibration and evaluation sub-catchments (shaded boxplots) for the model calibrated during "normal" climatic conditions.

4.3.3 Model evaluation for evapotranspiration and terrestrial water storage

The model generally performed well for ET during the whole study period and moderate droughts, but not during the severe drought. Integrated over the entire basin, the model simulated properly both ET monthly values (r = 0.94 and nRMSE = 0.36 over the entire period, Figure 4.5d) and seasonality (r = 0.99 and nRMSE = 0.18 for monthly mean ET, Figure 4.5e), although it overestimated slightly ET during winter and spring, and it simulated an earlier ET peak in summer (Figure 4.5e). The model performed less well in simulating ET deviations from seasonality, with r = 0.52 and nRMSE = 0.98 for monthly ET standardized anomalies over the whole study period (Figure 4.5f). Furthermore, across the study sub-catchments the simulation of monthly ET standardized anomalies was skillful during moderate droughts (mean r = 0.81 and mean nRMSE = 0.68, Figure 4.6a and d), but it deteriorated significantly during the severe drought (mean r = 0.05 and mean nRMSE = 1.61, Figure 4.6b and e). Performance decreases for monthly ET standardized anomalies during the severe drought were not uniform throughout the model domain (Figure 4.7b and e) and showed a clear pattern with land cover. Model deterioration was particularly strong for croplands, which are mostly located in the central part of the domain (Figure 4.1c), with mean r = 0.58 and mean nRMSE = 0.97 across the cells classified as cropland during moderate droughts, and mean r = -0.03 and mean nRMSE = 1.8 during the severe drought (Figure 4.7c and f).

Over the entire basin, the model simulated properly the decline in TWS over the recent years (Figure 4.5g), as well as TWS seasonality (r = 0.91 and nRMSE = 0.41, Figure 4.5h), with the refilling of storage in autumn and winter, and its depletion in spring and summer. The model simulated properly the negative storage conditions in autumn 2021 (simulated TWS = -65 mm and observed TWS = -92 mm in September 2021, Figure 4.5h) and it overestimated slightly TWS during the depletion (simulated TWS = -100 mm and observed TWS = -158 mm in August 2022).

The observed annual water imbalance (P-Q-ET-TWSC, with TWSC as the annual change in TWS) did not differ significantly between the moderate 2012 drought and the severe 2022 drought (Figure O.1). Across the study sub-catchments, the observed annual imbalance was 69±234 mm in 2012, 51±202 mm in 2022, and 108±244 mm on average over the study period. A slightly positive observed imbalance may have contributed to an overestimation in Q simulation for some catchments, but we did not detect any systematic increase in this net imbalance in 2022 to justify the Q overestimation for this year.

4.3.4 Impact of calibration period on model transferability

Including a moderate drought (the 2017 event) in the calibration period did not improve model skills during the severe drought (2022). Model performance during calibration was similar dur-

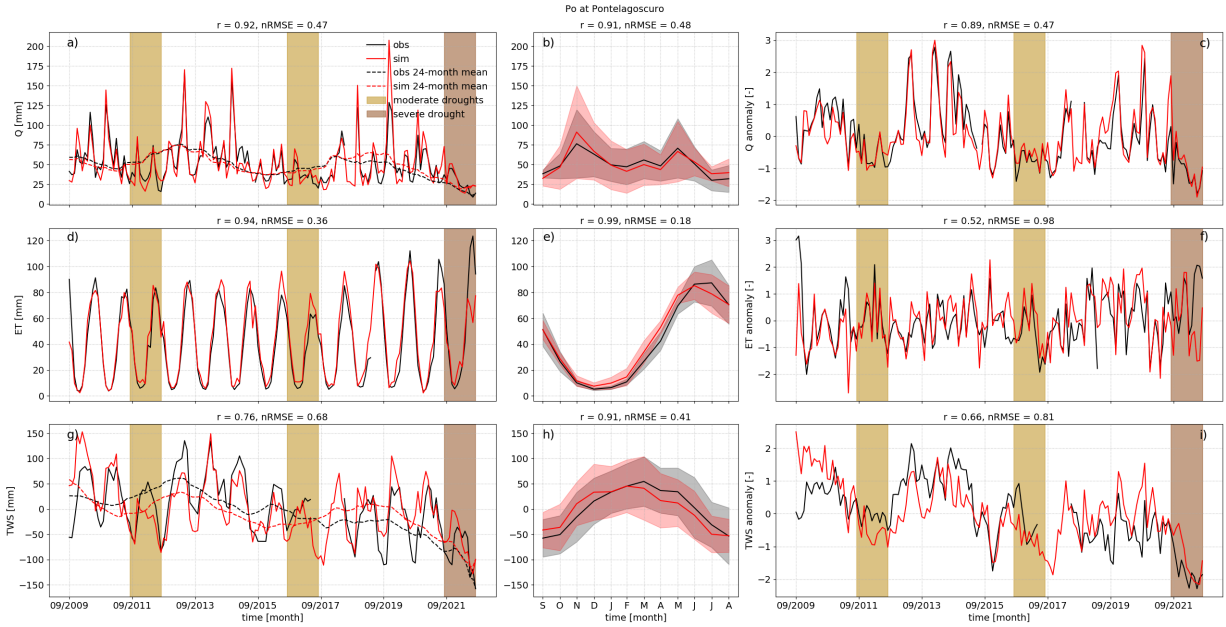

Figure 4.5: Time series of observed (black) and simulated (red) Q (first row), TWS (second row), and ET (third row) monthly values with 24-month rolling means (first column), monthly means (second column), and monthly standardized anomalies (third column) for the basin outlet. Shading in panels (a), (c), (d), (f), (g), and (i) refers to moderate and severe droughts, while shading in panels (b), (e), and (h) corresponds to ± 1 standard deviation in monthly values.

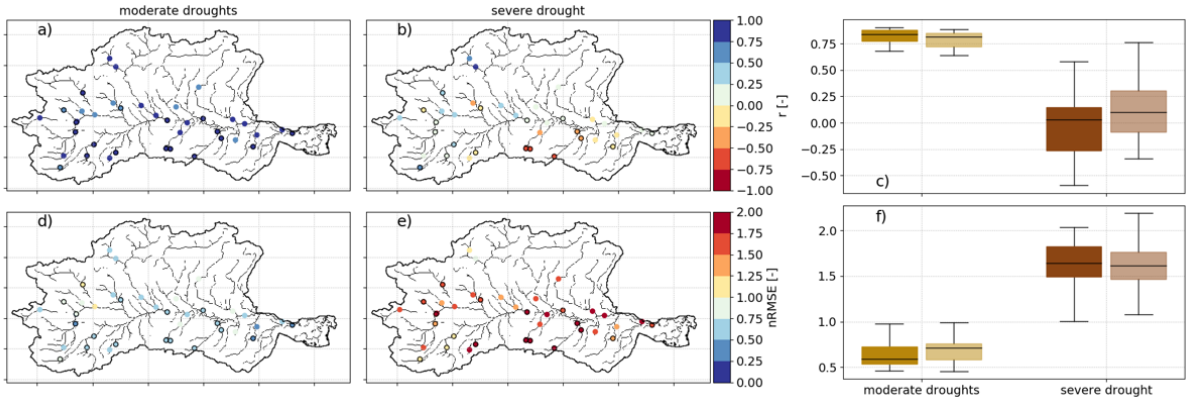

Figure 4.6: r and nRMSE on monthly ET standardized anomalies over moderate droughts (a and d) and the severe drought (b and e) for each study sub-catchment, and errors distributions as boxplots (c and f) grouped by calibration and evaluation sub-catchments (shaded boxplots).

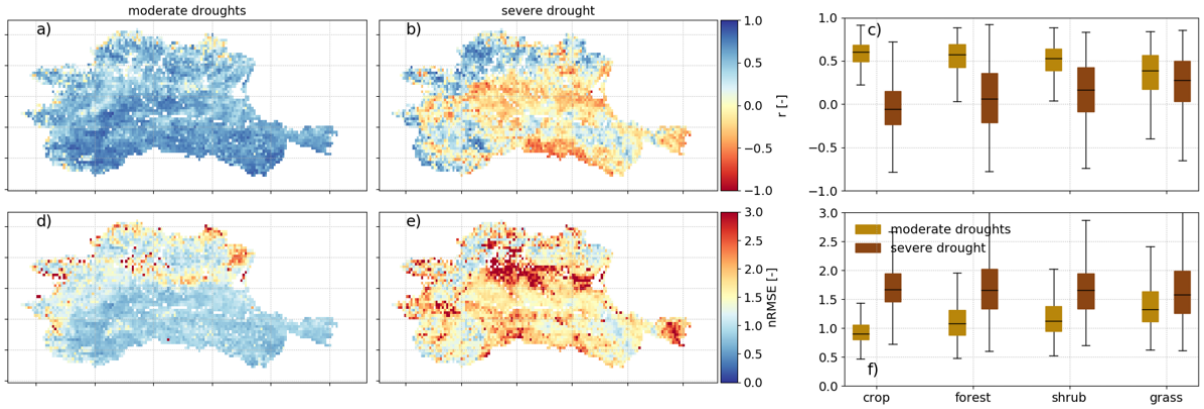

Figure 4.7: Maps of pixel-wise r and nRMSE on monthly ET standardized anomalies over moderate droughts (a and d) and the severe drought (b and e), and errors distributions as boxplots per each land cover type (c and f). Water bodies were excluded from the comparison. Model outputs were rescaled by bilinear interpolation to the resolution of the LSASAF product for comparison.

ing both calibration experiments – with a mean KGE across the calibrated sub-catchments = 0.58 for the "normal" calibration period and a mean KGE = 0.44 for the calibration period including a moderate drought (Table K.1). Also for the model calibrated during a drought, Q simulation performances across the study sub-catchments deteriorated significantly during the severe 2022 drought compared to model skills during moderate droughts (mean KGE = 0.5±0.27 during moderate droughts versus 0.18±0.63 during the severe drought, Figure 4.8c). The model calibrated during a moderate drought showed issues in simulating monthly ET standardized anomalies in the croplands during the severe drought, with mean r = -0.11 and mean nRMSE = 1.85 during the severe drought across the cropland model cells (Figure 4.8f and i), similarly to the model calibrated during "normal" climatic conditions.

4.4 Discussion

4.4.1 Main findings and implications

We investigated the skills of the distributed and process-based hydrological model Continuum to simulate Q under a range of climatic conditions, explored possible causes for the decrease in model performances during a severe drought, by analyzing the simulation performance for ET and TWS, and evaluated the benefit of including a moderate drought in the calibration.

Over the entire study period, we achieved a satisfactory Q simulation even in the heavily human-affected Po river basin in Italy (mean KGE = 0.7 across the 38 study sub-catchments, Table K.1), consistently to [69] who used the same model and study area. Focusing on specific climatic peri-

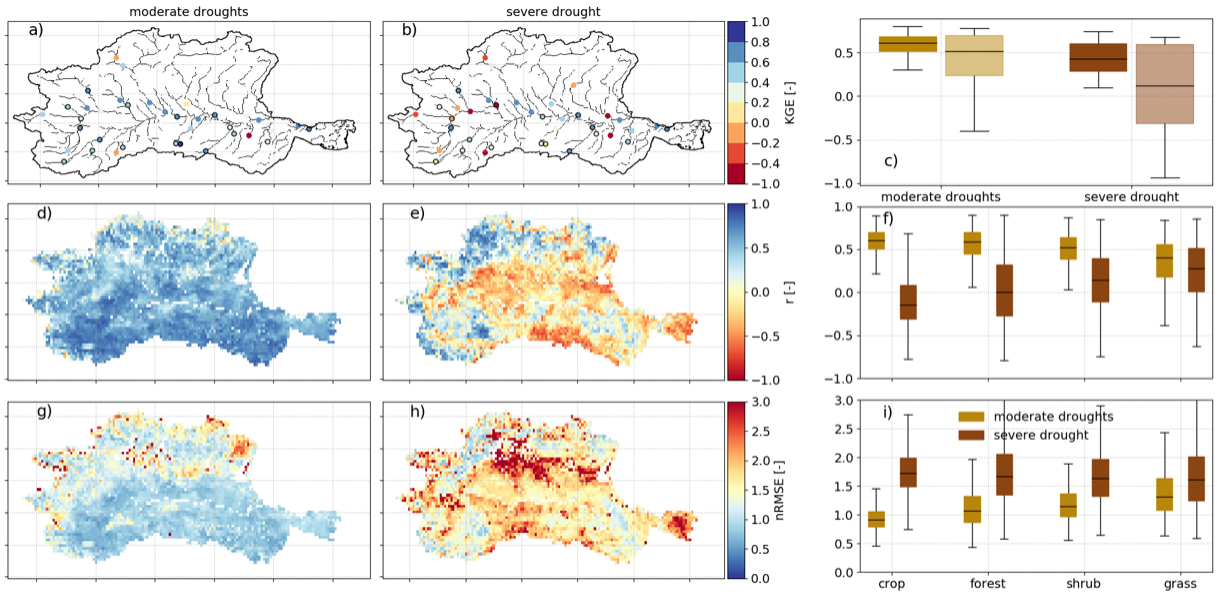

Figure 4.8: Summary of model performances for the model calibrated during a drought: KGE values on monthly Q over moderate droughts (a) and the severe drought (b) for each study sub-catchment, their distributions as boxplots (c) grouped by calibration and evaluation sub-catchments (shaded boxplots), maps of r and nRMSE on monthly ET standardized anomalies over moderate droughts (d and g) and the severe drought (e and h), and errors distributions as boxplots per each land cover types (f and i).

ods, we found that Continuum represented Q reasonably well during moderate droughts such as the 2012 and 2017 events (KGE = 0.55±0.25, Figure 3.3b), even in a model setup not specifically tailored to low flows simulation. During the severe 2022 drought, the model simulated Q still reliably for the basin outlet (KGE = 0.82), which weighted the most in the calibration procedure (Section 4.2.4.2). However, we found a decrease in model performances across the other study sub-catchments (KGE = 0.18±0.69, Figure 3.3c), especially in evaluation catchments and in terms of bias with a general overestimation of Q during the severe 2022 event (Figure L.1). On the one hand, our results showed the ability of the distributed hydrological model Continuum in simulating Q during moderate droughts. [195] found indeed that a distributed hydrological model outperformed lumped and semi-distributed models to simulate Q outside the climatic conditions during the calibration period for two catchments in south-eastern Australia. On the other hand, we found an overestimation of Q during the severe 2022 drought across the study sub-catchments that points to room for possible model improvement during severe droughts. A wide number of studies reported decreases in Q model skills for conceptual models when simulating prolonged and particularly severe droughts, such as the Millennium Drought in Australia [97] and the Californian multi-year drought between 2012 and 2016 [13]. The model performances we detected during a severe event can have relevant implications for operational applications. A proper representation of Q timing is encouraging for drought monitoring tools for instance, while

the overestimation of Q could stand for a potential underestimate of the severity of predicted extreme droughts in climate impact assessments.

Potential causes for the overestimation of Q during the severe 2022 drought are (i) an underestimation of simulated ET, (ii) an overestimation of simulated TWS contribution to Q, and (iii) an increased uncertainty in observed data used to force/evaluate the model. We indeed revealed that model capability in simulating spatial and temporal variability of monthly ET standardized anomalies decreased significantly during the severe drought compared to moderate droughts, especially in the human-affected areas with mean r = -0.03 and mean nRMSE = 1.8 across the croplands in 2022 (Figure 4.7). An overestimation of simulated TWS contribution to Q may have arisen from an (over-) underestimation of the (initial) final storage conditions. We showed that over the river basin the model overestimated slightly TWS both at the beginning and end of 2022 (Figure 4.5g), and thus it underestimated slightly its contribution to Q, rather than overestimating it. An increased uncertainty in observed data may have stemmed either from an overestimation of P or an underestimation of Q, due to increased uncertainty in the measurements under extremely low flow conditions [217] for instance. Yet, the uncertainty in observed data did not systematically increase across the study sub-catchments compared to the moderate 2012 drought (observed imbalance between ingoing and outgoing fluxes = 69±234 mm in 2012 and 51±202 mm in 2022, Figure O.1). Therefore, we identified the misrepresentation of ET - and its underestimation in particular - as the main cause for Q overestimation during the severe drought. Previous studies showed indeed that a poor ET simulation can hamper Q simulation during severe droughts [13] and ET has a prominent role particularly during severe and prolonged events [106, 218]. Model difficulties in representing monthly standardized anomalies in both ET and TWS (Figure 4.5), compared to seasonality and long-term changes, further agrees with previous literature. [105] for instance showed that a set of global hydrological and land surface models represented TWS seasonality and long-term variability well in a tropical basin, but not its deviations from seasonality. The misrepresentation in ET during the severe drought may have derived from (i) the model neglection of irrigation, which can have strongly increased water availability for ET during the exceptionally dry and warm summer 2022 over the study area [2], and (ii) uncertainties in model structure and parameterization for water-limited ET conditions. This latter cause would be also in line with the earlier ET suppression we detected in the simulated ET annual cycle compared to the one from the remote sensing-based ET product (Figure 4.5e). By identifying possible causes for the decrease in model performances during the severe drought, our results pave the way for future research to increase model robustness during severe events (Section 4.4.2).

Including a moderate drought (the 2017 event) in the calibration did not lead to an improvement in Q nor in ET during a severe drought (the 2022 event), with mean KGE = 0.18±0.63 for Q across the study sub-catchments, and mean r = -0.11 and nRMSE = 1.85 for ET across the croplands during 2022 (Figure 4.8). [8] tested different calibration strategies for an ecohydrological model for the simulation of the 2018-2019 German drought in an experimental catchment. They reported an improvement in model performances by including the drought in the calibration period, compared to those from an alternative calibration period. These findings partly contrast

our results and this may be due to several differences between the two studies, such as the experimental design, study areas, models, and calibration procedures used. However, we see our findings complementing those by [8], by demonstrating that calibrating during a drought may not be sufficient to ensure model transferability to a different and more severe drought.

Recent literature revealed that a changing climate may exacerbate the occurrence of severe and prolonged drought events [9]. Thus, our results further call for comprehensive evaluations of simulated hydrological fluxes and states, and the testing of alternative strategies to enhance the simulation of the hydrological cycle during severe droughts, especially for drought studies, drought monitoring and forecasting systems, and impact assessments of a drying climate.

4.4.2 Future work

Our study area encompassed a variety of climates and land cover types (Figure 4.1), and our study period included droughts of different severity (Figure 4.3). Nevertheless, our results referred to a particular model over specific region and drought events, and intercomparison studies over different areas and droughts would be helpful to generalize our conclusions.

In this work, we showed the usefulness of remote sensing-based products as benchmarks for distributed simulations of ET and TWS to unravel where they deviate most. However, ET and TWS retrieval through remote sensing still presents challenges, as we cannot measure ET directly and we can derive TWS only at large scales. For TWS, we applied the mean of three latest GRACE products (Section 4.2.3.2) to take into account uncertainties [125]. As ET dataset, we exploited the LSASAF product, which showed skilful performances over the study region, even during droughts [205]. However, benchmarking the model against alternative additional datasets for ET or other variables, such as soil moisture and snow, would be beneficial to assess model internal consistency during droughts.

Multivariable calibration may be helpful to improve model internal consistency [219, 67], also during low-flow periods [220] and droughts [8]. [8] for example showed that including tracer data in the calibration of an ecohydrological model increased model internal consistency during the 2018-2019 drought in Central Europe. Here we calibrated the model against Q data only (Section 4.2.4.2). Given the satisfactory performances we achieved for ET during moderate droughts, we argue that a multi-variable calibration approach will probably not enhance model transferability to a severe drought significantly. [221] showed that a multi-objective calibration with Q data aggregated at different time scales improved Q transferability outside the calibration conditions for a distributed model in a German medium-sized basin. Future work could test similar multi-objective or multi-metric approaches.

Human interference affects heavily the hydrological cycle in the study area, both in terms of water withdrawals and irrigation (Section 4.2.1). Here, Continuum included reservoirs - although we did not know their regulation -, but not irrigation and water withdrawals, which can be more

relevant during droughts than during wet periods. By calibrating the model against observed Q data, model parameterization partly accounts for the effects of human interference. However, an enhanced representation of human interference could improve hydrological modelling during severe droughts. For instance, [222] achieved a median 10.6% improvement in low-flows simulation by including monthly actual abstraction and discharge data in a distributed hydrological model for 605 English catchments. Further, [223] showed that assimilating vegetation variables into a land surface model led to an improved simulation of agricultural droughts and [224] proposed effective techniques for estimating irrigation over large areas through satellite data that can be incorporated into distributed hydrological modelling. Further research should investigate the benefits of assimilating new data in the representation of the human-affected hydrological cycle during severe droughts.

4.5 Conclusions

In this work, we comprehensively evaluated model capability in reproducing Q, ET, and TWS during droughts of different severity for the distributed hydrological model Continuum over 38 sub-catchments of the Po River basin in northern Italy, using ground- and remote sensing-based datasets as independent benchmarks. Further, we tested the value of calibrating during a moderate drought as possible strategy to improve model performances during a severe drought. We found that Continuum represented Q well during moderate droughts (the 2012 and 2017 events) even in this highly human-affected area, but overestimated Q for many of the study sub-catchments during the severe 2022 drought (Figure 4.4). We hypothesized and tested possible causes for this overestimation of Q, and we linked it to an underestimation of monthly ET standardized anomalies in the irrigated croplands during such period (Figure 4.7). Moreover, we demonstrated that the representation of Q and ET during the severe drought was not sensitive to the climatic conditions during calibration (Figure 4.8). Thus, we highlighted the need for holistic model evaluations and possibly model developments to enhance the representation of human and drought processes in distributed hydrological models, with the ultimate goal of increasing model robustness during severe droughts. This is highly relevant in a changing climate and the anthropogenic era to predict water availability throughout the hydrological cycle to inform water management, disaster risk reduction, and climate change adaptation measures.

Chapter 5

Synthesis

5.1 Main findings in context

The overarching goals of the thesis were to (i) study the role of evapotranspiration (ET) and subsurface storage in drought evolution (propagation and recovery) across climates and landscape, and (ii) evaluate how a process-based distributed hydrological model simulates streamflow (Q), ET, and Terrestrial Water Storage (TWS) during droughts, in order to better understand and simulate surface- and ground-water availability during droughts (Section 1.3). Hence, I collected a hydrometeorological dataset for Italy, as a valuable example of various hydroclimatological regimes (Section 2.2), I performed a large-sample data-based analysis of water balance components during droughts (Section 3), and I evaluated the performances of the Continuum model [198] in simulating Q, ET, and TWS during recent droughts - including the severe 2022 event - over the Po river basin in northern Italy (Section 4).

I found that variations in subsurface storage represent a significant fraction of the annual water balance (mean annual change in subsurface storage 11% of precipitation - P - on average across the 102 study catchments, Figure 3.3). Moreover, I illustrated how the depletion of subsurface storage during droughts (Figure 3.6) and its refilling during the recovery (Figure 3.9) generally sustained Q, regardless of catchment types and climates.

I further showed that Continuum properly simulated moderate droughts (mean KGE on monthly Q = 0.55±0.25 across the 38 study sub-catchments, Figure 4.4b), while the severe and complex 2022 drought - for human disturbance and concurrent heat wave - challenged it (mean KGE = 0.18±0.69, Figure 4.4c). I found that model deterioration could be linked to an uncertain representation of ET anomalies in the human-affected croplands (mean r = -0.03 and mean nRMSE = 1.8 during the severe drought, Figure 4.7) and calibrating during the moderate 2017 drought was

not sufficient to improve model skills in 2022 (mean KGE = 0.18±0.63, Figure 4.8).

In the thesis, I did not analyze specifically multi-year droughts over the study area, because of the general paucity of multi-year events during the study period. However, these findings can provide a consistent picture of the different roles ET and storage have in drought propagation and its modelling (Figure 5.1), also in the context of multi-year droughts (Section 1.2.5).

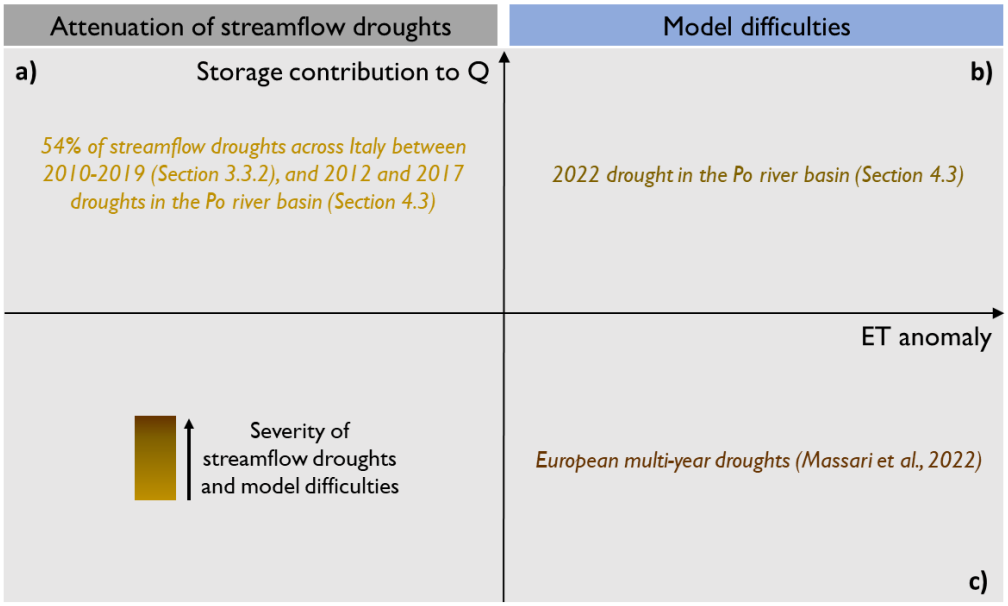

Figure 5.1: Illustration of evapotranspiration (ET) and storage contribution to streamflow (Q) during droughts, from main findings of the thesis and literature (in italic): (a) negative ET anomalies and enhanced storage contribution to Q attenuate streamflow droughts; (b) positive ET anomalies lead to model difficulties during severe droughts; (c) positive ET anomalies, and possibly reduced storage contribution to Q, exacerbate streamflow droughts during multi-year events. Yellowish to brownish colours refer to increasing severity of streamflow droughts and model difficulties.

The propagation of P deficits through the hydrological cycle is mainly regulated by ET and water storage in the catchment [60], and different hydrometeorological drivers can result in drought events of varying severity and duration [106].

I showed that negative anomalies in subsurface storage and ET characterized the 54% of streamflow droughts across Italy between 2010 and 2019, and attenuated them compared to the corresponding meteorological droughts (Figure 5.1a), consistently with typical perceptualization of streamflow droughts [88]. From model evaluation I revealed that Continuum well represented these moderate streamflow droughts (Figure 5.1a). Additionally, from remote sensing data I detected that concurrent negative storage anomalies and positive ET anomalies drove the severe streamflow drought in the Po river basin in 2022, and Continuum had decreased performances

for this event (Figure 5.1b). [3, 92] found similar features for the severe 2003 European summer drought, and [59] reported frequent ET enhancement during droughts at the expense of modelling capabilities.

During multi-year droughts, changes in the hydrological response of catchments to P can occurr, as documented for Mediterranean areas across the world [11, 12, 13]. Perceptual models for these shifts in P-Q relationship include a reduced contribution of storage to Q, either via an enhanced groundwater recharge [12] at the expense of Q generation or a decline in groundwater levels that feed Q [102], and/or an enhanced ET [13]. In [141] we analyzed data for 210 catchments in Europe from 1980 to 2015 to test (i) the occurrence of shifts in P-Q relationship during multi-year droughts across the variety of European climates and (ii) the ET enhancement as a potential driver for it. We found that shifts in the hydrological response of catchments occurred also during prolonged dry periods throughout Europe with concurrent positive ET anomalies, especially in catchments with high root depth and total available water content. This suggests that the deeper storage can support ET and further aggravate streamflow droughts during multi-year droughts (Figure 5.1 c). [13] showed similar drought features and poor model capabilities during the 2012-2016 Californian drought (Figure 5.1 b and c).

In summary, negative-to-positive ET anomalies may lead to increased severity of streamflow droughts (Figure 5.1a and b) and model difficulties in reproducing them (Figure 5.1b and c), while a reduction in the storage contribution to Q may lead to a further exacerbation of streamflow droughts, compared to the corresponding meteorological events (Figure 5.1c).

5.2 Study limitations and ways forward for future research

Some limitations in this thesis provide the opportunity for future research, as discussed in Section 3.4.3 for the large-sample analysis and Section 4.4.2 for the model evaluation. Here I summarized common limitations and ways forward for both the analyses.

The study catchments used in the thesis cover different hydroclimatological regimes (Section 2.2.6) and previous studies in different regions support most of the findings (Sections 3.4 and 4.4). Yet, extending the analyses to different climates would make the conclusions more general.

I considered a 10-year study period for the large-sample analysis and a 13-year study period for the model evaluation, mainly because of the difficulty in collecting a long-term water balance dataset for the study region (Section 2.2). Therefore, I analyzed specific drought events and the relatively short study period prevented the use of a fully standardized approach [76] for instance to study drought propagation. A longer study period would allow to generalize these findings for different drought events and to use alternative methodologies for drought identification and characterization (Section 1.2.2).

The cryosphere (snow and ice) can store winter precipitation to buffer later hydrological droughts.

In the large-sample analysis I did not explicitly consider snow as I used an annual temporal resolution to estimate changes in catchment (subsurface) storage, whereas in the modelling study I simulated snow dynamics through the Continuum snow module [203]. Recent developments in the S3M cryospheric model [225], which can be fully coupled to Continuum, and IT-SNOW [127], an Italian-scale snow reanalysis over the last decade based on S3M, in-situ and satellite data, could allow to explicitly consider the cryosphere. Snow estimates would allow one to derive subsurface storage changes and study drought propagation at a finer temporal resolution, by considering also the joint contribution of snow and subsurface storage. The coupling of S3M and Continuum [69] instead would let simulate the glacier dynamics during droughts as well.

Detailed information about human interference on the hydrological cycle is generally lacking for large samples of catchments [74]. In the large-sample analysis I did not explicitly consider human interference in the study catchments, by assuming that it possibly intensified the streamflow droughts I analyzed in line with the findings of [138]. In the modelling study, I partly considered human disturbance in the model by including reservoirs and calibrating against possible human-affected Q data. However, detailed information on human activities would be helpful to determine their influence on streamflow droughts and to properly model it in the study catchments, even in a socio-hydrological framework [226].

Hydrological data are inherently uncertain and so, hydrological models [227]. Throughout the thesis I used specific P, Q, and ET datasets. Regarding P and Q, I applied some filters on raw data to identify and remove possible outliers before using them (Section 3.2.2.1). Concerning ET, I firstly verified the suitability of the remote sensing-based product for the study region, even during droughts, in a multi-dataset comparison (Figure E.1). However, the use of multiple products would allow to explicitly quantify the uncertainties.

Finally, follow-up work could investigate ET and storage during multi-year droughts over the study area, and Continuum modelling skills in simulating them to further test the framework I proposed from the findings of the thesis and recent literature (Section 5.1).

5.3 Implications and relevance

Several implications can be drawn from the findings of this thesis (Sections 3.4.1 and 4.4.1).

As general outcome of the thesis, I revealed the feasibility of a multivariate approach in studying hydrological processes and model internal consistency during droughts, by merging traditional data and products from remote sensing. The dataset I collected was an initial effort for large-sample hydrology at Italian scale, and in so doing I provided further evidence of the value of large-sample datasets [72] and multiple data sources, to advance our hydrological understanding and modelling capabilities at large scales.

From the large-sample data-based analysis, the relevance of subsurface (soil and groundwater)

storage in annual water balance and in buffering streamflow droughts emerged. The buffering effect may be prevented in case of low antecedent storage conditions (Figure 3.7) and, of course, it comes at the expense of groundwater availability. Groundwater is a primary water source for many human communities and ecosystems, and is currently overexploited in many regions of the world [228]. Data from remote sensing showed indeed a decline in TWS over the last years also for the Po river basin (Figure 4.3). Furthermore, I detected room for improvement in the simulation of TWS by Continuum (Figure 4.3). These findings call for an enhanced consideration of storage conditions as driver for streamflow droughts, for instance in drought typologies [74, 106], and more broadly, for joint efforts by surface- and ground-water hydrology communities in analyzing and simulating surface- and ground-water availability during droughts.

From model evaluation, on the one hand, I revealed the ability of Continuum in reproducing most of drought conditions at a high resolution across the hydrological cycle and the landscape, even in a heavily human-affected area like the Po river basin. On the other hand, I provided further evidence of possible model performance decreases for particularly severe and complex droughts, which pose challenges in properly predicting climate impacts (Section 4.4.1). By identifying possible causes for this decrease, I also provided possible guidance for scientific model improvement, for example through an enhanced representation of human water uses into hydrological modelling [229] or the assimilation of satellite-derived irrigation data [224]. This emphasizes the need for integration between remote sensing and hydrological modelling to make hydrological models more robust even in heavily human-affected areas and outside the calibration conditions, as real digital twins of the hydrological cycle [69, 70].

Finally, I discussed that my findings fit consistently with recent pieces of literature on multi-year drought in a broader context. This should encourage unifying research on annual and multi-annual droughts, as their intertwined nature and the potential high impacts of prolonged events.

In conclusion, I showed that combining data analyses and model evaluations across catchments is the prerequisite for robust hydrological modelling to cope with drought risk and climate impacts.

Appendix A

The Asynchronicity Index (ASI) between precipitation (P) and potential evapotranspiration (PET) [126] is computed as

$$ASI = \sqrt{JS_{obs} - JS_{sim}}, \tag{A.1}$$

where JS_{obs} is the observed Jensen-Shannon distance and JS_{min} is the minimum Jensen-Shannon distance that can be obtained for the seasonality of P and PET. The Jensen-Shannon distances (JS) are derived as

$$JS = \sqrt{\frac{1}{2}D_P + \frac{1}{2}D_{PET}} \tag{A.2}$$

where D_P is the relative entropy of P and D_{PET} is the relative entropy of PET with reference to their average, obtained as

$$D_P = \sum_{m=1}^{12} P_m \log_2 \frac{P_m}{n_m} \tag{A.3}$$

and

$$D_{PET} = \sum_{m=1}^{12} PET_m \log_2 \frac{PET_m}{n_m} \tag{A.4}$$

with

$$P_m = \frac{r_m}{\sum_{m=1}^{12} r_m} \tag{A.5}$$

$$PET_m = \frac{k_m}{\sum_{m=1}^{12} k_m} \tag{A.6}$$

$$n_m = \frac{1}{2}\left(P_m + PET_m\right) \tag{A.7}$$

where r_m and k_m are the long-term mean monthly values for P and PET and the calender month m $\in [1, 12]$.

Appendix B

Table B.1: Catchment properties for the large-sample analysis in Chapter 3: basin and section name, catchment mean latitude, catchment area in km^2, catchment mean elevation in m a.s.l., aridity index (AI), dominant land cover type in the catchment, dominant topsoil texture in the catchment, and dominant geological class in the catchment. Sources and details about each property are provided in Section 3.2.2.2. Catchments are north to south ordered, according to the catchment mean latitude.

Basin	Section	Lat	Area	Elev	AI	Land cover	Soil texture	Geological class
Adige	S Michele all Adige	46.71	7299	1970	0.52	Coniferous forest	Medium	Igneous and metamorphic
Adige	Trento	46.64	9709	1935	0.55	Coniferous forest	Medium	Igneous and metamorphic
Adige	Verona	46.58	11029	1828	0.75	Coniferous forest	Medium	Igneous and metamorphic
Adige	Boara Pisani	46.52	12203	1708	0.63	Coniferous forest	Medium	Unconsolidated
Rabbies	S Bernardo Rabbi	46.43	105	2487	0.62	Bare soil	Medium	Igneous and metamorphic
Avisio	Cavalese Masi	46.38	569	2117	0.66	Coniferous forest	Medium	Unconsolidated
Noce	Mezzolombardo	46.37	1349	1870	0.58	Coniferous forest	Medium	Unconsolidated
Noce	Male	46.33	467	2288	0.55	Coniferous forest	Medium	Unconsolidated
Avisio	Lavis	46.3	933	1886	1.02	Coniferous forest	Medium	Unconsolidated
Cismon	Fiera di Primiero	46.25	124	1899	0.47	Coniferous forest	Coarse	Unconsolidated
Toce	Domodossola	46.24	828	1953	0.65	Bare soil	Coarse	Igneous and metamorphic
Sarca	Ragoli	46.16	539	2077	0.86	Coniferous forest	Medium	Igneous and metamorphic
Adda	Lodi	46.16	5584	1542	0.58	Broad-leaved forest	Medium	Unconsolidated
Toce	Candoglia	46.12	1441	1845	0.32	Bare soil	Coarse	Igneous and metamorphic
Fersina	Trento Fersina	46.11	174	1315	0.8	Coniferous forest	Coarse	Igneous and metamorphic
Brenta	Barzizza	46.08	1564	1473	0.35	Coniferous forest	Medium	Carbonate
Brenta	Grigno Ponte Filippini	46.06	616	1457	0.53	Coniferous forest	Medium	Igneous and metamorphic
Chiese	Cimego	46.01	238	2046	0.81	Coniferous forest	Medium	Igneous and metamorphic
Oglio	Capriolo	45.99	1883	1591	0.79	Coniferous forest	Medium	Unconsolidated
Chiese	Ponte dei Tedeschi	45.98	369	1841	0.43	Coniferous forest	Medium	Unconsolidated
Ticino	Vigevano	45.96	7071	1179	0.24	Broad-leaved forest	Medium	Igneous and metamorphic
Tesina	Bolzano Vicentino	45.85	809	1173	0.94	Coniferous forest	Medium	Carbonate
Ticino	Ponte della Liberta	45.85	8018	1018	0.28	Broad-leaved forest	Medium	Unconsolidated
Chiese	Gavardo	45.84	934	1430	0.45	Broad-leaved forest	Medium	Unconsolidated
Olona	Castellanza Olona	45.79	163	607	0.61	Broad-leaved forest	Medium	Unconsolidated
Lambro	Peregallo	45.79	273	654	0.63	Broad-leaved forest	Medium	Unconsolidated
Dorabaltea	Tavagnasco	45.75	3322	2300	0.44	Bare soil	Medium	Igneous and metamorphic
Bacchiglione	Montegalda	45.74	1470	844	0.65	Broad-leaved forest	Medium	Carbonate
Oglio	Marcaria	45.72	5840	979	0.58	Crops	Medium	Unconsolidated

DoraBaltea	Verolengo	45.68	3940	2063	0.67	Bare soil	Medium	Igneous and metamorphic
Agno	Ponte Brogliano	45.68	143	849	0.52	Broad-leaved forest	Medium	Silicatic
Sesia	Quinto Vercellese Cervo	45.56	1055	702	0.54	Broad-leaved forest	Medium	Unconsolidated
Agno	Borgofrassine	45.56	526	561	0.77	Broad-leaved forest	Medium	Unconsolidated
Orco	S.Benigno	45.45	733	1982	0.46	Bare soil	Medium	Igneous and metamorphic
Po	Cremona	45.43	50403	1064	0.56	Broad-leaved forest	Medium	Unconsolidated
SturadiLanzo	Lanzo	45.29	578	1992	0.42	Bare soil	Coarse,	Igneous and metamorphic
Po	Ficarolo	45.24	68619	977	0.59	Crops	Medium	Unconsolidated
Po	Casale Monferrato	45.19	13715	1478	0.73	Crops	Medium	Igneous and metamorphic
Po	Spessa	45.13	37500	1085	0.55	Broad-leaved forest	Medium	Unconsolidated
DoraRiparia	Torino	45.1	1416	1768	0.63	Broad-leaved forest	Medium	Igneous and metamorphic
DoraRiparia	Susa Via Mazzini	45.06	652	2273	0.53	Coniferous forest	Medium	Igneous and metamorphic
Po	Torino Murazzi	44.77	5177	1145	0.66	Crops	Medium	Unconsolidated
Po	Carignano	44.69	3785	1364	0.61	Crops	Medium	Igneous and metamorphic
Trebbia	Rivergaro	44.68	890	1060	0.56	Broad-leaved forest	Medium	Silicatic
Crostolo	Cadelbosco	44.65	257	426	0.99	Crops	Fine	Unconsolidated
Taro	S.Secondo	44.63	1488	836	0.56	Broad-leaved forest	Medium	Unconsolidated
Maira	Busca	44.5	580	1895	0.79	Bare soil	Medium	Igneous and metamorphic
Secchia	Pioppa	44.5	1631	774	0.72	Broad-leaved forest	Medium	Unconsolidated
Erro	Cartosio	44.5	199	531	0.65	Broad-leaved forest	Medium	Igneous and metamorphic
Secchia	Ponte Alto	44.44	1420	852	0.74	Broad-leaved forest	Medium	Unconsolidated
Bormida	Piana Crixia	44.38	279	535	1	Broad-leaved forest	Medium	Igneous and metamorphic
Rossenna	Rossenna	44.37	183	940	0.8	Broad-leaved forest	Medium	Unconsolidated
Tanaro	Alba Q.A.	44.35	3437	1281	0.6	Broad-leaved forest	Medium	Igneous and metamorphic
Panaro	Bomporto	44.34	1082	823	0.69	Broad-leaved forest	Medium	Unconsolidated
Tanaro	Farigliano	44.32	1517	1158	0.52	Broad-leaved forest	Medium	Igneous and metamorphic
Scoltenna	Pievepelago	44.2	126	1530	0.38	Broad-leaved forest	Medium	Silicatic
Reno	Vergato	44.17	535	785	0.52	Broad-leaved forest	Medium	Silicatic
Neva	Cisano sul Neva	44.13	128	741	0.69	Broad-leaved forest	Medium	Carbonate
Serchio	Calavorno	44.13	681	919	0.71	Broad-leaved forest	Medium	Silicatic
Lamone	Strada Casale	44.09	200	656	0.85	Broad-leaved forest	Medium	Silicatic
Serchio	Monte S.Quirico	44.09	1254	836	0.5	Broad-leaved forest	Medium	Silicatic
Serchio	Ripafratta	44.07	1401	769	0.48	Broad-leaved forest	Medium	Silicatic
Uso	Santarcangelo	44	112	307	0.96	Crops	Medium	Silicatic
Arno	S. Piero a Ponti	43.97	287	519	0.83	Broad-leaved forest	Medium	Silicatic
Arno	Fornacina 2 ul	43.95	828	563	0.82	Broad-leaved forest	Medium	Silicatic
Arno	Poggio a Caiano	43.94	440	352	0.86	Broad-leaved forest	Medium	Unconsolidated
Savio	S.Carlo	43.92	578	586	0.72	Broad-leaved forest	Medium	Silicatic
Casentino	Subbiano	43.73	750	817	0.72	Broad-leaved forest	Medium	Silicatic
Arno	Ponte di Scandicci	43.67	275	362	1.5	Crops	Medium	Silicatic
Arno	S.Giovanni alla Vena valle	43.58	8601	416	1.06	Broad-leaved forest	Medium	Silicatic
Tevere	SLucia	43.55	937	640	0.86	Broad-leaved forest	Medium	Silicatic
Aspio	Aspio 2	43.54	134	143	1.39	Crops	Medium	Unconsolidated
Carpina	Montone	43.42	133	601	1.19	Broad-leaved forest	Medium	Silicatic
Arno	Incisa Valle	43.41	3414	513	1.05	Broad-leaved forest	Medium	Silicatic
Tevere	Mocaiana	43.39	108	659	1.04	Crops	Medium	Silicatic
Nestore	Trestina	43.35	204	572	1.05	Broad-leaved forest	Medium	Silicatic
Chiascio	Branca	43.32	242	712	0.81	Crops	Medium	Silicatic
Niccone	Migianella	43.27	134	514	1.05	Broad-leaved forest	Medium	Silicatic
Ombrone	Sasso dOmbrone	43.12	2706	425	1.19	Broad-leaved forest	Medium	Silicatic
Topino	Valtopina	43.11	196	745	0.81	Broad-leaved forest	Medium	Silicatic
Tevere	Alviano	43.03	7438	524	1.21	Broad-leaved forest	Medium	Silicatic
Puglia	Collepepe	42.91	162	443	1.25	Crops	Medium	Silicatic
Nera	Ponte Buggianino	42.88	396	1227	1.02	Broad-leaved forest	Medium	Carbonate
Carcaione	Orvieto Scalo	42.83	1306	512	1.07	Broad-leaved forest	Medium	Unconsolidated
Tevere	Cantalupo	42.81	554	550	1.24	Crops	Medium	Carbonate
Tevere	Vallo di Ner	42.79	1238	1126	1.1	Broad-leaved forest	Medium	Carbonate

Tevere	Ponte Felice	42.75	12896	660	0.95	Broad-leaved forest	Medium	Silicatic
Tevere	Torreorsina	42.75	1467	1080	1.07	Broad-leaved forest	Medium	Carbonate
Tevere	Ripetta	42.64	16595	610	1.01	Broad-leaved forest	Medium	Silicatic
Nera	Serravalle	42.64	429	1160	0.98	Broad-leaved forest	Medium	Carbonate
Fiora	Montalto di Castro	42.61	824	421	1.21	Crops	Medium	Igneous and metamorphic
Marta	Tarquinia	42.41	1070	340	1.59	Crops	Coarse	Igneous and metamorphic
Velino	Terria	42.26	2194	1036	0.65	Broad-leaved forest	Medium	Carbonate
Turano	Rocca Sinibalda	42.08	503	1039	0.92	Broad-leaved forest	Medium	Silicatic
Aniene	Lunghezza	41.93	1201	673	0.92	Broad-leaved forest	Medium	Carbonate
Aniene	Ponte Mammolo	41.92	1494	586	0.7	Broad-leaved forest	Medium	Igneous and metamorphic
Liri	Pontecorvo	41.76	3759	737	0.86	Broad-leaved forest	Medium	Carbonate
Melfa	Atina	41.66	169	1071	0.84	Broad-leaved forest	Medium	Carbonate
Rapido	Cassino	41.57	189	627	0.62	Broad-leaved forest	Medium	Carbonate
Ofanto	San Samuele	40.99	2697	499	1.36	Crops	Medium	Silicatic
Bradano	Ponte Bradano	40.75	2999	429	1.52	Crops	Medium	Silicatic
Agri	Ponte La Marmora	40.37	276	975	0.86	Broad-leaved forest	Medium	Silicatic

Appendix C

Table C.1: Shapiro-Wilk rejection frequency for each candidate distribution for monthly SPI12 calculation across the study catchments in Chapter 3.

Gamma	Gumbel	Logistic	Loglogistic	Lognormal	Normal	Weibull
0.62	10.07	20.19	5.31	0.96	12.01	0.87

Appendix D

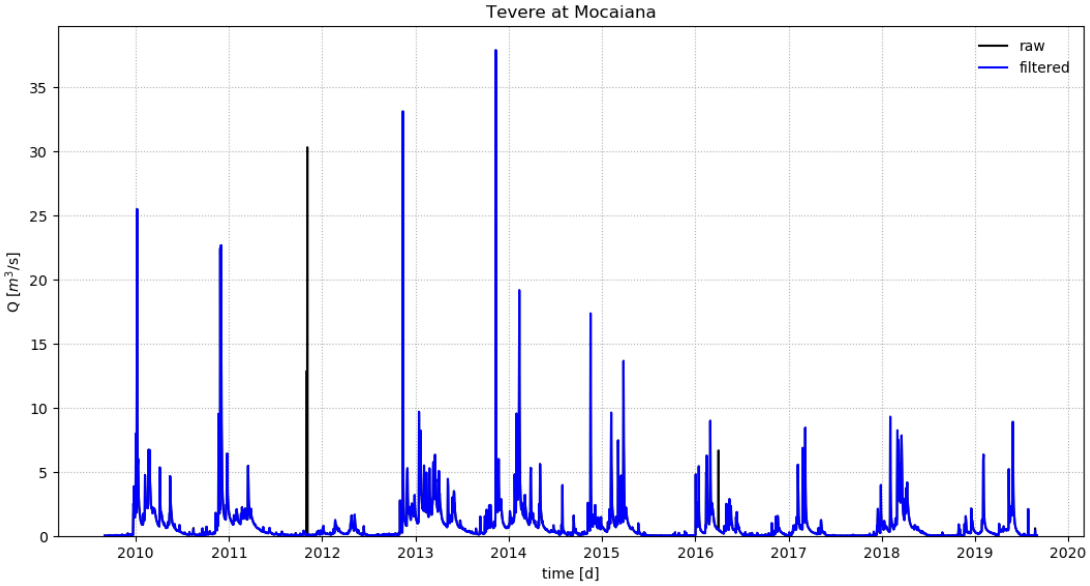

Figure D.1: Example of raw and filtered mean daily discharge (Q) data, according to the quality-check procedure described in Section 3.2.2.1.

Appendix E

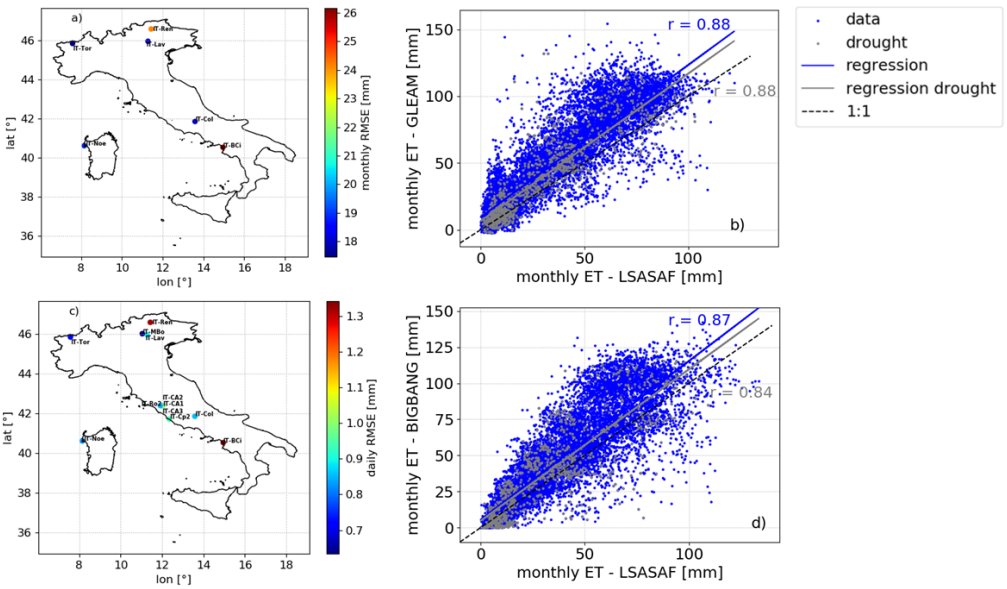

Figure E.1: Multi-dataset evapotranspiration (ET) comparison across the study region: (a) monthly root mean square error (RMSE) over the whole comparison period and (c) daily RMSE for the 2012 drought year between ET data from FLUXNET2015 dataset and LSASAF product at flux tower-scale (site IDs, according to the FLUXNET2015 dataset, are reported); (b) scatterplot between monthly catchment-average ET from LSASAF and GLEAM datasets over the whole comparison period (grey) and drought months (red); (d) same as (b) with catchment-average ET from the BIGBANG dataset on the y axis. Description of datasets is provided in Section 3.2.2.1. In (b) and (d), Pearson correlation coefficients (r) are reported.

Appendix F

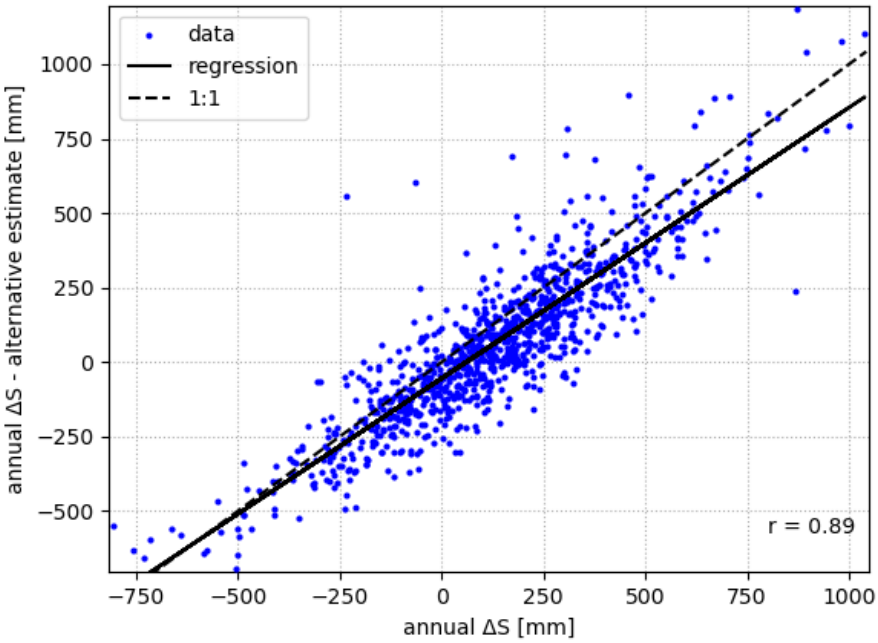

Figure F.1: Scatterplot between annual change in subsurface storage (ΔS) estimates used in in Chapter 3 and alternative estimates. Alternative ΔS estimates are annual residual from precipitation and evapotranspiration data from the BIGBANG dataset, and discharge data collected in this study (Section 3.2.2.1), according to the water balance equation (Equation 3.1). Pearson correlation coefficient (r) is reported.

Appendix G

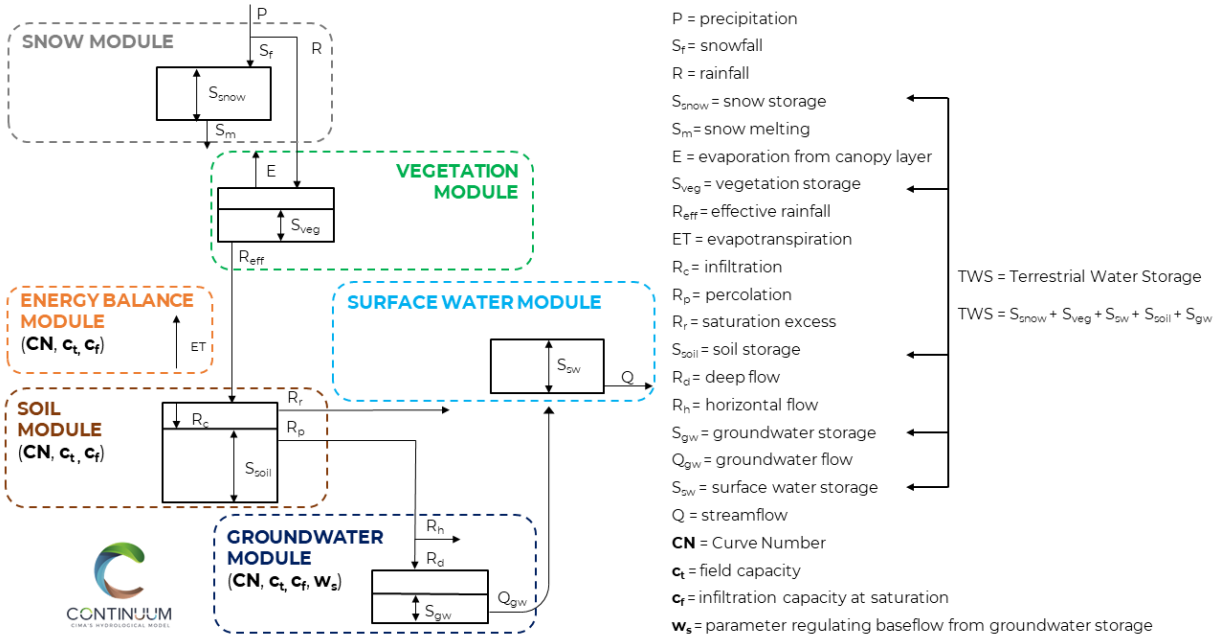

Figure G.1: Diagram of the hydrological model Continuum [198], with model modules, output, states, and calibration parameters (in bold).

Appendix H

Table H.1: Overview of datasets used in Chapter 4.

Variable	Dataset	Reference	Purpose
Digital Elevation Model	HDMA	[114]	Model setup
Hydrological Soil Group	HYSOGs250m	[230]	Model setup
Soil texture	ISRIC SoilGrids	[231]	Model setup
Soil porosity	ESACCI Soil Moisture	[232]	Model setup
Land Cover	ESACCI 2018 Land Cover	[202]	Model setup
Dams	DPC and GranD database	[233] for GranD database	Model setup
Lakes	DPC		Model setup
Glaciers	RGIv6	[158]	Model setup
Meteo data	DPC	[117, 69]	Model simulation
Streamflow	DPC and regional hydrometeorological offices	[69, 205]	Model calibration and evaluation
Evapotranspiration	LSASAF	[122, 123][1]	Model evaluation
Terrestrial Water Storage	GRACE JPL mascon RL06	[209, 210][2]	Model evaluation
Terrestrial Water Storage	GRACE CSR mascon RL06	[207, 208][3]	Model evaluation
Terrestrial Water Storage	GRACE GSFC mascon RL06	[211][4]	Model evaluation

[1] `https://landsaf.ipma.pt/en/products/evapotranspiration-energy-flxs/met/` (last access on 06 October 2022)

[2] `https://podaac-tools.jpl.nasa.gov/drive/files/GeodeticsGravity/tellus/L3/mascon/RL06/JPL/v02/CRI/netcdf` (last access on 06 October 2022)

[3] `http://www2.csr.utexas.edu/grace/RL06_mascons.html` (last access on 06 October 2022)

[4] `https://earth.gsfc.nasa.gov/geo/data/grace-mascons` (last access on 06 October 2022)

Appendix I

Table I.1: Properties of study sub-catchments in Chapter 4: ID, name, location, drainage area [km^2], mean elevation [m a.s.l.], dominant climate and land cover type. For data sources please refer to Table H.1. Sub-catchments are ordered west-to-east.

ID	Section	Basin	Lat	Lon	Area [km^2]	Elev [m a.s.l.]	Climate	Land cover
1	Susa Via Mazzini	Dora Riparia	45.14	7.05	832	2120	Cold	Forest
2	Gaiola	Stura di Demonte	44.33	7.42	562	1744	Cold	Grass
3	Lanzo	Stura di Lanzo	45.27	7.48	580	1767	Cold	Grass
4	Busca	Maira	44.52	7.48	613	1514	Cold	Forest
5	Carignano	Po	44.91	7.69	3957	1021	Temperate no dry	Forest
6	Torino Murazzi	Po	45.07	7.71	5152	971	Temperate no dry	Crop
7	Torino	Dora Riparia	45.08	7.72	1475	1373	Cold	Grass
8	S.Benigno	Orco	45.25	7.81	852	1645	Cold	Grass
9	Tavagnasco	Dora Baltea	45.55	7.82	3297	2124	Alpine	Grass
10	Farigliano	Tanaro	44.52	7.9	1505	916	Temperate dry	Forest
11	Alba Q.A.	Tanaro	44.71	8.03	3468	1313	Temperate dry	Forest
12	Verolengo	Dora Baltea	45.19	8.04	3962	1802	Alpine	Grass
13	Domodossola	Toce	46.11	8.31	954	1928	Alpine	Grass
14	Piana Crixia	Bormida	44.48	8.31	249	610	Temperate dry	Forest
15	Quinto Vercellese Cervo	Sesia	45.38	8.37	840	578	Temperate no dry	Forest
16	Candoglia	Toce	45.97	8.42	1564	1896	Alpine	Grass
17	Cartosio	Erro	44.57	8.42	196	544	Temperate dry	Forest
18	Palestro	Sesia	45.30	8.51	2709	826	Temperate no dry	Forest
19	Vigevano	Ticino	45.34	8.88	7467	1453	Cold	Forest
20	Ponte della Libertà	Ticino	45.18	9.15	8378	1383	Cold	Forest
21	Valsigiara	Trebbia	44.64	9.33	209	959	Cold	Forest
22	Spessa	Po	45.10	9.35	38626	1094	Temperate no dry	Forest
23	Salsominore	Aveto	44.63	9.41	186	1060	Cold	Forest
24	Lodi	Adda	45.32	9.51	6127	1515	Cold	Forest
25	Rivergaro	Trebbia	44.9	9.58	886	820	Cold	Forest
26	Ostia Parmense	Taro	44.51	9.84	422	859	Temperate no dry	Forest
27	Piacenza	Po	45.06	9.71	42090	992	Temperate no dry	Forest
28	Capriolo	Oglio	45.64	9.92	1921	1347	Cold	Forest
29	Cremona	Po	45.13	10.00	51163	1214	Temperate no dry	Forest
30	S.Secondo	Taro	44.92	10.25	1545	645	Temperate no dry	Forest
31	Ponte Verdi	Parma	44.81	10.25	527	649	Temperate no dry	Forest

32	Marcaria	Oglio	45.11	10.53	6085	723	Temperate no dry	Crop
33	Cadelbosco	Crostolo	44.78	10.58	258	247	Temperate no dry	Crop
34	Borgoforte	Po	45.04	10.75	63575	954	Temperate no dry	Forest
35	Ponte Alto	Secchia	44.67	10.9	1174	743	Temperate no dry	Forest
36	Pioppa	Secchia	44.86	10.97	1330	661	Temperate no dry	Forest
37	Ficarolo	Po	44.95	11.43	69315	867	Temperate no dry	Forest
38	Pontelagoscuro	Po	44.89	11.61	72545	832	Temperate no dry	Forest

Appendix J

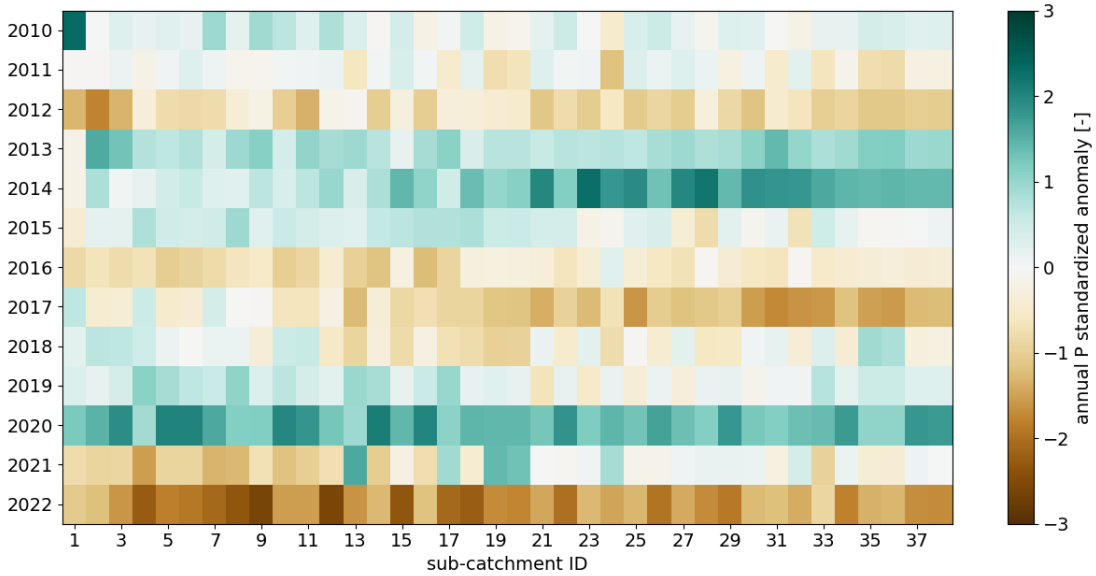

Figure J.1: Annual P standardized anomalies (Equation 4.1) for each study sub-catchment in Chapter 4 (ordered west-to-east, from the left to the right end side) over the study period.

Appendix K

Table K.1: Kling Gupta Efficiency (KGE) [213] for calibration and evaluation periods for each study sub-catchment in Chapter 4 (Table I.1). KGE_1 refers to calibration experiment 1 and KGE_2 refers to calibration experiment 2(Section 4.2.4.1).

ID	KGE_1	$KGE_{1,whole}$	$KGE_{1,wet}$	$KGE_{1,moderate}$	$KGE_{1,severe}$	KGE_2	$KGE_{2,whole}$	$KGE_{2,wet}$	$KGE_{2,moderate}$	$KGE_{2,severe}$
1	-	0.58	0.48	0.43	0.01	-	0.53	0.46	0.49	<0
2	0.52	0.58	0.52	0.31	0.31	0.47	0.55	0.51	0.41	0.17
3	0.47	0.67	0.71	0.47	0.34	<0	0.67	0.76	0.51	0.32
4	-	0.49	0.32	0.69	0.1	-	0.63	0.49	0.59	<0
5	0.85	0.85	0.74	0.48	<0	0.74	0.82	0.88	0.67	0.63
6	0.81	0.86	0.7	0.59	0.11	0.62	0.79	0.85	0.62	0.4
7	-	0.47	0.33	0.08	<0	-	0.58	0.46	0.37	<0
8	-	0.79	0.86	0.84	<0	-	0.76	0.81	0.76	<0
9	0.71	0.74	0.67	0.72	0.65	0.7	0.69	0.63	0.68	0.6
10	0.84	0.81	0.85	0.64	0.43	0.58	0.76	0.84	0.56	0.28
11	0.79	0.89	0.79	0.71	0.07	0.59	0.85	0.81	0.62	0.57
12	-	0.39	0.34	0.29	<0	-	0.45	0.36	0.28	<0
13	-	0.38	0.37	<0	<0	-	0.39	0.38	<0	<0
14	-	0.28	0.29	0.28	<0	-	0.02	0.01	<0	<0
15	-	0.54	0.43	0.2	0.51	-	0.63	0.61	0.71	0.68
16	-	0.55	0.45	0.5	0.19	-	0.57	0.51	0.55	0.26
17	0.55	0.83	0.96	0.9	0.46	0.25	0.7	0.87	0.52	0.39
18	0.74	0.7	0.52	0.84	<0	0.08	0.6	0.44	0.6	¡0
19	-	0.85	0.79	0.71	0.77	-	0.79	0.73	0.78	0.62
20	-	0.89	0.74	0.75	0.77	-	0.84	0.64	0.76	0.64
21	0.46	0.89	0.91	0.69	0.47	<0	0.82	0.92	0.6	0.27
22	0.87	0.85	0.71	0.76	0.7	0.84	0.89	0.91	0.76	0.64
23	<0	0.4	<0	0.59	<0	0.67	0.35	<0	0.8	0.1
24	-	0.77	0.76	0.32	0.66	-	0.74	0.82	0.06	0.59
25	-	0.78	0.73	0.64	<0	-	0.84	0.77	0.58	0.37
26	0.54	0.94	0.89	0.83	0.82	0.2	0.89	0.88	0.77	0.74
27	-	0.88	0.76	0.72	0.68	-	0.87	0.89	0.76	0.61
28	-	0.44	0.39	0.16	<0	-	0.51	0.49	0.21	<0
29	0.81	0.78	0.68	0.71	0.83	0.78	0.91	0.95	0.76	0.61
30	0.46	0.81	0.86	0.71	0.51	0.25	0.69	0.76	0.36	0.61
31	0.23	0.67	0.76	0.69	0.42	0.44	0.57	0.72	0.46	0.38

32	-	0.67	0.56	0.46	<0	-	0.63	0.53	0.24	<0
33	-	0.34	<0	<0	<0	-	0.14	<0	<0	<0
34	-	0.81	0.66	0.72	0.85	-	0.88	0.96	0.69	0.67
35	0.67	0.81	0.83	0.43	0.65	0.12	0.67	0.81	0.3	0.46
36	-	0.78	0.87	0.52	0.76	-	0.62	0.74	0.38	0.49
37	-	0.83	0.63	0.74	0.81	-	0.86	0.95	0.65	0.61
38	0.79	0.81	0.58	0.77	0.82	0.71	0.88	0.94	0.64	0.64

Appendix L

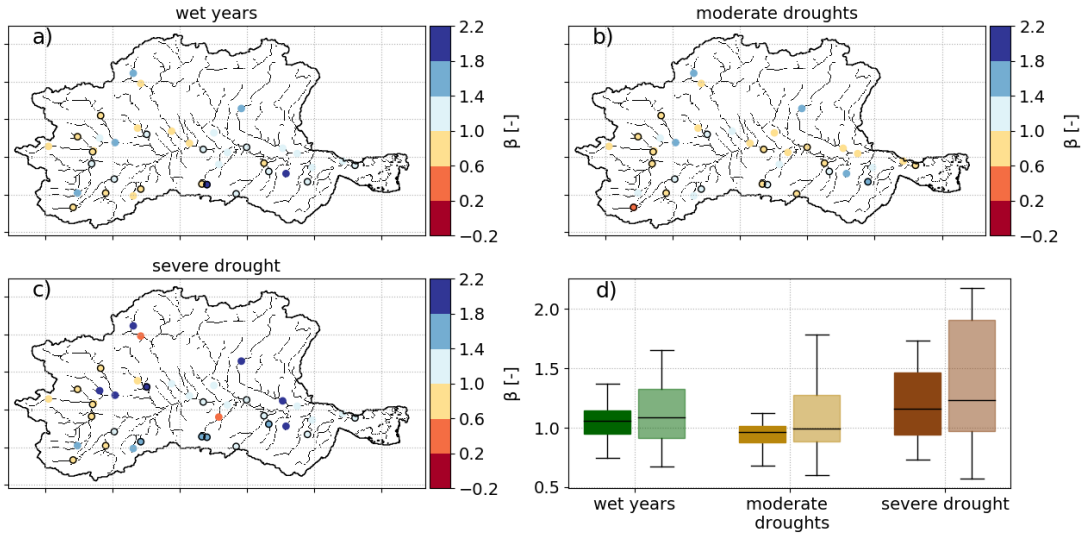

Figure L.1: Values of the bias component (β) of the Kling Gupta Efficiency (KGE [213]) on monthly Q during (a) wet years, (b) moderate droughts, and (c) the severe drought for each study sub-catchment in Chapter 4, and (d) their distributions as boxplots grouped by calibration and evaluation sub-catchments (shaded boxplots), from the model calibrated during ”normal” climatic conditions (Section 4.2.4.1).

Appendix M

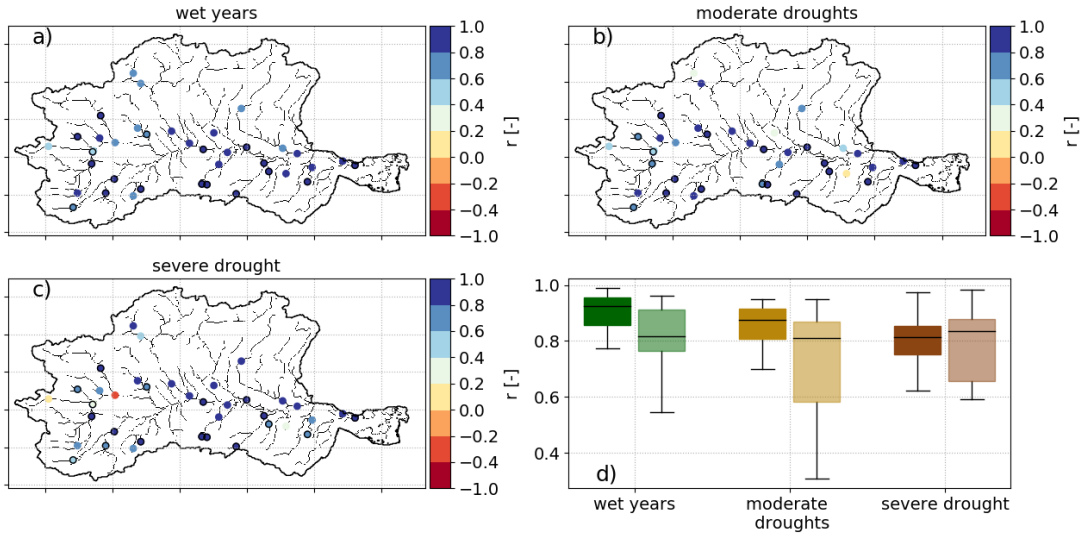

Figure M.1: Same as L.1, but for the r component of KGE (Equation 4.2).

Appendix N

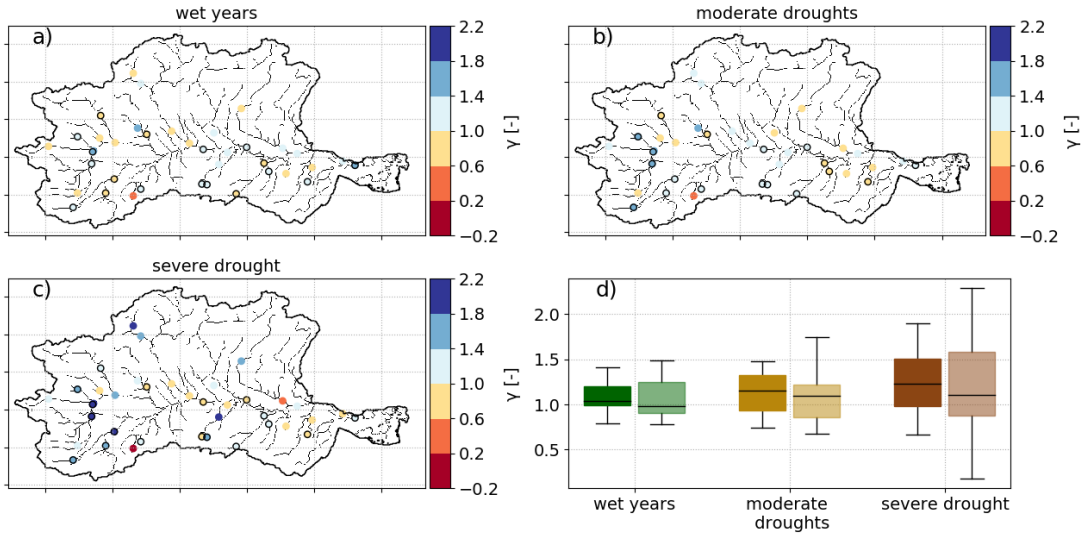

Figure N.1: Same as L.1, but for the γ component of KGE (Equation 4.2).

Appendix O

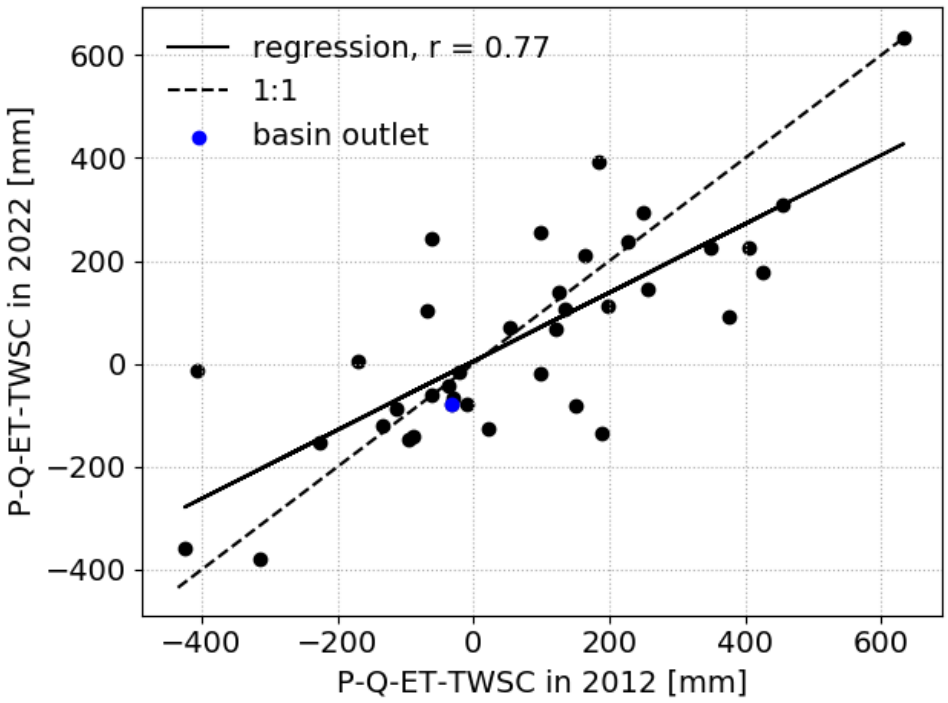

Figure O.1: Scatterplot between the observed imbalance (P-Q-ET-TWSC) in 2012 and 2022 for each study sub-catchment (black) and the basin outlet (blue) in Chapter 4. P, Q, ET, and TWSC are the annual precipitation, streamflow, evapotranspiration, and changes in Terrestrial Water Storage.

Bibliography

[1] L. M. Tallaksen, H. A. Van Lanen, Hydrological drought: processes and estimation methods for streamflow and groundwater (2004).

[2] A. Toreti, D. Bavera, J. Acosta Navarro, C. Cammalleri, A. de Jager, C. Di Ciollo, A. Hrast Essenfelder, W. Maetens, D. Magni, D. Masante, M. Mazzeschi, S. Niemeyer, J. Spinoni, Drought in europe august 2022 (JRC130493) (2022). doi:doi:10.2760/264241.

[3] A. J. Teuling, A. F. Van Loon, S. I. Seneviratne, I. Lehner, M. Aubinet, B. Heinesch, C. Bernhofer, T. Grünwald, H. Prasse, U. Spank, Evapotranspiration amplifies european summer drought, Geophysical Research Letters 40 (10) (2013) 2071–2075.

[4] M. Ionita, L. M. Tallaksen, D. G. Kingston, J. H. Stagge, G. Laaha, H. A. Van Lanen, P. Scholz, S. M. Chelcea, K. Haslinger, The european 2015 drought from a climatological perspective, Hydrology and Earth System Sciences 21 (3) (2017) 1397–1419.

[5] M. I. Brunner, K. Liechti, M. Zappa, Extremeness of recent drought events in switzerland: dependence on variable and return period choice, Natural Hazards and Earth System Sciences 19 (10) (2019) 2311–2323.

[6] C. Soulsby, B. Scheliga, A. Neill, J.-C. Comte, D. Tetzlaff, A longer-term perspective on soil moisture, groundwater and stream flow response to the 2018 drought in an experimental catchment in the scottish highlands, Hydrological Processes 35 (6) (2021) e14206.

[7] A. Toreti, A. Belward, I. Perez-Dominguez, G. Naumann, J. Luterbacher, O. Cronie, L. Seguini, G. Manfron, R. Lopez-Lozano, B. Baruth, et al., The exceptional 2018 european water seesaw calls for action on adaptation, Earth's Future 7 (6) (2019) 652–663.

[8] X. Yang, D. Tetzlaff, C. Soulsby, A. Smith, D. Borchardt, Catchment functioning under prolonged drought stress: Tracer-aided ecohydrological modeling in an intensively managed agricultural catchment, Water Resources Research 57 (3) (2021) e2020WR029094.

[9] O. Rakovec, L. Samaniego, V. Hari, Y. Markonis, V. Moravec, S. Thober, M. Hanel, R. Kumar, The 2018–2020 multi-year drought sets a new benchmark in europe, Earth's Future 10 (3) (2022) e2021EF002394.

[10] K. van der Wiel, T. J. Batelaan, N. Wanders, Large increases of multi-year droughts in north-western europe in a warmer climate, Climate Dynamics (2022) 1–20.

[11] M. Saft, A. W. Western, L. Zhang, M. C. Peel, N. J. Potter, The influence of multiyear drought on the annual rainfall-runoff relationship: An australian perspective, Water Resources Research 51 (4) (2015) 2444–2463.

[12] C. Alvarez-Garreton, J. P. Boisier, R. Garreaud, J. Seibert, M. Vis, Progressive water deficits during multiyear droughts in basins with long hydrological memory in chile, Hydrology and Earth System Sciences 25 (1) (2021) 429–446.

[13] F. Avanzi, J. Rungee, T. Maurer, R. Bales, Q. Ma, S. Glaser, M. Conklin, Climate elasticity of evapotranspiration shifts the water balance of mediterranean climates during multi-year droughts, Hydrology and Earth System Sciences 24 (9) (2020) 4317–4337.

[14] S. D. Schubert, M. J. Suarez, P. J. Pegion, R. D. Koster, J. T. Bacmeister, On the cause of the 1930s dust bowl, Science 303 (5665) (2004) 1855–1859.

[15] L. Kuil, G. Carr, A. Prskawetz, J. L. Salinas, A. Viglione, G. Blöschl, Learning from the ancient maya: Exploring the impact of drought on population dynamics, Ecological Economics 157 (2019) 1–16.

[16] A. Harpold, M. Dettinger, S. Rajagopal, Defining snow drought and why it matters, eos, 98, Eos 98 (2017).

[17] A. F. Van Loon, Hydrological drought explained, Wiley Interdisciplinary Reviews: Water 2 (4) (2015) 359–392.

[18] S. Parry, C. Prudhomme, R. L. Wilby, P. J. Wood, Drought termination: Concept and characterisation, Progress in Physical Geography 40 (6) (2016) 743–767.

[19] S. Parry, R. L. Wilby, C. Prudhomme, P. J. Wood, A systematic assessment of drought termination in the united kingdom, Hydrology and Earth System Sciences 20 (10) (2016) 4265–4281.

[20] J. Margariti, S. Rangecroft, S. Parry, D. Wendt, A. Van Loon, Anthropogenic activities alter drought termination, Elementa: Science of the Anthropocene 7 (2019).

[21] J.-C. Domec, D. M. Johnson, Does homeostasis or disturbance of homeostasis in minimum leaf water potential explain the isohydric versus anisohydric behavior of vitis vinifera l. cultivars?, Tree physiology 32 (3) (2012) 245–248.

[22] A. Van Loon, G. Laaha, Hydrological drought severity explained by climate and catchment characteristics, Journal of hydrology 526 (2015) 3–14.

[23] A. F. Van Loon, K. Stahl, G. Di Baldassarre, J. Clark, S. Rangecroft, N. Wanders, T. Gleeson, A. I. Van Dijk, L. M. Tallaksen, J. Hannaford, et al., Drought in a human-modified world: reframing drought definitions, understanding, and analysis approaches, Hydrology and Earth System Sciences 20 (9) (2016) 3631–3650.

[24] A. AghaKouchak, A. Mirchi, K. Madani, G. Di Baldassarre, A. Nazemi, A. Alborzi, H. Anjileli, M. Azarderakhsh, F. Chiang, E. Hassanzadeh, et al., Anthropogenic drought: Definition, challenges, and opportunities (2021).

[25] S. D. Crausbay, A. R. Ramirez, S. L. Carter, M. S. Cross, K. R. Hall, D. J. Bathke, J. L. Betancourt, S. Colt, A. E. Cravens, M. S. Dalton, et al., Defining ecological drought for the twenty-first century, Bulletin of the American Meteorological Society 98 (12) (2017) 2543–2550.

[26] UNDRR, Gar special report on drought 2021 (2021).

[27] A. K. Mishra, V. P. Singh, A review of drought concepts, Journal of hydrology 391 (1-2) (2010) 202–216.

[28] X. Zhang, N. Chen, H. Sheng, C. Ip, L. Yang, Y. Chen, Z. Sang, T. Tadesse, T. P. Y. Lim, A. Rajabifard, et al., Urban drought challenge to 2030 sustainable development goals, Science of the Total Environment 693 (2019) 133536.

[29] I. Meza, S. Siebert, P. Döll, J. Kusche, C. Herbert, E. Eyshi Rezaei, H. Nouri, H. Gerdener, E. Popat, J. Frischen, et al., Global-scale drought risk assessment for agricultural systems, Natural Hazards and Earth System Sciences 20 (2) (2020) 695–712.

[30] M. T. Van Vliet, J. Sheffield, D. Wiberg, E. F. Wood, Impacts of recent drought and warm years on water resources and electricity supply worldwide, Environmental Research Letters 11 (12) (2016) 124021.

[31] M. L. Goulden, R. C. Bales, California forest die-off linked to multi-year deep soil drying in 2012–2015 drought, Nature Geoscience 12 (8) (2019) 632–637.

[32] M. Van Vliet, F. Ludwig, J. Zwolsman, G. Weedon, P. Kabat, Global river temperatures and sensitivity to atmospheric warming and changes in river flow, Water Resources Research 47 (2) (2011).

[33] E. Wolff, M. T. van Vliet, Impact of the 2018 drought on pharmaceutical concentrations and general water quality of the rhine and meuse rivers, Science of the Total Environment 778 (2021) 146182.

[34] D. Maxwell, M. Fitzpatrick, The 2011 somalia famine: Context, causes, and complications, Global Food Security 1 (1) (2012) 5–12.

[35] G. E. Charnley, I. Kelman, K. A. Murray, Drought-related cholera outbreaks in africa and the implications for climate change: a narrative review, Pathogens and Global Health 116 (1) (2022) 3–12.

[36] S. Adaawen, C. Rademacher-Schulz, B. Schraven, N. Segadlo, Drought, migration, and conflict in sub-saharan africa: what are the links and policy options?, Current directions in water scarcity research 2 (2019) 15–31.

[37] N. Von Uexkull, M. Croicu, H. Fjelde, H. Buhaug, Civil conflict sensitivity to growing-season drought, Proceedings of the National Academy of Sciences 113 (44) (2016) 12391–12396.

[38] UNCCD, Gender mainstreaming in drought management (2021).

[39] E. K. Austin, T. Handley, A. S. Kiem, J. L. Rich, T. J. Lewin, H. H. Askland, S. S. Askarimarnani, D. A. Perkins, B. J. Kelly, Drought-related stress among farmers: findings from the australian rural mental health study, Medical Journal of Australia 209 (4) (2018) 159–165.

[40] S. J. Sutanto, C. Vitolo, C. Di Napoli, M. D'Andrea, H. A. Van Lanen, Heatwaves, droughts, and fires: Exploring compound and cascading dry hazards at the pan-european scale, Environment international 134 (2020) 105276.

[41] M. M. de Brito, Compound and cascading drought impacts do not happen by chance: A proposal to quantify their relationships, Science of the Total Environment 778 (2021) 146236.

[42] J. V. Vogt, G. Naumann, D. Masante, J. Spinoni, C. Cammalleri, W. Erian, F. Pischke, R. Pulwarty, P. Barbosa, Drought risk assessment and management: A conceptual framework (2018).

[43] U. Cred, Human cost of disasters. an overview of the last 20 years: 2000–2019, CRED, UNDRR, Geneva (2020).

[44] M. I. Brunner, D. L. Swain, E. Gilleland, A. W. Wood, Increasing importance of temperature as a contributor to the spatial extent of streamflow drought, Environmental Research Letters 16 (2) (2021) 024038.

[45] A. Baronetti, J. C. González-Hidalgo, S. M. Vicente-Serrano, F. Acquaotta, S. Fratianni, A weekly spatio-temporal distribution of drought events over the po plain (north italy) in the last five decades, International Journal of Climatology 40 (10) (2020) 4463–4476.

[46] G. G. Haile, Q. Tang, S.-M. Hosseini-Moghari, X. Liu, T. Gebremicael, G. Leng, A. Kebede, X. Xu, X. Yun, Projected impacts of climate change on drought patterns over east africa, Earth's Future 8 (7) (2020) e2020EF001502.

[47] L. Samaniego, S. Thober, R. Kumar, N. Wanders, O. Rakovec, M. Pan, M. Zink, J. Sheffield, E. F. Wood, A. Marx, Anthropogenic warming exacerbates european soil moisture droughts, Nature Climate Change 8 (5) (2018) 421–426.

[48] M. Dembélé, M. Vrac, N. Ceperley, S. J. Zwart, J. Larsen, S. J. Dadson, G. Mariéthoz, B. Schaefli, Contrasting changes in hydrological processes of the volta river basin under global warming, Hydrology and earth system sciences 26 (5) (2022) 1481–1506.

[49] IPCC, Climate change 2022: Impacts, adaptation and vulnerability. contribution of working group ii to the sixth assessment report of the intergovernmental panel on climate change (2022) 3056pp.

[50] A. Baronetti, V. Dubreuil, A. Provenzale, S. Fratianni, Future droughts in northern italy: high-resolution projections using euro-cordex and med-cordex ensembles, Climatic Change 172 (3-4) (2022) 22.

[51] G. Naumann, C. Cammalleri, L. Mentaschi, L. Feyen, Increased economic drought impacts in europe with anthropogenic warming, Nature Climate Change 11 (6) (2021) 485–491.

[52] S. J. Sutanto, M. van der Weert, N. Wanders, V. Blauhut, H. A. Van Lanen, Moving from drought hazard to impact forecasts, Nature Communications 10 (1) (2019) 1–7.

[53] C. Cammalleri, P. Barbosa, J. Vogt, Evaluating simulated daily discharge for operational hydrological drought monitoring in the global drought observatory (gdo), Hydrological Sciences Journal 65 (8) (2020) 1316–1325.

[54] K. Wang, R. E. Dickinson, A review of global terrestrial evapotranspiration: Observation, modeling, climatology, and climatic variability, Reviews of Geophysics 50 (2) (2012).

[55] D. Baldocchi, E. Falge, L. Gu, R. Olson, D. Hollinger, S. Running, P. Anthoni, C. Bernhofer, K. Davis, R. Evans, et al., Fluxnet: A new tool to study the temporal and spatial variability of ecosystem-scale carbon dioxide, water vapor, and energy flux densities, Bulletin of the American Meteorological Society 82 (11) (2001) 2415–2434.

[56] S. I. Seneviratne, I. Lehner, J. Gurtz, A. J. Teuling, H. Lang, U. Moser, D. Grebner, L. Menzel, K. Schroff, T. Vitvar, et al., Swiss prealpine rietholzbach research catchment and lysimeter: 32 year time series and 2003 drought event, Water Resources Research 48 (6) (2012).

[57] J. W. Roche, Q. Ma, J. Rungee, R. C. Bales, Evapotranspiration mapping for forest management in california's sierra nevada, Frontiers in Forests and Global Change 3 (2020) 69.

[58] D. Duethmann, G. Blöschl, Why has catchment evaporation increased in the past 40 years? a data-based study in austria, Hydrology and Earth System Sciences 22 (10) (2018) 5143–5158.

[59] M. Zhao, Y. Liu, A. G. Konings, et al., Evapotranspiration frequently increases during droughts, Nature Climate Change (2022) 1–7.

[60] R. C. Bales, M. L. Goulden, C. T. Hunsaker, M. H. Conklin, P. C. Hartsough, A. T. O'Geen, J. W. Hopmans, M. Safeeq, Mechanisms controlling the impact of multi-year drought on mountain hydrology, Scientific reports 8 (1) (2018) 1–8.

[61] I. Pechlivanidis, B. Jackson, N. Mcintyre, H. Wheater, et al., Catchment scale hydrological modelling: A review of model types, calibration approaches and uncertainty analysis methods in the context of recent developments in technology and applications, Global NEST journal 13 (3) (2011) 193–214.

[62] M. I. Brunner, A. Bárdossy, R. Furrer, Stochastic simulation of streamflow time series using phase randomization, Hydrology and Earth System Sciences 23 (8) (2019) 3175–3187.

[63] S. M. Hauswirth, M. F. Bierkens, V. Beijk, N. Wanders, The potential of data driven approaches for quantifying hydrological extremes, Advances in Water Resources 155 (2021) 104017.

[64] S. Fatichi, E. R. Vivoni, F. L. Ogden, V. Y. Ivanov, B. Mirus, D. Gochis, C. W. Downer, M. Camporese, J. H. Davison, B. Ebel, et al., An overview of current applications, challenges, and future trends in distributed process-based models in hydrology, Journal of Hydrology 537 (2016) 45–60.

[65] S. Kuppel, D. Tetzlaff, M. P. Maneta, C. Soulsby, Ech 2 o-iso 1.0: Water isotopes and age tracking in a process-based, distributed ecohydrological model, Geoscientific Model Development 11 (7) (2018) 3045–3069.

[66] M. Dembélé, N. Ceperley, S. J. Zwart, E. Salvadore, G. Mariethoz, B. Schaefli, Potential of satellite and reanalysis evaporation datasets for hydrological modelling under various model calibration strategies, Advances in Water Resources 143 (2020) 103667.

[67] D. Duethmann, A. Smith, C. Soulsby, L. Kleine, W. Wagner, S. Hahn, D. Tetzlaff, Evaluating satellite-derived soil moisture data for improving the internal consistency of process-based ecohydrological modelling, Journal of Hydrology 614 (2022) 128462.

[68] P. Hulsman, H. H. Savenije, M. Hrachowitz, Learning from satellite observations: increased understanding of catchment processes through stepwise model improvement, Hydrology and Earth System Sciences 25 (2) (2021) 957–982.

[69] L. Alfieri, F. Avanzi, F. Delogu, S. Gabellani, G. Bruno, L. Campo, A. Libertino, C. Massari, A. Tarpanelli, D. Rains, et al., High-resolution satellite products improve hydrological modeling in northern italy, Hydrology and Earth System Sciences 26 (14) (2022) 3921–3939.

[70] R. Rigon, G. Formetta, M. Bancheri, N. Tubini, C. D'Amato, O. David, C. Massari, Hess opinions: Participatory digital earth twin hydrology systems (darths) for everyone: a blueprint for hydrologists, Hydrology and Earth System Sciences Discussions (2022) 1–38.

[71] B. W. Abbott, K. Bishop, J. P. Zarnetske, C. Minaudo, F. Chapin, S. Krause, D. M. Hannah, L. Conner, D. Ellison, S. E. Godsey, et al., Human domination of the global water cycle absent from depictions and perceptions, Nature Geoscience 12 (7) (2019) 533–540.

[72] N. Addor, H. X. Do, C. Alvarez-Garreton, G. Coxon, K. Fowler, P. A. Mendoza, Large-sample hydrology: recent progress, guidelines for new datasets and grand challenges, Hydrological Sciences Journal 65 (5) (2020) 712–725.

[73] Y. Wada, M. F. Bierkens, A. De Roo, P. A. Dirmeyer, J. S. Famiglietti, N. Hanasaki, M. Konar, J. Liu, H. Müller Schmied, T. Oki, et al., Human–water interface in hydrological modelling: current status and future directions, Hydrology and Earth System Sciences 21 (8) (2017) 4169–4193.

[74] M. I. Brunner, L. Slater, L. M. Tallaksen, M. Clark, Challenges in modeling and predicting floods and droughts: A review, Wiley Interdisciplinary Reviews: Water 8 (3) (2021) e1520.

[75] W. M. Organization, Standardized precipitation index user guide, World Meteorological Organization (1090) (2012).

[76] L. J. Barker, J. Hannaford, A. Chiverton, C. Svensson, From meteorological to hydrological drought using standardised indicators, Hydrology and Earth System Sciences 20 (6) (2016) 2483–2505.

[77] V. M. Yevjevich, Objective approach to definitions and investigations of continental hydrologic droughts, an, Ph.D. thesis, Colorado State University. Libraries (1967).

[78] T. B. McKee, N. J. Doesken, J. Kleist, et al., The relationship of drought frequency and duration to time scales, in: Proceedings of the 8th Conference on Applied Climatology, Vol. 17, Boston, MA, USA, 1993, pp. 179–183.

[79] S. M. Vicente-Serrano, S. Beguería, J. I. López-Moreno, A multiscalar drought index sensitive to global warming: the standardized precipitation evapotranspiration index, Journal of climate 23 (7) (2010) 1696–1718.

[80] S. M. Vicente-Serrano, J. I. López-Moreno, S. Beguería, J. Lorenzo-Lacruz, C. Azorin-Molina, E. Morán-Tejeda, Accurate computation of a streamflow drought index, Journal of Hydrologic Engineering 17 (2) (2012) 318–332.

[81] H. Carrão, S. Russo, G. Sepulcre-Canto, P. Barbosa, An empirical standardized soil moisture index for agricultural drought assessment from remotely sensed data, International journal of applied earth observation and geoinformation 48 (2016) 74–84.

[82] J. Bloomfield, B. Marchant, Analysis of groundwater drought building on the standardised precipitation index approach, Hydrology and Earth System Sciences 17 (12) (2013) 4769–4787.

[83] A. Zargar, R. Sadiq, B. Naser, F. I. Khan, A review of drought indices, Environmental Reviews 19 (NA) (2011) 333–349.

[84] S. Kchouk, L. A. Melsen, D. W. Walker, P. R. van Oel, A geography of drought indices: mismatch between indicators of drought and its impacts on water and food securities, Natural Hazards and Earth System Sciences 22 (2) (2022) 323–344.

[85] A. F. Van Loon, H. A. Van Lanen, A process-based typology of hydrological drought, Hydrology and Earth System Sciences 16 (7) (2012) 1915–1946.

[86] M. Staudinger, K. Stahl, J. Seibert, A drought index accounting for snow, Water Resources Research 50 (10) (2014) 7861–7872.

[87] C. Cammalleri, C. Arias-Muñoz, P. Barbosa, A. de Jager, D. Magni, D. Masante, M. Mazzeschi, N. McCormick, G. Naumann, J. Spinoni, et al., A revision of the combined drought indicator (cdi) used in the european drought observatory (edo), Natural Hazards and Earth System Sciences 21 (2) (2021) 481–495.

[88] A. F. Van Loon, H. A. Van Lanen, A process-based typology of hydrological drought, Hydrology and Earth System Sciences 16 (7) (2012) 1915–1946.

[89] A. Van Loon, S. Ploum, J. Parajka, A. Fleig, E. Garnier, G. Laaha, H. Van Lanen, Hydrological drought types in cold climates: quantitative analysis of causing factors and qualitative survey of impacts, Hydrology and Earth System Sciences 19 (4) (2015) 1993–2016.

[90] H. K. McMillan, A review of hydrologic signatures and their applications, Wiley Interdisciplinary Reviews: Water 8 (1) (2021) e1499.

[91] R. Orth, G. Destouni, Drought reduces blue-water fluxes more strongly than green-water fluxes in europe, Nature communications 9 (1) (2018) 1–8.

[92] T. Mastrotheodoros, C. Pappas, P. Molnar, P. Burlando, G. Manoli, J. Parajka, R. Rigon, B. Szeles, M. Bottazzi, P. Hadjidoukas, et al., More green and less blue water in the alps during warmer summers, Nature Climate Change 10 (2) (2020) 155–161.

[93] L. Melsen, B. Guse, Hydrological drought simulations: How climate and model structure control parameter sensitivity, Water Resources Research 55 (12) (2019) 10527–10547.

[94] M. Staudinger, K. Stahl, J. Seibert, M. Clark, L. Tallaksen, Comparison of hydrological model structures based on recession and low flow simulations, Hydrology and Earth System Sciences 15 (11) (2011) 3447–3459.

[95] V. Klemeš, Operational testing of hydrological simulation models, Hydrological sciences journal 31 (1) (1986) 13–24.

[96] D. Duethmann, G. Blöschl, J. Parajka, Why does a conceptual hydrological model fail to correctly predict discharge changes in response to climate change?, Hydrology and Earth System Sciences 24 (7) (2020) 3493–3511.

[97] M. Saft, M. C. Peel, A. W. Western, J.-M. Perraud, L. Zhang, Bias in streamflow projections due to climate-induced shifts in catchment response, Geophysical Research Letters 43 (4) (2016) 1574–1581.

[98] A. Van Loon, M. Van Huijgevoort, H. Van Lanen, Evaluation of drought propagation in an ensemble mean of large-scale hydrological models, Hydrology and Earth System Sciences 16 (11) (2012) 4057–4078.

[99] A. Kumar, S. N. Gosling, M. F. Johnson, M. D. Jones, J. Zaherpour, R. Kumar, G. Leng, H. M. Schmied, J. Kupzig, L. Breuer, et al., Multi-model evaluation of catchment-and global-scale hydrological model simulations of drought characteristics across eight large river catchments, Advances in Water Resources (2022) 104212.

[100] T. R. Saha, P. K. Shrestha, O. Rakovec, S. Thober, L. Samaniego, A drought monitoring tool for south asia, Environmental Research Letters 16 (5) (2021) 054014.

[101] S. Gabellani, R. Rudari, L. Rossi, Assessing floods and droughts direct impacts in subsaharan africa by using a regional hydrologic model: a fully probabilistic approach, in: EGU General Assembly Conference Abstracts, 2021, pp. EGU21–7585.

[102] K. Fowler, W. Knoben, M. Peel, T. Peterson, D. Ryu, M. Saft, K.-W. Seo, A. Western, Many commonly used rainfall-runoff models lack long, slow dynamics: Implications for runoff projections, Water Resources Research 56 (5) (2020) e2019WR025286.

[103] K. J. Fowler, G. Coxon, J. E. Freer, W. J. Knoben, M. C. Peel, T. Wagener, A. W. Western, R. A. Woods, L. Zhang, Towards more realistic runoff projections by removing limits on simulated soil moisture deficit, Journal of Hydrology 600 (2021) 126505.

[104] O. Rakovec, R. Kumar, J. Mai, M. Cuntz, S. Thober, M. Zink, S. Attinger, D. Schäfer, M. Schrön, L. Samaniego, Multiscale and multivariate evaluation of water fluxes and states over european river basins, Journal of Hydrometeorology 17 (1) (2016) 287–307.

[105] S. Bolaños Chavarría, M. Werner, J. F. Salazar, T. Betancur Vargas, Benchmarking global hydrological and land surface models against grace in a medium-sized tropical basin, Hydrology and Earth System Sciences 26 (16) (2022) 4323–4344.

[106] M. I. Brunner, A. F. Van Loon, K. Stahl, Moderate and severe hydrological droughts in europe differ in their hydrometeorological drivers, Water Resources Research 58 (10) (2022) e2022WR032871.

[107] K. Fowler, M. Peel, M. Saft, T. Peterson, A. Western, L. Band, C. Petheram, S. Dharmadi, K. S. Tan, L. Zhang, et al., Explaining changes in rainfall-runoff relationships during and after australia's millennium drought: a community perspective, Hydrology and Earth System Sciences Discussions (2022) 1–56.

[108] M. Saft, M. C. Peel, A. W. Western, L. Zhang, Predicting shifts in rainfall-runoff partitioning during multiyear drought: Roles of dry period and catchment characteristics, Water Resources Research 52 (12) (2016) 9290–9305.

[109] M. I. Brunner, L. M. Tallaksen, Proneness of european catchments to multiyear streamflow droughts, Water Resources Research 55 (11) (2019) 8881–8894.

[110] K. Fowler, M. Peel, M. Saft, R. Nathan, A. Horne, R. Wilby, C. McCutcheon, T. Peterson, Hydrological shifts threaten water resources, Water Resources Research 58 (8) (2022) e2021WR031210.

[111] P. Billi, M. Fazzini, Global change and river flow in italy, Global and Planetary Change 155 (2017) 234–246.

[112] H. E. Beck, N. E. Zimmermann, T. R. McVicar, N. Vergopolan, A. Berg, E. F. Wood, Present and future köppen-geiger climate classification maps at 1-km resolution, Scientific data 5 (1) (2018) 1–12.

[113] R. Seager, T. J. Osborn, Y. Kushnir, I. R. Simpson, J. Nakamura, H. Liu, Climate variability and change of mediterranean-type climates, Journal of Climate 32 (10) (2019) 2887–2915.

[114] K. L. Verdin, Hydrologic derivatives for modeling and analysis—a new global high-resolution database, Tech. rep., US Geological Survey (2017).

[115] R. Hiederer, Mapping soil properties for europe—spatial representation of soil database attributes, Luxembourg: Publications Office of the European Union (2013).

[116] R. Hiederer, Mapping soil typologies-spatial decision support applied to european soil database, EUR25932EN Scientific and Technical Research Series (2013) 1831–9424.

[117] G. Bruno, F. Pignone, F. Silvestro, S. Gabellani, F. Schiavi, N. Rebora, P. Giordano, M. Falzacappa, Performing hydrological monitoring at a national scale by exploiting rain-gauge and radar networks: The italian case, Atmosphere 12 (6) (2021) 771.

[118] G. Braca, D. Ducci, Development of a gis based procedure (bigbang 1.0) for evaluating groundwater balances at national scale and comparison with groundwater resources evaluation at local scale, in: Groundwater and Global Change in the Western Mediterranean Area, Springer, 2018, pp. 53–61.

[119] G. Braca, M. Bussettini, D. Ducci, B. Lastoria, S. Mariani, Evaluation of national and regional groundwater resources under climate change scenarios using a gis-based water budget procedure, Rendiconti Lincei. Scienze Fisiche e Naturali 30 (1) (2019) 109–123.

[120] Il Bilancio Idrologico Gis BAsed a scala Nazionale su Griglia regolare – BIGBANG: metodologia e stime. Rapporto sulla disponibilità naturale della risorsa idrica. (in Italian), Tech. rep., ISPRA (2021).

[121] Programma nazionale di misure di portata in corsi d'acqua finalizzate alla definizione della scala di deflusso. Valutazione tecnico-economica, https://www.isprambiente.gov.it/pre_meteo/idro/documenti_tavolo/Programma%20nazionale%20misure%20portata_agg_nov2017.pdf, in Italian, Tech. rep., ISPRA (2017).

[122] N. Ghilain, A. Arboleda, F. Gellens-Meulenberghs, Evapotranspiration modelling at large scale using near-real time msg seviri derived data, Hydrology and Earth System Sciences 15 (3) (2011) 771–786.

[123] Algorithm Theoretical Basis Document, LSA-SAF ETv2 HLE, version 1.1, Tech. rep., EUMETSAT (2016).

[124] F. Lehmann, B. D. Vishwakarma, J. Bamber, How well are we able to close the water budget at the global scale?, Hydrology and Earth System Sciences 26 (1) (2022) 35–54.

[125] B. Scanlon, Z. Zhang, A. Rateb, A. Sun, D. Wiese, H. Save, H. Beaudoing, M. Lo, H. Müller-Schmied, P. Döll, et al., Tracking seasonal fluctuations in land water storage using global models and grace satellites, Geophysical Research Letters 46 (10) (2019) 5254–5264.

[126] X. Feng, S. E. Thompson, R. Woods, A. Porporato, Quantifying asynchronicity of precipitation and potential evapotranspiration in mediterranean climates, Geophysical Research Letters 46 (24) (2019) 14692–14701.

[127] F. Avanzi, S. Gabellani, F. Delogu, F. Silvestro, F. Pignone, G. Bruno, L. Pulvirenti, G. Squicciarino, E. Fiori, L. Rossi, et al., It-snow: a snow reanalysis for italy blending modeling, in-situ data, and satellite observations (2010–2021), Earth System Science Data Discussions (2022) 1–30.

[128] G. Chiogna, P. Skrobanek, T. S. Narany, R. Ludwig, C. Stumpp, Effects of the 2017 drought on isotopic and geochemical gradients in the adige catchment, italy, Science of the Total Environment 645 (2018) 924–936.

[129] C. Marchina, C. Natali, G. Bianchini, The po river water isotopes during the drought condition of the year 2017, Water 11 (1) (2019) 150.

[130] Drought news march 2012 - european drought observatory, `https://edo.jrc.ec.europa.eu/documents/news/EDODroughtNews201203.pdf`, accessed: 2022-04-29.

[131] Severe drought in italy – july 2017 - edo analytical report, `https://edo.jrc.ec.europa.eu/documents/news/EDODroughtNews201707_Italy.pdf`, accessed: 2022-04-29.

[132] A. TORETI, D. BAVERA, F. AVANZI, C. CAMMALLERI, M. DE FELICE, A. DE JAGER, C. DI CIOLLO, S. GABELLANI, W. MAETENS, D. MAGNI, et al., Drought in northern italy-march 2022: Gdo analytical report.

[133] T. Apurv, M. Sivapalan, X. Cai, Understanding the role of climate characteristics in drought propagation, Water Resources Research 53 (11) (2017) 9304–9329.

[134] R. D. Garreaud, C. Alvarez-Garreton, J. Barichivich, J. P. Boisier, D. Christie, M. Galleguillos, C. LeQuesne, J. McPhee, M. Zambrano-Bigiarini, The 2010–2015 megadrought in central chile: Impacts on regional hydroclimate and vegetation, Hydrology and earth system sciences 21 (12) (2017) 6307–6327.

[135] J. H. Stagge, L. M. Tallaksen, L. Gudmundsson, A. F. Van Loon, K. Stahl, Candidate distributions for climatological drought indices (spi and spei), International Journal of Climatology 35 (13) (2015) 4027–4040.

[136] C. Svensson, J. Hannaford, I. Prosdocimi, Statistical distributions for monthly aggregations of precipitation and streamflow in drought indicator applications, Water Resources Research 53 (2) (2017) 999–1018.

[137] R. Stephan, M. Erfurt, S. Terzi, M. Žun, B. Kristan, K. Haslinger, K. Stahl, An inventory of alpine drought impact reports to explore past droughts in a mountain region, Natural Hazards and Earth System Sciences 21 (8) (2021) 2485–2501.

[138] A. F. Van Loon, S. Rangecroft, G. Coxon, M. Werner, N. Wanders, G. Di Baldassarre, E. Tijdeman, M. Bosman, T. Gleeson, A. Nauditt, et al., Streamflow droughts aggravated by human activities despite management, Environmental Research Letters 17 (4) (2022) 044059.

[139] W. Tian, X. Liu, C. Liu, P. Bai, Investigation and simulations of changes in the relationship of precipitation-runoff in drought years, Journal of hydrology 565 (2018) 95–105.

[140] T. Maurer, F. Avanzi, S. D. Glaser, R. C. Bales, Drivers of drought-induced shifts in the water balance through a budyko approach, Hydrology and Earth System Sciences 26 (3) (2022) 589–607.

[141] C. Massari, F. Avanzi, G. Bruno, S. Gabellani, D. Penna, S. Camici, Evaporation enhancement drives the european water-budget deficit during multi-year droughts, Hydrology and Earth System Sciences 26 (6) (2022) 1527–1543.

[142] J. Wu, X. Chen, Z. Yu, H. Yao, W. Li, D. Zhang, Assessing the impact of human regulations on hydrological drought development and recovery based on a 'simulated-observed'comparison of the swat model, Journal of Hydrology 577 (2019) 123990.

[143] J. Lorenzo-Lacruz, S. M. Vicente-Serrano, J. C. González-Hidalgo, J. I. López-Moreno, N. Cortesi, Hydrological drought response to meteorological drought in the iberian peninsula, Climate Research 58 (2) (2013) 117–131.

[144] J. Wu, X. Chen, H. Yao, D. Zhang, Multi-timescale assessment of propagation thresholds from meteorological to hydrological drought, Science of the Total Environment 765 (2021) 144232.

[145] J. Wu, X. Chen, X. Yuan, H. Yao, Y. Zhao, A. AghaKouchak, The interactions between hydrological drought evolution and precipitation-streamflow relationship, Journal of Hydrology 597 (2021) 126210.

[146] T. Apurv, X. Cai, Drought propagation in contiguous us watersheds: A process-based understanding of the role of climate and watershed properties, Water Resources Research 56 (9) (2020) e2020WR027755.

[147] Y. Yang, T. R. McVicar, R. J. Donohue, Y. Zhang, M. L. Roderick, F. H. Chiew, L. Zhang, J. Zhang, Lags in hydrologic recovery following an extreme drought: Assessing the roles of climate and catchment characteristics, Water Resources Research 53 (6) (2017) 4821–4837.

[148] M. Safeeq, R. R. Bart, N. F. Pelak, C. K. Singh, D. N. Dralle, P. Hartsough, J. W. Wagenbrenner, How realistic are water-balance closure assumptions? a demonstration from the southern sierra critical zone observatory and kings river experimental watersheds, Hydrological Processes 35 (5) (2021) e14199.

[149] L. Bouaziz, A. Weerts, J. Schellekens, E. Sprokkereef, J. Stam, H. Savenije, M. Hrachowitz, Redressing the balance: quantifying net intercatchment groundwater flows, Hydrology and Earth System Sciences 22 (12) (2018) 6415–6434.

[150] Y. Fan, Are catchments leaky?, Wiley Interdisciplinary Reviews: Water 6 (6) (2019) e1386.

[151] A. N. Wlostowski, N. Molotch, S. P. Anderson, S. L. Brantley, J. Chorover, D. Dralle, P. Kumar, L. Li, K. A. Lohse, J. M. Mallard, et al., Signatures of hydrologic function across the critical zone observatory network, Water Resources Research 57 (3) (2021) e2019WR026635.

[152] J. Han, Y. Yang, M. L. Roderick, T. R. McVicar, D. Yang, S. Zhang, H. E. Beck, Assessing the steady-state assumption in water balance calculation across global catchments, Water Resources Research 56 (7) (2020) e2020WR027392.

[153] F. W. Landerer, S. Swenson, Accuracy of scaled grace terrestrial water storage estimates, Water resources research 48 (4) (2012).

[154] S. Wang, D. W. McKenney, J. Shang, J. Li, A national-scale assessment of long-term water budget closures for canada's watersheds, Journal of Geophysical Research: Atmospheres 119 (14) (2014) 8712–8725.

[155] K. Stahl, I. Kohn, V. Blauhut, J. Urquijo, L. De Stefano, V. Acácio, S. Dias, J. H. Stagge, L. M. Tallaksen, E. Kampragou, et al., Impacts of european drought events: insights from an international database of text-based reports, Natural Hazards and Earth System Sciences 16 (3) (2016) 801–819.

[156] J. Spinoni, P. Barbosa, A. De Jager, N. McCormick, G. Naumann, J. V. Vogt, D. Magni, D. Masante, M. Mazzeschi, A new global database of meteorological drought events from 1951 to 2016, Journal of Hydrology: Regional Studies 22 (2019) 100593.

[157] L. Alfieri, V. Lorini, F. A. Hirpa, S. Harrigan, E. Zsoter, C. Prudhomme, P. Salamon, A global streamflow reanalysis for 1980–2018, Journal of Hydrology X 6 (2020) 100049.

[158] Randolph Glacier Inventory – A Dataset of Global Glacier Outlines: Version 6.0: Technical Report, Global Land Ice Measurements from Space, Colorado, USA. Digital Media. DOI: https://doi.org/10.7265/N5-RGI-60, Tech. rep., RGI Consortium (2017).

[159] M. Van Tiel, A. F. Van Loon, J. Seibert, K. Stahl, Hydrological response to warm and dry weather: do glaciers compensate?, Hydrology and Earth System Sciences 25 (6) (2021) 3245–3265.

[160] G. Pastorello, C. Trotta, E. Canfora, H. Chu, D. Christianson, Y.-W. Cheah, C. Poindexter, J. Chen, A. Elbashandy, M. Humphrey, et al., The fluxnet2015 dataset and the oneflux processing pipeline for eddy covariance data, Scientific data 7 (1) (2020) 1–27.

[161] D. G. Miralles, T. Holmes, R. De Jeu, J. Gash, A. Meesters, A. Dolman, Global land-surface evaporation estimated from satellite-based observations, Hydrology and Earth System Sciences 15 (2) (2011) 453–469.

[162] F. R. Hampel, The influence curve and its role in robust estimation, Journal of the american statistical association 69 (346) (1974) 383–393.

[163] L. Gudmundsson, H. X. Do, M. Leonard, S. Westra, The global streamflow indices and metadata archive (gsim)–part 2: Quality control, time-series indices and homogeneity assessment, Earth System Science Data 10 (2) (2018) 787–804.

[164] C. Murphy, S. Harrigan, J. Hall, R. L. Wilby, Climate-driven trends in mean and high flows from a network of reference stations in ireland, Hydrological Sciences Journal 58 (4) (2013) 755–772.

[165] G. Hu, L. Jia, M. Menenti, Comparison of mod16 and lsa-saf msg evapotranspiration products over europe for 2011, Remote Sensing of Environment 156 (2015) 510–526.

[166] G. P. Petropoulos, G. Ireland, S. Lamine, H. M. Griffiths, N. Ghilain, V. Anagnostopoulos, M. R. North, P. K. Srivastava, H. Georgopoulou, Operational evapotranspiration estimates from seviri in support of sustainable water management, International Journal of Applied Earth Observation and Geoinformation 49 (2016) 175–187.

[167] G. Sepulcre-Canto, J. Vogt, A. Arboleda, T. Antofie, Assessment of the eumetsat lsa-saf evapotranspiration product for drought monitoring in europe, International Journal of Applied Earth Observation and Geoinformation 30 (2014) 190–202.

[168] B. Martens, D. G. Miralles, H. Lievens, R. Van Der Schalie, R. A. De Jeu, D. Fernández-Prieto, H. E. Beck, W. A. Dorigo, N. E. Verhoest, Gleam v3: Satellite-based land evaporation and root-zone soil moisture, Geoscientific Model Development 10 (5) (2017) 1903–1925.

[169] S. Dingman, Physical hydrology (2002).

[170] A. Crespi, M. Brunetti, G. Lentini, M. Maugeri, 1961–1990 high-resolution monthly precipitation climatologies for italy, International Journal of Climatology 38 (2) (2018) 878–895.

[171] D. Koffler, G. Laaha, Lfstat-low-flow analysis in r, in: EGU General Assembly Conference Abstracts, 2013, pp. EGU2013–7770.

[172] S. J. Sutanto, H. A. Van Lanen, Catchment memory explains hydrological drought forecast performance, Scientific reports 12 (1) (2022) 1–11.

[173] A. R. Ladson, R. Brown, B. Neal, R. Nathan, A standard approach to baseflow separation using the lyne and hollick filter, Australasian Journal of Water Resources 17 (1) (2013) 25–34.

[174] J. W. Kirchner, Catchments as simple dynamical systems: Catchment characterization, rainfall-runoff modeling, and doing hydrology backward, Water Resources Research 45 (2) (2009).

[175] T. Gleeson, B. Richter, How much groundwater can we pump and protect environmental flows through time? presumptive standards for conjunctive management of aquifers and rivers, River research and applications 34 (1) (2018) 83–92.

[176] S. K. Kampf, S. J. Burges, J. C. Hammond, A. Bhaskar, T. P. Covino, A. Eurich, H. Harrison, M. Lefsky, C. Martin, D. McGrath, et al., The case for an open water balance: Re-envisioning network design and data analysis for a complex, uncertain world, Water Resources Research 56 (6) (2020) e2019WR026699.

[177] W. Abera, G. Formetta, L. Brocca, R. Rigon, Modeling the water budget of the upper blue nile basin using the jgrass-newage model system and satellite data, Hydrology and Earth System Sciences 21 (6) (2017) 3145–3165.

[178] W. Abera, G. Formetta, M. Borga, R. Rigon, Estimating the water budget components and their variability in a pre-alpine basin with jgrass-newage, Advances in water resources 104 (2017) 37–54.

[179] M. G. Floriancic, W. R. Berghuijs, T. Jonas, J. W. Kirchner, P. Molnar, Effects of climate anomalies on warm-season low flows in switzerland, Hydrology and Earth System Sciences 24 (11) (2020) 5423–5438.

[180] A. Conte, S. Fares, L. Salvati, F. Savi, G. Matteucci, F. Mazzenga, D. Spano, C. Sirca, S. Marras, M. Galvagno, et al., Ecophysiological responses to rainfall variability in grassland and forests along a latitudinal gradient in italy, Frontiers in Forests and Global Change 2 (2019) 16.

[181] N. Ghajarnia, Z. Kalantari, R. Orth, G. Destouni, Close co-variation between soil moisture and runoff emerging from multi-catchment data across europe, Scientific reports 10 (1) (2020) 1–11.

[182] N. Ghajarnia, Z. Kalantari, G. Destouni, Data-driven worldwide quantification of large-scale hydroclimatic co-variation patterns and comparison with reanalysis and earth system modeling, Water Resources Research (2020) e2020WR029377.

[183] W. C. Palmer, Meteorological drought, Vol. 30, US Department of Commerce, Weather Bureau, 1965.

[184] A. Mangin, Pour une meilleure connaissance des systèmes hydrologiques à partir des analyses corrélatoire et spectrale, Journal of hydrology 67 (1-4) (1984) 25–43.

[185] M. F. Bierkens, V. A. Bell, P. Burek, N. Chaney, L. E. Condon, C. H. David, A. de Roo, P. Döll, N. Drost, J. S. Famiglietti, et al., Hyper-resolution global hydrological modelling: what is next? "everywhere and locally relevant", Hydrological processes 29 (2) (2015) 310–320.

[186] M. Van Huijgevoort, H. Van Lanen, A. Teuling, R. Uijlenhoet, Identification of changes in hydrological drought characteristics from a multi-gcm driven ensemble constrained by observed discharge, Journal of Hydrology 512 (2014) 421–434.

[187] C. Cammalleri, G. Naumann, L. Mentaschi, B. Bisselink, E. Gelati, A. De Roo, L. Feyen, Diverging hydrological drought traits over europe with global warming, Hydrology and Earth System Sciences 24 (12) (2020) 5919–5935.

[188] C. Cammalleri, J. Vogt, P. Salamon, Development of an operational low-flow index for hydrological drought monitoring over europe, Hydrological Sciences Journal 62 (3) (2017) 346–358.

[189] P. Trambauer, M. Werner, H. Winsemius, S. Maskey, E. Dutra, S. Uhlenbrook, Hydrological drought forecasting and skill assessment for the limpopo river basin, southern africa, Hydrology and Earth System Sciences 19 (4) (2015) 1695–1711.

[190] T. C. Van Hateren, S. J. Sutanto, H. A. Van Lanen, Evaluating skill and robustness of seasonal meteorological and hydrological drought forecasts at the catchment scale–case catalonia (spain), Environment international 133 (2019) 105206.

[191] S. J. Sutanto, F. Wetterhall, H. A. Van Lanen, Hydrological drought forecasts outperform meteorological drought forecasts, Environmental Research Letters 15 (8) (2020) 084010.

[192] B. W. Abbott, K. Bishop, J. P. Zarnetske, D. M. Hannah, R. J. Frei, C. Minaudo, F. S. Chapin, S. Krause, L. Conner, D. Ellison, et al., A water cycle for the anthropocene, Hydrological Processes 33 (23) (2019).

[193] V. Klemeš, Operational testing of hydrological simulation models, Hydrological sciences journal 31 (1) (1986) 13–24.

[194] C. Li, L. Zhang, H. Wang, Y. Zhang, F. Yu, D. Yan, The transferability of hydrological models under nonstationary climatic conditions, Hydrology and Earth System Sciences 16 (4) (2012) 1239–1254.

[195] P. Deb, A. S. Kiem, Evaluation of rainfall–runoff model performance under non-stationary hydroclimatic conditions, Hydrological Sciences Journal 65 (10) (2020) 1667–1684.

[196] S. Westra, M. Thyer, M. Leonard, D. Kavetski, M. Lambert, A strategy for diagnosing and interpreting hydrological model nonstationarity, Water Resources Research 50 (6) (2014) 5090–5113.

[197] D. Guo, S. Westra, H. R. Maier, Impact of evapotranspiration process representation on runoff projections from conceptual rainfall-runoff models, Water Resources Research 53 (1) (2017) 435–454.

[198] F. Silvestro, S. Gabellani, F. Delogu, R. Rudari, G. Boni, Exploiting remote sensing land surface temperature in distributed hydrological modelling: the example of the continuum model, Hydrology and Earth System Sciences 17 (1) (2013) 39–62.

[199] D. Masante, J. Vogt, N. McCormick, C. Cammalleri, D. Magni, A. de Jager, Severe drought in italy – july 2017 (2017). doi:https://edo.jrc.ec.europa.eu/documents/news/EDODroughtNews201707_Italy.pdf.

[200] A. Toreti, D. Bavera, F. Avanzi, C. Cammalleri, M. De Felice, A. de Jager, C. Di Ciollo, M. Gardella, S. Gabellani, P. Leoni, W. Maetens, D. Magni, M. G., D. Masante, M. Mazzeschi, N. McCormick, G. Naumann, S. Niemeyer, L. Rossi, L. Seguini, J. Spinoni, M. van den Berg, Drought in europe april 2022 (JRC129395) (2022). doi:doi:10.2760/40384.

[201] P. R. B. Authority, Caratteristiche del bacino del fiume po e primo esame dell' impatto ambientale delle attivitá umane sulle risorse idriche (characteristics of po river basin and first analysis of the impact of human activities on water resources) (2006). doi:adbpo.it/download/bacino_Po/AdbPo_Caratteristiche-bacino-Po_2006.pdf(inItalian).

[202] ESA, Land cover cci product user guide version 2. tech. rep., Tech. rep. (2017). doi:https://maps.elie.ucl.ac.be/CCI/viewer/download/ESACCI-LC-Ph2-PUGv2_2.0.pdf(lastaccess:28July2022).

[203] F. Silvestro, S. Gabellani, R. Rudari, F. Delogu, P. Laiolo, G. Boni, Uncertainty reduction and parameter estimation of a distributed hydrological model with ground and remote-sensing data, Hydrology and Earth System Sciences 19 (4) (2015) 1727–1751.

[204] F. Silvestro, G. Ercolani, S. Gabellani, P. Giordano, M. Falzacappa, Improving real-time operational streamflow simulations using discharge data to update state variables of a distributed hydrological model, Hydrology Research 52 (6) (2021) 1239–1260.

[205] G. Bruno, F. Avanzi, S. Gabellani, L. Ferraris, E. Cremonese, M. Galvagno, C. Massari, Disentangling the role of subsurface storage in the propagation of drought through the hydrological cycle, Advances in Water Resources 169 (2022) 104305.

[206] B. R. Scanlon, Z. Zhang, H. Save, D. N. Wiese, F. W. Landerer, D. Long, L. Longuevergne, J. Chen, Global evaluation of new grace mascon products for hydrologic applications, Water Resources Research 52 (12) (2016) 9412–9429.

[207] H. Save, S. Bettadpur, B. D. Tapley, High-resolution csr grace rl05 mascons, Journal of Geophysical Research: Solid Earth 121 (10) (2016) 7547–7569.

[208] H. Save, Csr grace and grace-fo rl06 mascon solutions v02 (2020). doi:doi:10.15781/cgq9-nh24.

[209] M. M. Watkins, D. N. Wiese, D.-N. Yuan, C. Boening, F. W. Landerer, Improved methods for observing earth's time variable mass distribution with grace using spherical cap mascons, Journal of Geophysical Research: Solid Earth 120 (4) (2015) 2648–2671.

[210] D. N. Wiese, D.-N. Yuan, C. Boening, F. W. Landerer, M. M. Watkins., Jpl grace mascon ocean, ice, and hydrology equivalent water height rl06 cri filtered version 02. ver. 02. po.daac, ca, usa. dataset accessed [2022-08-03] (2019). doi:https://doi.org/10.5067/TEMSC-3JC62.

[211] B. Loomis, S. Luthcke, T. Sabaka, Regularization and error characterization of grace mascons, Journal of geodesy 93 (9) (2019) 1381–1398.

[212] L. Poggio, L. M. De Sousa, N. H. Batjes, G. Heuvelink, B. Kempen, E. Ribeiro, D. Rossiter, Soilgrids 2.0: producing soil information for the globe with quantified spatial uncertainty, Soil 7 (1) (2021) 217–240.

[213] H. Kling, M. Fuchs, M. Paulin, Runoff conditions in the upper danube basin under an ensemble of climate change scenarios, Journal of hydrology 424 (2012) 264–277.

[214] W. J. Knoben, J. E. Freer, R. A. Woods, Inherent benchmark or not? comparing nash–sutcliffe and kling–gupta efficiency scores, Hydrology and Earth System Sciences 23 (10) (2019) 4323–4331.

[215] R. Pushpalatha, C. Perrin, N. Le Moine, V. Andréassian, A review of efficiency criteria suitable for evaluating low-flow simulations, Journal of Hydrology 420 (2012) 171–182.

[216] D. N. Moriasi, J. G. Arnold, M. W. Van Liew, R. L. Bingner, R. D. Harmel, T. L. Veith, Model evaluation guidelines for systematic quantification of accuracy in watershed simulations, Transactions of the ASABE 50 (3) (2007) 885–900.

[217] G. Coxon, J. Freer, I. K. Westerberg, T. Wagener, R. Woods, P. Smith, A novel framework for discharge uncertainty quantification applied to 500 uk gauging stations, Water resources research 51 (7) (2015) 5531–5546.

[218] C. Massari, F. Avanzi, G. Bruno, S. Gabellani, D. Penna, S. Camici, Evaporation enhancement drives the european water-budget deficit during multi-year droughts, Hydrology and Earth System Sciences 26 (6) (2022) 1527–1543.

[219] M. Dembélé, M. Hrachowitz, H. H. Savenije, G. Mariéthoz, B. Schaefli, Improving the predictive skill of a distributed hydrological model by calibration on spatial patterns with multiple satellite data sets, Water resources research 56 (1) (2020) e2019WR026085.

[220] O. Rakovec, R. Kumar, S. Attinger, L. Samaniego, Improving the realism of hydrologic model functioning through multivariate parameter estimation, Water Resources Research 52 (10) (2016) 7779–7792.

[221] G. Hartmann, A. Bárdossy, Investigation of the transferability of hydrological models and a method to improve model calibration, Advances in Geosciences 5 (2005) 83–87.

[222] P. Rameshwaran, V. A. Bell, M. J. Brown, H. N. Davies, A. L. Kay, A. C. Rudd, C. Sefton, Use of abstraction and discharge data to improve the performance of a national-scale hydrological model, Water Resources Research 58 (1) (2022) e2021WR029787.

[223] D. M. Mocko, S. V. Kumar, C. D. Peters-Lidard, S. Wang, Assimilation of vegetation conditions improves the representation of drought over agricultural areas, Journal of Hydrometeorology 22 (5) (2021) 1085–1098.

[224] J. Dari, P. Quintana-Seguí, R. Morbidelli, C. Saltalippi, A. Flammini, E. Giugliarelli, M. J. Escorihuela, V. Stefan, L. Brocca, Irrigation estimates from space: Implementation of different approaches to model the evapotranspiration contribution within a soil-moisture-based inversion algorithm, Agricultural Water Management 265 (2022) 107537.

[225] F. Avanzi, S. Gabellani, F. Delogu, F. Silvestro, E. Cremonese, U. Morra di Cella, S. Ratto, H. Stevenin, Snow multidata mapping and modeling (s3m) 5.1: a distributed cryospheric model with dry and wet snow, data assimilation, glacier mass balance, and debris-driven melt, Geoscientific Model Development 15 (12) (2022) 4853–4879.

[226] M. Sivapalan, H. H. Savenije, G. Blöschl, et al., Socio-hydrology: A new science of people and water, Hydrol. Process 26 (8) (2012) 1270–1276.

[227] H. K. McMillan, I. K. Westerberg, T. Krueger, Hydrological data uncertainty and its implications, Wiley Interdisciplinary Reviews: Water 5 (6) (2018) e1319.

[228] I. E. de Graaf, T. Gleeson, E. H. Sutanudjaja, M. F. Bierkens, et al., Environmental flow limits to global groundwater pumping, Nature 574 (7776) (2019) 90–94.

[229] E. H. Sutanudjaja, R. Van Beek, N. Wanders, Y. Wada, J. H. Bosmans, N. Drost, R. J. Van Der Ent, I. E. De Graaf, J. M. Hoch, K. De Jong, et al., Pcr-globwb 2: a 5 arcmin global hydrological and water resources model, Geoscientific Model Development 11 (6) (2018) 2429–2453.

[230] C. W. Ross, L. Prihodko, J. Anchang, S. Kumar, W. Ji, N. P. Hanan, Hysogs250m, global gridded hydrologic soil groups for curve-number-based runoff modeling, Scientific data 5 (1) (2018) 1–9.

[231] T. Hengl, J. Mendes de Jesus, G. B. Heuvelink, M. Ruiperez Gonzalez, M. Kilibarda, A. Blagotić, W. Shangguan, M. N. Wright, X. Geng, B. Bauer-Marschallinger, et al., Soilgrids250m: Global gridded soil information based on machine learning, PLoS one 12 (2) (2017) e0169748.

[232] W. Dorigo, W. Wagner, C. Albergel, F. Albrecht, G. Balsamo, L. Brocca, D. Chung, M. Ertl, M. Forkel, A. Gruber, et al., Esa cci soil moisture for improved earth system understanding: State-of-the art and future directions, Remote Sensing of Environment 203 (2017) 185–215.

[233] B. Lehner, C. R. Liermann, C. Revenga, C. Vörösmarty, B. Fekete, P. Crouzet, P. Döll, M. Endejan, K. Frenken, J. Magome, et al., High-resolution mapping of the world's reservoirs and dams for sustainable river-flow management, Frontiers in Ecology and the Environment 9 (9) (2011) 494–502.